ANALYSIS OF A HIGH TEMPERATURE FOULING UNIT FOR HEAVY HYDROCARBON FRACTIONS

By

Martial Simard

B. A. Sc., Université Laval, 1996

A THESIS SUBMITTED IN PARTIAL FULFILLMENT OF

THE REQUIREMENTS FOR THE DEGREE OF

MASTER OF APPLIED SCIENCE

in

THE FACULTY OF GRADUATE STUDIES

DEPARTMENT OF CHEMICAL AND BIO-RESOURCE ENGINEERING

We accept this thesis as conforming

to the required standard

THE UNIVERSITY OF BRITISH COLUMBIA

March 2000

In presenting this thesis in partial fulfilment of the requirements for an advanced degree at the University of British Columbia, I agree that the Library shall make it freely available for reference and study. I further agree that permission for extensive copying of this thesis for scholarly purposes may be granted by the head of my department or by his or her representatives. It is understood that copying or publication of this thesis for financial gain shall not be allowed without my written permission.

Department of CHEMICAL ENGINEERING

The University of British Columbia
Vancouver, Canada

Date MARCH 31, 2000

Abstract

With the depletion and increase in the price of light crude oil, the conversion of heavy oils and bitumens into distillable fractions in upgrading units has become an important source in meeting the demand for fuels and petrochemical products. Fouling, or the deposition of any undesirable material on heat exchangers surfaces, is a costly operational problem in conventional refineries because it increases the resistance to heat transmission and flow. The precipitation problem is worse with heavy petroleum streams because of the higher concentration of fouling precursors such as asphaltenes and polar heteroatomic species and the higher temperatures of processing required to convert the high molecular weight components. At temperatures above 300°C, heavy oil streams undergo thermal decomposition or free-radical reactions which lead to the formation of coke defined as toluene insoluble carbonaceous solid which fouls processing units.

In order to design and operate upgrading units with minimum coke deposition, the chemical, thermal, and fluid mechanical factors causing the problem must be known. A research project which involved kinetic and thermal fouling studies on pitch, gas oils, and their blends was initiated to generate such information. As part of this research, a re-circulation flow loop had been constructed to study coke deposition during flow through a vertical tube placed in an electrically heated fluidized bed. The present work was conducted to develop the apparatus, to analyze its behaviour, to evaluate the tendency of pitch–gas oils blends to form coke and to assess the capability of the unit to detect it under the appropriate conditions of bulk and surface temperatures.

A series of fouling experiments was carried out by recirculating a 50:50% vol. pitch-coker heavy gas oil blend over 11–56 hour periods with average bulk fluid temperatures of 200–375°C, tube side velocities of 0.3–2.2 m/s (laminar flow), and average fluid bed temperatures in the range of 500–615°C. A number of improvements to the high-temperature unit were made to reach the desired temperature conditions, to provide the necessary measurements for adequate interpretation of results, and to increase the quality of the data. In order to determine the flow regime and to account for possible viscosity changes

during recirculation, the density of the above mixture and the viscosity of pitch, gas oils, and their blends were measured over a wide range of temperatures. Additional tests were performed to monitor the viscosity change during recirculation of the test fluid and also the change in the amount of toluene insolubles in the 50:50% vol. pitch-heavy gas oil blend. Coke deposition was determined by mass deposition and by thermal measurements. Interpretation of the latter was made by use of different data analysis techniques and of empirical correlations found between process variables. Moreover, in order to see whether the absence of fouling observed was due to the fouling unit and/or to the nature of the test fluid, a blend of de-asphalted oil known to give measurable fouling rates in turbulent flow and in similar periods of time as for the coking experiments was studied. Finally, measurements of heat transfer coefficients were made in order to estimate the sensitivity of the unit to detect fouling by thermal measurements.

Correlations were developed over a wide temperature range for the viscosity (80–310°C) and density (60–145°C) prediction of any blend of pitch and gas oil. As a result, the flow regime could be determined and the viscosity drop observed in some of the runs revealed a possible bias effect on the mass flowrate measurement. Moreover, the use of different data analysis techniques and empirical equations found between process variables confirmed the liquid flowrate variations as the reason for the observed changes in the thermal resistance for the runs with the 50:50% vol. pitch-gas oil blend. The liquid flowrate variations were essentially eliminated by modifying the configuration of the bypass circuit. Also, the thermal resistance of the fluid bed was found to be as high as 38% of the total resistance, which substantially reduced the sensitivity of the unit to detect coke deposition. Finally, no significant fouling was observed both from the thermal and mass deposition measurements with the 50:50% vol. pitch-gas oil blend over the range of conditions mentioned above. As for the experiments involving a blend of de-asphalted oil, the evidence obtained was judged insufficient to draw a definite conclusion as whether sufficient fouling actually took place.

Table of Contents

List of Tables

List of Figures

List of Symbols

A, a	constants
A_i, A_o	inner and outer tube surfaces, respectively
B, b, b_1, b_2	constants
C	constant (Chapter 3), discharge coefficient elsewhere
C_p, c_p, c_g	heat capacity of test fluid, particles, and gas, respectively
C_R	ratio of heat transfer coefficient for vertical tube to that for tube located on bed axis
D	rate of shear (p.25) and tube diameter elsewhere
D_{th}	diameter of orifice throat
d_p	particle diameter
D_v	bed internal diameter
E	activation energy
G, g	superficial mass fluidizing velocity and gravity constant, resp.
h	convective heat transfer coefficient
$\hat{h}$	predicted convective heat transfer coefficient
j	$\sqrt{-1}$
k, k_d, k_g, k_l	thermal conductivity of tube wall, deposit, gas, and liquid, resp.
K	instrument factor
L	length of vector (Section 6.4), length of heated tube elsewhere
L_e, L_{et}	hydrodynamic and thermal entry lengths, respectively
l_l	laminar flow length scale
m	mass of deposit per unit heat transfer area
$\dot{m}, \overline{\dot{m}}$	mass flowrate, average (over time) mass flowrate
$\Delta\dot{m}_\nu$	change in $\dot{m}$ predicted from viscosity data
$\Delta\dot{m}_{\Delta T_{loss}}$	change in $\dot{m}$ predicted from Eq. 6.16
n	test speed (Eq. 3.6), number of data points elsewhere
N	number of data points

p	period
ΔP	pressure drop across orifice plate
ΔP_{dist}	pressure drop across air distributor
$\Delta P_t, \Delta P_v$	total pressure drop, and pressure drop across the fluid bed
$Q, \overline{Q}$	heat flow, average (over time) heat flow
$\dot{q}$	heat flux
q^{-1}	backward shift operator
R	universal gas constant
R_f, R_t, R_w	thermal resistance (fouling, total, and tube wall, respectively)
$\dot{R}_f$	thermal fouling rate
r	tube radius
r_k	cross-correlation function at lag k
S, s	torque, and constant, respectively
$\hat{S}_p, S_p$	periodogram, and power spectral density, respectively
$T, \overline{T}$	temperature, and average temperature, respectively
TI	toluene insolubles
t	time index
t_r	recirculation time
ΔT	temperature difference
$\Delta T_{lm}, \overline{\Delta T}_{lm}$	log mean temperature difference (LMTD), and average LMTD
$\Delta T_{loss}, \overline{\Delta T}_{loss}$	temperature difference between bulk temperature of test fluid in the tank and bulk inlet temperature, and average ΔT_{loss}
U	gas superficial velocity
U_i, U_o	overall heat transfer coefficient (based on inner and outer surfaces of tube, respectively)
U_{or}	gas velocity at air distributor nozzle
V, v	volatile yield, and liquid velocity, respectively
w	defined by Eq. 6.27
w_c	weight of coke in test section at the end of a run
$\%wt_p$	weight percent of pitch

W_N	defined by Eq. 6.24
X	discrete fourier transform of sequence $\{x_t\}$
x	tube length
x_d	deposit thickness
$x_{fd,T}, x_{fd,H}$	thermal and hydrodynamic entrance regions
x_i	weight fraction of component i
x_p	weight fraction of pitch
x_{res}	equivalent liquid thickness of residue which would give rise to w_c
x_t	time series
y	data
z	coordinate

Dimensionless groups

Ar	Archimedes number
Gz	Graetz number
Nu	Nusselt number
Pr	Prandtl number
Re	Reynolds number

Greek letters

β	orifice-to-pipe diameter ratio
ϵ	fluid bed voidage
θ	frequency
μ	dynamic viscosity of liquid
μ_g	dynamic viscosity of gas
ν	kinematic viscosity of liquid
ρ	density of liquid
ρ_d	density of deposit

ρ_g	density of gas
ρ_p	density of particles
ρ_{res}	density of residue
σ	standard error
τ	shear stress

Subscripts

0	initial
air	air entering the fluid bed
b	bulk
bot	bottom of fluid bed
c	calculated with a constant flowrate value measured at the end of each run
cb	at calibration
d	deposit
f	final
fb	fluid bed
h	hot medium
i	inside (or inner) of the tube or liquid side
in	inlet
j	component j
M	by Molerus
m	mixture
max	maximum
mf	minimum fluidization conditions
mid	middle of fluid bed
o	outside (or outer) of the tube or fluid bed side
out	outlet
p	pitch
s	surface

T	at a given temperature
t	time index
top	top of fluid bed
v	calculated with actual flowrate value

Abbreviations

AAD	average absolute deviation
CHGO	coker heavy gas oil
CI	confidence interval
DAO	de-asphalted oil
FO	fuel oil
HO	heavy oil
LHS	left hand side
MCR	micro carbon residue (amount of solid left behind when a sample is pyrolyzed in an inert gas)
RHS	right hand side
SS	time required to get to thermal steady-state

Acknowledgement

I would like to thank my supervisors, Dr. Paul Watkinson and Dr. Ezra Kwok, for their support, guidance, and helpful suggestions throughout my research.

Special thanks must go to Dr. K. L. Pinder for his help regarding viscosity measurements and to Dr. D. Posarac who helped me solve several technical difficulties.

Support and technical advice from the staff of Mechanical workshop, Electrical shop, Stores, and Chemical Engineering office are truly appreciated.

Also I would like to thank my colleagues Michael Chong Ping, Petar Knezevich, Eman Al-Atar, and Ian Rose for their friendship and assistance.

The financial support of Syncrude Canada Limited and NSERC are gratefully acknowledged.

Finally, to my family for their encouragement and love, this thesis is dedicated.

Chapter 1

Introduction

1.1 Background

The increase in the price of conventional crude oil and its depletion have increased the interest for exploitation of alternate sources such as the vast reserves of heavy oils and bitumens found in tar sands of Western Canada. These feedstocks contain much larger amounts of residuum—the 524°C+ fraction of a crude oil or bitumen—than conventional crude oil, and hence require more processing. The current practice consists of converting the residua, and pitch—524°C+ product from processing a crude oil or bitumen—to produce synthetic crude oil that is suitable for conventional refinery processing. Gray (1994) has provided an excellent description of the upgrading processes of heavy oils and bitumens.

1.2 Fouling by Coke Deposition

Fouling can be defined as the accumulation of unwanted material at a phase interface. Fouling of heat exchanger surfaces in which organic streams are heated is the cause of important economic penalties that have been discussed by Van Nostrand Jr. et al. (1981), by Bott (1995), and others. At temperatures above 300°C, heavy oil streams undergo thermal or free-radical reactions which lead to the formation of coke, defined as toluene-insoluble carbonaceous solid. In processing petroleum streams, coke frequently deposits on the surface of processing equipment and causes fouling. Precipitation of carbon-rich material is worse with heavy petroleum streams such as bitumen from oil sands because of the higher temperatures of processing required and the higher concentration of precursors to coke formation such as asphaltenes and polar heteroatomic species.

1.3 Objectives of Work

As heavier feedstocks are processed in upgrading and refinery units, efforts are made to know the conditions which lead to coke and deposit precursors formation and deposition. The design and operation of units with minimum deposits require an understanding of the chemical, thermal and fluid mechanical factors which govern the processes leading to solids formation.

The ultimate goal of this research is to generate information on deposition processes taking place in heavy hydrocarbon streams, such as pitch and gas oil blends, through thermal fouling studies. To this end, a re-circulation flow loop capable of reaching high surface and bulk temperatures was constructed. The objective of the present work was to develop the new fouling unit, to analyze its behaviour, and to evaluate its capability to detect coke formation in pitch–gas oil blends so that progress towards the primary goal stated above can be achieved.

More specifically the objectives of this study are

- To modify the fouling unit so that viscous hydrocarbon streams can be processed and such that higher bulk temperatures are achieved.
- To provide additional measurements to ensure adequate monitoring and control of the unit and to facilitate the analysis of the fouling data.
- To characterize pitch, heavy gas oils, and blends by measuring the density and viscosity in the temperature range of thermal fouling studies to permit the flow regime to be determined.
- To perform a series of fouling experiments to test the coke detection limits in the fouling unit.
- To distinguish fouling from other process variable effects, to improve the quality of the data by eliminating known effects, and to reduce variations in process variables.

Chapter 2

Literature Review

2.1 Introduction

The build-up of undesired material on a surface, or fouling, is a widespread problem that has been observed to occur in many applications of heat exchangers. Because the subject matter of such a universal problem is quite broad, only the issues directly relevant to the present work are briefly discussed. This literature review is intended to provide a general background to the fouling problem and covers some aspects which occur in processing heavy petroleum streams typical of the heavy oil upgrading industry.

2.2 The Fouling Problem – Fundamentals

The accumulation of deposits considered here is the one occurring on the surface of a heat exchanger. In the following paragraphs, the basic equations governing the rate of heat transfer in heat exchangers will be recalled along with implications of fouling.

Consider a simple double pipe heat exchanger. An energy balance around a differential control volume for the flow in a tube leads to the following equations after certain assumptions are made—fluid is not undergoing a phase change, negligible potential and kinetic energy changes, constant mass flow rate, and negligible heat transfer between the exchanger and its surroundings—and integration from the tube inlet *in* to the outlet *out* (Incropera and DeWitt (1996)):

$$\begin{aligned} dQ &= \dot{m} \cdot C_p \cdot dT_b \\ Q &= \dot{m} \cdot \bar{C}_p \cdot (T_{b,out} - T_{b,in}) \end{aligned} \tag{2.1}$$

where the subscript b refers to mean (or bulk) temperature of the fluid at a given cross-section. The total heat flow, Q, can also be related to the heat exchanger surface area

and the temperature difference between the cold and the hot medium (denoted by the subscripts b and h, respectively). If an overall heat transfer coefficient U is used in place of a single convection coefficient, an extension of Newton's law of cooling is obtained, which applies to the entire tube:

$$Q = U_o \cdot A_o \cdot \Delta T_{lm} = U_i \cdot A_i \cdot \Delta T_{lm} \tag{2.2}$$

where ΔT_{lm} is an appropriate log mean temperature difference to account for the axial variation of the radial temperature gradient and the subscripts i and o indicate that U can be based on either the inner ($A_i = \pi D_i L$) or outer ($A_o = \pi D_o L$) tube surface area. The specific form of ΔT depends on the flow configuration and can be derived by applying energy balances to differential elements in the hot and cold media.

For a smooth, and clean single-tube heat exchanger, the overall heat transfer coefficient is given as:

$$U_o \cdot A_o = U_i \cdot A_i = \frac{1}{R_t} = \frac{1}{\left(\frac{1}{h_i A_i} + \frac{ln(r_o/ri)}{2\pi kL} + \frac{1}{h_o A_o}\right)} \tag{2.3}$$

The thermal resistance under clean conditions is therefore:

$$R_t = \frac{1}{U_o \cdot A_o} = \frac{1}{U_i \cdot A_i} = \left(\frac{1}{h_i A_i} + \frac{ln(r_o/ri)}{2\pi kL} + \frac{1}{h_o A_o}\right) \tag{2.4}$$

During normal heat exchanger operation, surfaces are usually subject to deposit formation and this represents an additional heat transfer resistance which increases with time. The technical problems associated with this layer are numerous and have been discussed by several authors, among them Bott (1988), but can be summarized in terms of two major effects. The thermal conductivity of the fouling layer is generally lower than the other resistances and this results in a loss of heat transfer efficiency. Also, the reduction of the flow area due to the presence of the deposit causes a blockage effect, which coupled with the usually rough surface presented by the foulant, increases the pressure drop through the heat exchanger.

This layer can be accounted for by introducing a fouling resistance, R_f. If we now consider deposit formation only on the inside surface of the tube, then the increase in

fouling resistance inside the tube over time t can be described as:

$$R_{f,i}(t) = \frac{A_i}{A_o}\left(\frac{1}{U_o(t)} - \frac{1}{U_o(0)}\right) \tag{2.5}$$

$$\approx \frac{x_d(t)}{k_d} = \frac{m(t)}{\rho_d k_d} \tag{2.6}$$

where m is mass deposited per unit heat transfer area, ρ_d is deposit density, and k_d is deposit thermal conductivity. Equation 2.6 is valid only for thin deposits. This situation is illustrated in Figure 2.1 which also shows the various thermal resistances acting in series. In addition, the initial fouling rate is an important parameter in thermal fouling studies and is given by:

$$\dot{R}_f(0) = \frac{A_i}{A_o}\frac{d}{dt}\left(\frac{1}{U_o(t)}\right)_{t=0} \tag{2.7}$$

The two special cases of interest in heat transfer—constant hot fluid temperature and constant surface heat flux—have some important implications on fouling. The former is

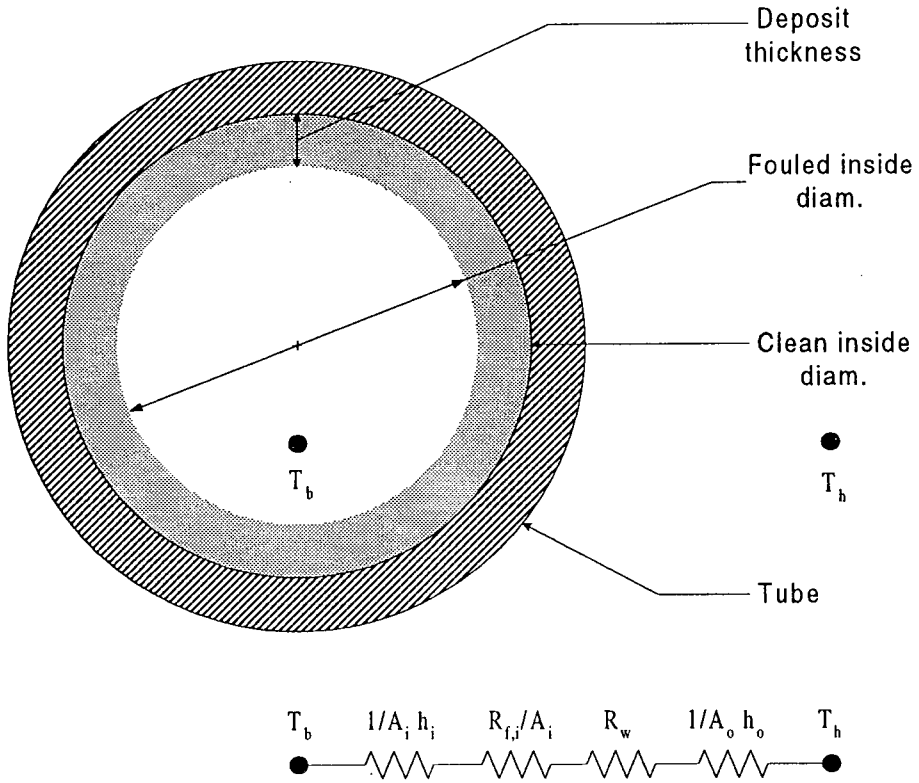

Figure 2.1: Schematic of Thermal Resistances in a Fouled Tube.

closely approximated, for example, when the surface is in contact with a freezing liquid or a condensing vapor while the latter may be realized from an electric heater. If we consider a local heat transfer at any axial position z, the heat flux may be obtained from Equation 2.2 where ΔT_{lm} simplifies to yield:

$$\dot{q}(z,0) = U_o(z,0)[T_h(z,0) - T_b(z,0)] \tag{2.8}$$

At time t we have by making use of Equation 2.5:

$$\dot{q}(z,t) = \frac{1}{\frac{1}{U_o(z,0)} + \frac{A_o}{A_i}R_{f,i}(z,t)}[T_h(z,t) - T_b(z,t)] \tag{2.9}$$

For constant local T_h, as $R_{f,i}$ increases, the local heat flux decreases over time. Provided that T_h is constant over time, the total heat flux will decrease whether or not the hot fluid temperature is uniform over the surface. If T_h is also uniform over the surface and the surface temperature is an important factor determining fouling, the measured initial fouling rate is expected to apply to the whole tube. However, when constant hot fluid temperature conditions prevail, the deposit/fluid interface temperature decreases as the surface fouls.

Equations 2.8 and 2.9 also reveal that to maintain a constant local heat flux implies that the local hot fluid temperature must be increased as $R_{f,i}$ increases:

$$U_o(z,0)[T_h(z,0) - T_b(z,0)] = \frac{1}{\frac{1}{U_o(z,0)} + \frac{A_o}{A_i}R_{f,i}(z,t)}[T_h(z,t) - T_b(z,t)] \tag{2.10}$$

If the heat flux is also uniform over the surface, it can be shown (Incropera and DeWitt (1996)) that the mean temperature T_b varies linearly between $T_{b,in}$ and $T_{b,out}$; the variation of the mean temperature along the tube may also be obtained if $\dot{q}$ is a known function of the distance. Note that a uniform heat flux implies that the surface temperature varies along the tube. Furthermore, in the case of a thin and hydrodynamically smooth deposit, the local deposit/fluid interface temperature remains constant at the clean wall temperature value as the surface fouls.

2.3 Fouling in The Heavy Oil Upgrading Industry

Heavy oils and bitumens are solid and semi-solid petroleum materials consisting of high molecular weight hydrocarbons, and contain large quantities of residuum which is defined

as material boiling above 524°C. The conversion of heavy oil residua to distillates (C_5+ to 524°C-) is of particular importance in Canada because of the vast bitumen reserves in Western Canada. These feedstocks are considerably heavier and more difficult to process than traditional crudes; the current practice consists of converting the residua and pitch to produce synthetic crude oil that is suitable for conventional refinery treatment.

Primary upgrading followed by hydrotreating are the two stages in which residua are upgraded, as explained by Gray (1994). Primary upgrading requires breakage of the carbon-carbon bonds in the residua and there are two approaches for doing this: hydrocracking and thermal processes. In the latter, the residuum is heated in an inert atmosphere and carbon in the form of coke is rejected.

Thermal-cracking processes are commonly used commercially to convert residua into distillable liquid products. Example processes include visbreaking, delayed coking and fluid coking. Within the coking units, coke formation is desired and promoted, leaving a lighter liquid as gaseous products. The coke is recovered as a by-product. When bitumen is processed under the severe temperature conditions of these thermal processes, there is usually a tendency for coke formation outside the units as well, and this can lead to technical difficulties. Fouling of processing equipment and heat exchanger surfaces by coke deposition is especially severe during the upgrading of heavy oils because of the higher temperatures of processing. These deposits must ultimately be removed from the equipment and disposed of.

The processing of heavy oils with minimum deposit formation hinges on understanding the reaction fundamentals of the heavy ends and the thermal and fluid mechanical factors which govern the process. However, hydrocarbon processing deals with undefined mixtures. Trace metal contaminants, heteroatoms (S, N, O containing species), short-lived radicals, catalytic effects and the large number of components combine to make the chemistry involved in this type of fouling exceedingly complex (Watkinson (1992)). The complicated nature of fouling chemistry in turn affects the thermal and physical processes involved.

In the remaining sections, some of the literature dealing with the key factors involved in the chemical and physical processes which lead to solid formation will be briefly reviewed.

Experimental techniques that have been used in previous thermal fouling studies will also be described. Finally, principles and correlations for heat transfer in a bubbling fluidized bed will be discussed, since a fluid bed unit was used in the current work.

2.4 Classification of Fouling

In order to facilitate analysis of fouling and to provide a conceptual framework for systematic research, Epstein (1983) has classified fouling into five primary categories. Crystallization fouling includes precipitation and solidification fouling. The former is due to formation of crystals from dissolved substances on the surface while the latter refers to the freezing of the process fluid—or constituents—onto a subcooled surface. Particulate fouling is the accumulation of suspended solids from the fluid stream on a surface. Deposit formation at the heat transfer surface resulting from chemical reactions in the flowing fluid in which the wall is not a reactant has been called chemical reaction fouling. Corrosion fouling occurs when the wall is involved in the formation of indigenous corrosion products on the surface. Biofouling was another category defined which accounts for the deposition and growth of organisms on a heat transfer surface.

Epstein (1983) also proposed a general sequence of events which may play a role in all of the above fouling types:

1. Initiation
2. Transport of foulant
3. Attachment to the surface
4. Removal of the deposit
5. Aging of the deposit on the surface

The deposits resulting from organic fluid fouling are usually strong such that no removal processes are significant (Watkinson (1992)). On the other hand, aging of deposits is particularly important (Watkinson and Wilson (1997)).

This classification should be used with care since it is not likely that practical heat exchanger fouling is due to only one type. Most fouling problems are the result of combinations and interactions of factors which belong to more than one of the above categories. This was pointed out by Murphy and Campbell (1992) who discussed fouling in refinery heat exchangers under seven categories, of which the following four—inorganic salts, sediments, filterable solids, and corrosion products—arise from impurities. Three others—oxidative polymerization, asphaltene precipitation, and coke formation—arise from chemical reactions of constituents of the oil. Nevertheless, fouling in organic fluids is generally regarded as belonging primarily to chemical reaction fouling, but may be intrinsically related to other categories.

2.5 Chemical Reaction Fouling

Chemical reaction fouling was defined by Watkinson (1988) as a deposition process in which a chemical reaction either forms the deposit directly on a surface or is involved in forming precursors (or foulants) which subsequently become deposited. Unlike corrosion fouling, reaction does not take place with the wall itself. Reviews of chemical reaction fouling by organic fluids include those by Watkinson—Watkinson (1988), Watkinson (1992), Watkinson and Wilson (1997)—, by Crittenden (1988), and by Bott (1995).

Watkinson (1988) attributed chemical reaction fouling for organic fluids to three general classes of reactions: autoxidation, polymerization, and thermal decomposition. Other terms for thermal decomposition include thermolysis, pyrolysis, cracking, etc. A final polymerization step to form insolubles occurs in both autoxidation and thermal decomposition and, when precursors are already present, insolubles can be directly formed by polymerization. Although these reaction classes overlap in many fouling problems, at temperatures typical of thermal processes (i.e. $T \geq 350°C$), thermal decomposition becomes the predominant route in the production of fouling precursors.

2.5.1 Thermal Decomposition

Since coke formation from pitch and residuum involves the liquid phase and the gas phase, it is important to consider the reactions that can occur in both phases.

Reviews of carbon deposition from gas-phase pyrolysis have been given by Oblad et al. (1979) and by Albright et al. (1983). Coke is formed from light feedstocks such as methane, ethane, propylene, butadiene or medium cuts such as naphthas, which are pyrolyzed at temperatures over 700°C. The gas phase reactions result in formation of aromatics which then react to produce coke. The kinetics of possible thermal reactions of olefins has been reviewed by Albright et al. (1983) and by Sakai (1983). These systems are also discussed by Froment (1981) in his review of chemical reaction fouling. More recent information includes the works by Kumar and Kunzru (1987), Kopinke et al. (1993), and Huntrods et al. (1989). Also a survey of recent work in the light hydrocarbon pyrolysis area has been given by Bach et al. (1995) in which additional mechanisms for deposit formation in transfer line exchangers are given.

Pyrolysis reactions in the liquid phase occur from temperatures below 300–350°C on upwards. Accumulation of high molar mass species on heat transfer surfaces may be the result of degradation reactions followed by synthesis of high molecular weight compounds. Synthesis reactions include cyclization, aromatization and ring condensation. These observations have been described by Fitzer et al. (1971) in an extensive review of pyrolytic conversion of organic compounds related primarily to carbon or coke formation. Their schematic for the conversion of organic compounds to carbonaceous solids can be summarized as shown in Figure 2.2. The same authors pointed out that unsubstituted aromatics

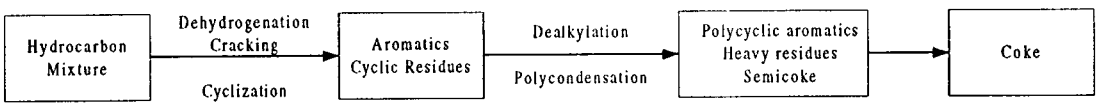

Figure 2.2: Schematic of Hydrocarbon Pyrolysis.

react by chemical condensation to produce polynuclear aromatics; anthracene was found very active as was also reported by Madison and Roberts (1958). These thermal decom-

position reactions proceed via free radical mechanisms and have also been discussed by Lewis (1980) who emphasizes thermal polymerization reactions for polynuclear aromatics.

2.5.2 The Role of Asphaltenes in Coke Deposition

Since petroleum residua are complex mixtures of thousands of compounds, the identification of specific fouling precursors involved in the reactions leading to coke deposition is not possible. For that matter, a common approach has been to separate residua and their reaction products into pseudocomponents by the use of solvents and then to identify the pathway for chemical change by the conversion of each pseudocomponent into others. One such pseudocomponent is the asphaltenes that are soluble in aromatic solvents (e.g. benzene, toluene) and insoluble in paraffinic solvents (e.g. *n*-pentane, *n*-heptane) and are high-molecular weight substances. Strausz et al. (1992) proposed a structure for asphaltene which was consistent with recent research and reported aromatic clusters with side chains and heteroatoms in its structure.

The predominant role of asphaltenes in crude oil fouling under nonoxidative conditions has been claimed by several authors including Murphy and Campbell (1992), Eaton and Lux (1984) and Dickakian and Seay (1988), although confusion remains about the role of the physical and chemical processes involved. Mechanisms for deposit formation by asphaltenes have also been given by Dickakian and Seay (1988), Eaton and Lux (1984) and by Lambourn and Durrieu (1983).

The residuum processing literature suggests some approaches for dealing with fouling and coke formation in processes such as those described in Section 2.3 (see e.g. Lott et al. (1996)). The thermal reactions of asphaltenes leading to coke formation under conditions typical of these processes have been discussed by many authors including Speight (1991), Trimm (1983), Lott et al. (1996) and have been recently reviewed by Asomaning (1997). Furthermore, an important model of residuum thermolysis based on asphaltene solubility and phase behaviour has been developed by Wiehe (1993).

2.6 Effects of Process Variables

2.6.1 Surface and Bulk Temperatures

The effect of surface temperature is certainly a critical factor in deposition processes which are chemically controlled and has been reviewed by Watkinson and Wilson (1997), Bott (1995), Crittenden (1988), and others. Since there may be several reactions leading to coke deposition, and given that selectivity may be a strong function of temperature, a simple dependence of fouling rate on temperature is not always exhibited. Nevertheless, several investigations—see e.g. Watkinson and Epstein (1969), Vranos et al. (1981), Braun (1977), Crittenden et al. (1987), Taylor (1969)—have shown that the initial fouling data can be correlated by an Arrhenius-type equation, i.e.

$$\dot{R}_f(0) \; \alpha \; exp\left(\frac{-E}{R \cdot T_s}\right) \tag{2.11}$$

where T_s is the surface temperature. Watkinson (1988) provides a summary of published activation energies.

The role of bulk temperature for fouling in which chemical reactions are involved must also be investigated. However, where bulk temperature effects have been studied, its effect, as opposed to that of wall temperature, has not been clarified as mentioned by Watkinson (1992).

2.6.2 Velocity

The effects of velocity on organic fouling at a fixed wall temperature are contradictory as described by Bott (1995), Watkinson (1992), and Crittenden (1988). It is generally accepted that the problem of hydrocarbon fouling can be reduced to some extent by the use of higher velocities and this idea is reinforced by TEMA (1978), which gives design fouling resistances that conform to this trend. However, many investigations discussed in the preceding articles—see e.g. Vranos et al. (1981), Crittenden et al. (1987)—do not agree with this result. This confusion may be attributed to the effects of velocity on heat and mass transfer which complicate the analysis to find the dominant effect. For example, if the fouling rate is solely controlled by a chemical reaction, then enhanced mass transfer

to the surface as a result of increasing the velocity will not change the situation. As well, increasing the velocity may reduce the wall temperature through the heat transfer coefficient thereby affecting the reaction kinetics of the deposition process. On the other hand, if the fouling process is mass-transfer controlled, an increase in velocity will result in an improved mass transfer, thereby promoting the deposition process.

2.7 Models of Chemical Reaction Fouling

As was shown in Sections 2.5 and 2.6, chemical reaction fouling is explained through chemistry and operating variables effects. As a result, understanding of chemical reaction fouling may require (Watkinson and Wilson (1997)):

1. Identification of the reactants and precursors;
2. Determination of the kinetics of reactions that form precursors; and
3. Determination of whether the solid fouling phase is initially formed in the bulk, in the thermal boundary layer, or on the heated surface.

A general multistep chemical reaction fouling model that can take into account the chemical and physical processes involved has been proposed by Watkinson and Wilson (1997)—see also Watkinson and Panchal (1993)—and is reproduced in Figure 2.3. Based on this

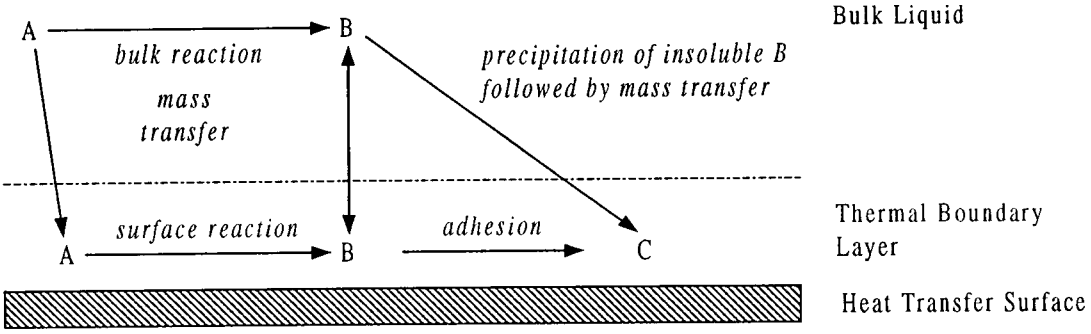

Figure 2.3: General multistep chemical reaction fouling mechanism where A is the soluble precursor, B is insoluble foulant and C is the deposit.

model, they have described several pathways leading to deposit formation. The critical issues discussed in the literature associated with modeling chemical reaction fouling and in this paper in particular, are bulk reaction versus surface reaction and adhesion or attachment versus mass transfer. This model has been used to visualize different controlling mechanisms.

2.8 Experimental Techniques in Thermal Fouling

According to Equations 2.5 and 2.6, we may measure fouling by thermal resistance R_f, deposit thickness, x_d, or mass per unit heat transfer area, m. Thermal fouling studies refer to cases in which the thermal fouling resistance is the primary response measured whereas in mass deposition studies, the fouling deposit is weighed. The experimental techniques used in fouling studies have been reviewed by Braun and Hausler (1976), subsequently by Knudsen (1981) and Fetissoff (1982), and more recently by Bott (1995).

Thermal fouling resistances may be obtained from laboratory studies and from plant data. In-plant measurements are useful but do not usually lend themselves to the degree of control necessary for acquiring reliable fouling data. Much of the literature associated with fouling of heat exchangers is based on laboratory work. However, laboratory data have also important shortcomings which have been discussed by Bott (1995). Because fouling in refinery exchangers can take weeks or months to reach significant levels, it is common practice in the laboratory to modify one or more of the operating parameters so that an accelerated test lasting only hours or days can be achieved. Thus, processes which may occur in industrial exchangers over periods of months are measured under more severe conditions over periods of days or weeks. The uncertainties introduced by using such an approach are undoubtedly worse in chemical reaction fouling than in the other types of fouling, since the nature of the reactions occurring and the selectivity to certain reaction products may be a strong function of conditions as stated by Watkinson (1988). Furthermore, in laboratory thermal fouling studies, recirculation of the process liquid is generally employed in order to use reasonable quantities of fluid. Recycle of the fluid across a simulated heat exchanger surface that is at a raised temperature may bring about permanent chemical changes in the fluid so that the fluid is no longer representative of

the process fluid. This phenomenon is particularly acute where chemical reaction fouling occurs.

Despite these concerns however and given the generally poor state of knowledge in chemical reaction fouling from residua, laboratory investigations can provide insights into fouling mechanisms and as such, give valuable data that may be useful in formulating models of fouling. It is also possible to study the effects of velocity and temperature on the fouling process that will be invaluable in the design and operation of full scale heat exchangers.

2.8.1 Fouling Surface Heating Techniques

Numerous methods for heating a fouling surface have been used in the past and have been discussed and described by Fetissoff (1982) and by others. However, none of them were suitable for reaching the high surface temperatures required for the present study. To address this issue, other kinds of devices were considered.

When the fouling process occurs inside a tube and is measured via an overall heat transfer coefficient, say U_o, representing several resistances in series (see Equation 2.4), it is crucial that U_o be sensitive to h_i in order to detect fouling. If the other resistances are large compared to the resistance inside the tube, the measurement of U_o will be insensitive to fouling inside. The fluidized bed was selected for the heating method because of the high temperature it can reach and of its well-known temperature uniformity that exists in both the radial and axial directions. Heat transfer coefficients in gas fluidized beds have been found to be considerably higher than in single-phase gas flow in an empty tube (see Gelperin and Einstein (1971)). Hence the fouling unit consisted of a vertical tube in a heated fluidized bed. The heavy oil flowed in the tube, and the bed was fluidized with air.

A quantitative value of the heat transfer coefficient between surface and bed is often required when dealing with fluidized beds—for example in estimating the surface temperature or the relative importance of the resistances involved as discussed above. In the present work, three tests were performed in which wall temperature measurements were obtained for this matter. In the following paragraphs, some calculation procedures for h_o

(see Equation 2.4) that have been reported in the literature and which are applicable to the fouling unit will be given and briefly discussed. It should be noted that these correlations are far from universal and most are limited to a narrow range of conditions because of the complex nature of fluidized contacting. Also, their predictions usually differ widely as stated by Grace (1982) who mentioned that the accuracy of several correlations should not be assumed to be better than ±50% within their ranges of application. Because the present work does not focus on heat transfer in a fluidized bed, a general background relevant to the system used is outside the scope of this thesis. A good summary of the principles involved with several references can be found in Kunii and Levenspiel (1991).

2.8.2 Heat Transfer Coefficient in a Bubbling Fluidized Bed

The hydrodynamic and thermal behavior of fluidized beds are commonly characterized by the powder classification scheme proposed by Geldart (1973) or by that of Saxena and Ganzha (1984), which is based on the Archimedes number defined by:

$$Ar = \frac{d_p^3 \; g \; \rho_g \; (\rho_p - \rho_g)}{\mu_g^2} \tag{2.12}$$

where g is the gravity constant and ρ_g and μ_g are the gas density and viscosity respectively. The sand used in the fouling unit belongs to Group B of Geldart's scheme which comprises particles of mean diameter, d_p, and density, ρ_p, lying in the range of 40 μm $< d_p <$500 μm, and 1400 kg/m^3 $< \rho_p <$ 4000 kg/m^3. Under the conditions studied in the present work, the sand used belongs to group I powders of Saxena and Ganzha (1984), which are defined by $3.55 \leq \text{Ar} \leq 21700$.

Numerous empirical and semiempirical formulae have been proposed for calculating heat transfer coefficients and they can be classified into two groups, one of which relates to the determination of the maximum heat transfer coefficient, h_{max}, and the other to the dependence of h on fluid velocity. Because of the shortcomings of these equations, a number of models have been developed to explain the mechanism of heat transfer in fluidized beds. The calculation procedures given below were selected based on their validity with the system used, which was characterized according to the above schemes, and on the availability of the parameters required in the equations. Previous reviews of

heat transfer in fluidized beds have been given by Gelperin and Einstein (1971), Grace (1982), Xavier and Davidson (1985), Baskakov (1985), and more recently by Saxena (1989).

Theoretical Studies

From his review, Saxena (1989) observed that the heat transfer rate from an immersed surface in a gas-fluidized bed depends upon a number of factors, such as the size, size range, shape, and properties of the bed particles; operating conditions, namely, temperature, pressure, fluidizing velocity, and properties of the gas; shape, size, surface finish, and orientation of the heat transfer surface; the relative size of the heat transfer surface and the fluidized bed; and on the design of the gas distributor plate.

Many models have been proposed to explain the mechanism of heat transfer (see e.g. Mickley and Fairbanks (1955), Bock and Molerus (1983), Martin (1984), etc.). However, the majority of them could not be applied to our system due to a lack of data required in the computations. The model developed by Kunii and Levenspiel (1991) was selected because it was general enough to account for many of the above factors and because of the availability of the information required.

They developed a general expression for the heat transfer coefficient between a bubbling fluidized bed and an exchanger surface. The expression accounts for the fact that part of the time the surface is bathed by gas and part of the time by emulsion packets:

$$h = (h_{bubble\ at\ surface}) \cdot \delta_w + (h_{emulsion\ at\ surface}) \cdot (1 - \delta_w) \tag{2.13}$$

where δ_w is the volume fraction of bubbles in the vicinity of the surface, and is equal to the time that the surface is bathed by bubbles. The bubble term represents the contributions of convection and radiation from the gas:

$$h_{bubble\ present} = (h_r + h_g) \tag{2.14}$$

When the emulsion packet is present on the surface, the heat transfer occurs in series—at the wall region followed by transfer at the emulsion packet. In addition, both convection

and radiation occur throughout the wall region. Combining all of the above terms yields:

$$h = [\delta_w \cdot (h_r + h_g)]_{bubble\ at\ surface} + \left[\frac{1-\delta_w}{\frac{1}{h_r+h_w} + \frac{1}{h_{packet}}}\right]_{emulsion\ at\ surface} \tag{2.15}$$

This model has been applied with success for both horizontal and vertical tubes (see Kunii and Levenspiel (1991) for more details about the different terms of Equation 2.15).

Empirical and Semiempirical Correlations

The theories and mechanisms that have been proposed, such as the one outlined above, show the general features of bed-to-surface heat transfer in gas-fluidized beds and the importance of different variables. However, despite the elaboration of a number of mechanistic models, empirical and semiempirical correlations are still the most common means for predicting heat transfer rates (Grace (1982)). Experts in the field (see e.g. Botterill and Hawkes (1989)) prefer empirical equations such as the one given by Zabrodsky et al. (1976).

The heat transfer coefficient for an immersed surface in a gas-fluidized bed of systems belonging to groups I and IIA will depend upon the orientation of the surface with the flow of gas in the fluidized bed (Saxena (1989)). Experimental investigations of h for vertical tubes are relatively more scarce than for horizontal tubes, as reviewed by Saxena (1989).

One of the best-known correlation for heat transfer to a single vertical unfinned tube positioned on the axis of a cylindrical column is that due to Vreedenburg (1960), who obtained:

$$\frac{h(D_v - D_o)}{k_g}\left(\frac{D_o}{D_v}\frac{d_p}{(D_v - D_o)}\frac{k_g}{\mu_g\ c_g}\right)^{1/3} = 0.105 \times 10^{-3}\left(\frac{G(D_v - D_o)}{\rho_g(d_p^3\ g)^{1/2}}\right)^2 \tag{2.16}$$

where D_v is the bed diameter, k_g is the gas thermal conductivity, and c_g is the gas heat capacity. This equation is valid for $(G\ d_p\ \rho_p/\rho_g\ \mu_g) > 2.5 \times 10^3$ and $G(D_v - D_o)/\rho_g\ d_p^{3/2}\ g^{1/2} < 1070$. According to a review of Saxena (1989), the correlations by Vreedenburg (1960) reproduced the available experimental data within $\pm 100\%$. However, these do not predict a maximum in the plot of h versus superficial mass fluidizing velocity, G, as was found in the experiments.

Borodulya et al. (1980) reported h data for an 18-mm vertical heat transfer probe immersed in a 45-cm deep and 10.5-cm diameter fluidized beds of quartz sand (d_p=126–1220 μm. They proposed:

$$Nu_p = 0.96\ Re^{0.71}\ Pr^{0.31} \tag{2.17}$$

for $Re < 20$. The agreement of experimental data of Verma and Saxena (1983) with the predictions of Equation 2.17 was considered inadequate.

The following dimensionless correlation given by Wender and Cooper (1958) has also been widely used:

$$\frac{h\ d_p}{k_g(1-\epsilon)}\left(\frac{k_g}{c_g\ \rho_g}\right)^{0.43} = 3.5\times 10^{-4}\ C_R\left(\frac{d_p\ G}{\mu_g}\right)^{0.23}\left(\frac{c_p}{c_g}\right)^{0.8}\left(\frac{\rho_p}{\rho_g}\right)^{0.66} \tag{2.18}$$

for $0.01 < (d_p\ G/\mu_g) < 100$. In Equation 2.18, C_R is a correction factor and is unity if tube is in the center of the fluid bed, ϵ is the bed voidage, and c_p is the particle heat capacity. An average deviation of $\pm 20\%$ was found for the 323 data points used to develop this expression. Saxena (1989) found that this correlation reproduced their data best and was recommended as being about the best.

The following recent correlation to predict h has been given by Molerus et al. (1995) in the intermediate range of $10^2 < Ar < 10^5$:

$$\begin{aligned}
\frac{hl_l}{k_g} &= \frac{0.125(1-\epsilon_{mf})\left(1+33.3\left\{\left[\frac{U-U_{mf}}{U_{mf}}\right]^{1/3}\left(\frac{\rho_p c_p}{k_g g}\right)^{1/3}(U-U_{mf})\right\}^{-1}\right)^{-1}}{1+\left(\frac{k_g}{2c_p\mu_g}\right)\left\{1+0.28(1-\epsilon_{mf})^2\left[\frac{\rho_g}{\rho_p-\rho_g}\right]^{0.5}\left[\left(\frac{\rho_p c_p}{k_g g}\right)^{1/3}(U-U_{mf})\right]^2\frac{U_{mf}}{U-U_{mf}}\right\}} \\
&\quad +0.165\ Pr^{1/3}\left(\frac{\rho_g}{\rho_p-\rho_g}\right)^{1/3}\left[1+0.05\left(\frac{U-U_{mf}}{U_{mf}}\right)^{-1}\right]^{-1} \\
l_l &\equiv \left[\frac{\mu_g}{g^{0.5}(\rho_p-\rho_g)}\right]^{2/3}
\end{aligned} \tag{2.19}$$

where U is the gas superficial velocity and the subscript mf denotes minimum fluidization conditions. The correctness of the prediction was tested by comparison with more than 20 measurements covering a relatively wide range of system data and operational conditions. The accuracy of the deduced correlation was judged excellent.

Maximum Heat Transfer Coefficient

The correlation of Zabrodsky et al. (1976) covers a relatively broad range of data, including beds operated at high temperature and may be applied for vertical or horizontal tubes or for transfer to the external wall:

$$Nu_{max} = \frac{h_{max}\ d_p}{k_g} = 0.88\ Ar^{0.213} \qquad 10^2 < Ar < 2 \times 10^5 \tag{2.20}$$

A similar correlation has also been given previously by Varygin and Martyushin (1959):

$$Nu_{max} = \frac{h_{max}\ d_p}{k_g} = 0.86\ Ar^{0.2} \qquad 30 < Ar < 1.35 \times 10^5 \tag{2.21}$$

The following correlations have also been given to predict experimental data:

- Grewal and Saxena (1981):

$$Nu_{max} = 0.9\ (0.0127\ Ar/D_o)^{0.21}(c_p/c_g)^{0.2} \qquad 75 < Ar < 2 \times 10^4 \tag{2.22}$$

- Denloye and Botterill (1978):

$$Nu_{max} = 0.843\ Ar^{0.15} + 0.86\ Ar^{0.39} d_p^{0.5} \qquad 10^3 < Ar < 2 \times 10^6 \tag{2.23}$$

- Molerus and Mattmann (1992):

$$Nu_{max} = \frac{5}{\left(1 + \frac{k_g}{2c_p\mu_g}\right)} + 0.146\ (Ar\ Pr)^{1/3} \qquad 10^2 < Ar < 2 \times 10^5 \tag{2.24}$$

Mathur et al. (1986) have compared some of the above correlations with experimental data of 13 different workers comprising 86 data points and a brief summary of their comments is given in Saxena (1989). The percentage deviations between experimental and predicted values, based on the correlation of Zabrodsky et al. (1976), range between the limits of -34.5% and 59.6% with a root-mean-square deviation of 25.1%. Equation 2.20 predicts 90% of the data points within ±35%. On the other hand, most of the 86 data points were underpredicted by the correlation of Varygin and Martyushin (1959). The deviations range between -46.9% and 12.6% with a root-mean-square of 19.4%. The correlation of Denloye and Botterill (1978) was also found to underpredict all the data points; the deviations were about -10% to -55%. Finally, comparison of 61 experimental points with prediction by Molerus and Mattmann (1992) suggested that an excellent estimate can be expected from Equation 2.24.

Chapter 3

Characterization of Feed Materials

3.1 Properties of Fluids

The deposition of coke-like materials was studied by recirculating through the fouling unit a blend of pitch and coker heavy gas oil (52%wt. pitch-48%wt. CHGO or 50:50%vol. under ambient conditions). These fluids were supplied by Syncrude Canada Ltd. and are typical of the streams associated with their coking units. Some characteristics of these fluids provided by Syncrude Ltd. are given in Table B.1. The high temperature simulated distillation TBP curve for coker heavy gas oil is given in Figure B.1. Note that whenever the term '52%wt. pitch mixture' is used, the balance is CHGO.

Other tests were done with a blend of fuel oil (75%wt. FO), Cold Lake heavy oil (10%wt. HO), and de-asphalted oil (15%wt. DAO) to evaluate the capability of the unit to detect fouling by thermal measurement. This blend was chosen because of the high fouling rates measured when recirculated in another fouling unit. The composition and properties of these fluids are reported in Table B.2.

3.2 Density

Density is a fundamental physical property used to characterize bitumen and is required as an input in many process calculations. In this section, the density measurements on the 52%wt. pitch blend are presented. Also, density-temperature equations are derived to model the variation of density with temperature for other blends of pitch and CHGO.

3.2.1 Density of 52%wt. Pitch–48%wt. CHGO Blend

Several standardized procedures issued by the American Society for Testing and Materials can be used for determining the density of bituminous materials (Lu (1989)). The density

of the 52%wt. pitch blend was measured by use of a pycnometer according to the standard designated as ASTM D70 using a constant-temperature bath Model 1130-2 from VWR Scientific which was filled with mineral oil. In this method, due to the high viscosity of the materials involved, the pycnometer is partially filled with the mixture and water is normally added to fill it completely. For this work, since densities at temperatures higher than 100°C were desired, a mineral oil from Fischer Co. (same as in the constant-temperature bath) for use up to 176°C was used instead of water for all the density measurements. The pycnometer was first calibrated with water in a water bath at several temperatures up to 89°C and a constant volume of 27.560 cm^3 was found. The densities of mineral oil and of the 52%wt. pitch mixture were measured between 60 and 145°C and the following linear relationships were fitted:

$$\rho_{T,m.oil} = 866.7 - 0.621 \cdot T \tag{3.1}$$

$$\rho_{T,52\%} = 1042.4 - 0.621 \cdot T \tag{3.2}$$

The results are shown in Figure 3.1 with the fitted lines.

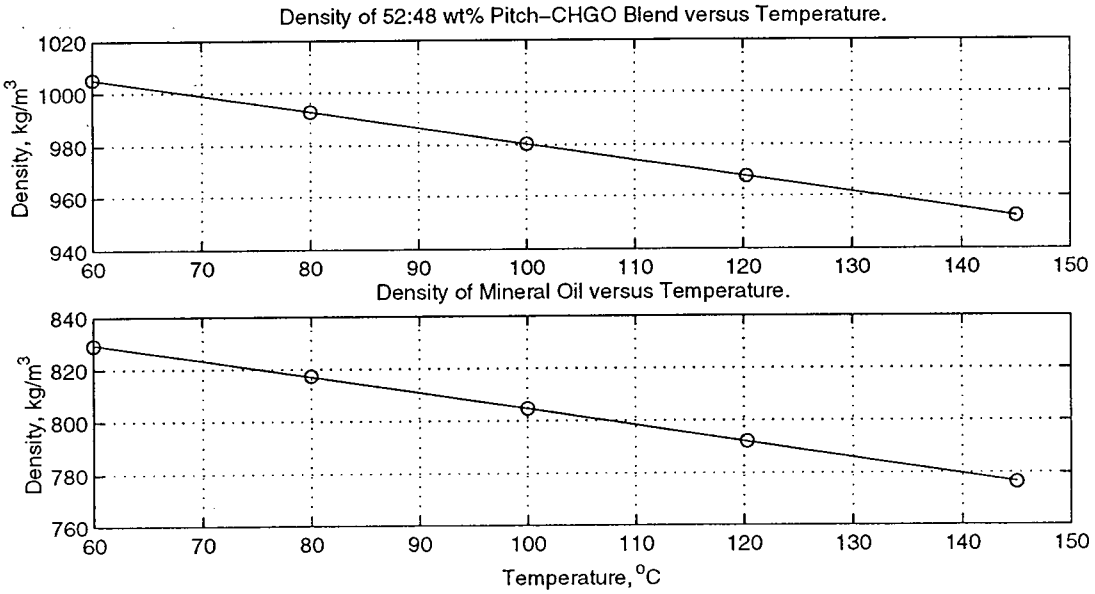

Figure 3.1: Density of mineral oil and of 52%wt. pitch blend.

3.2.2 Generalization of Results

The data of Bulkowski and Prill (1978) on four Athabasca bitumen samples with different treatment histories in the 0 to 150°C temperature range were reported by Lu (1989). They developed the following linear relationship between temperature and density:

$$\rho_{T,j} = \rho_{T^\circ,j} - A \cdot T \tag{3.3}$$

In this equation, ρ_T and ρ_{T° refer to the densities in kg/m^3 at temperatures T and T° (=0°C) respectively. The constant A was assigned a value of 0.62 °C^{-1}, which is the same as the constant derived from our measurements (see Equation 3.2). Furthermore, the densities measured by Polikar (1980)—as reported by Lu (1989)—in the temperature range 0°C to 260°C for bitumen extracted from high-grade Athabasca oil sands can also be represented by Equation 3.3 with A=0.62 °C^{-1}. Based on these findings, a value of A of 0.62°C^{-1} was assumed for any blend of pitch and CHGO. The intercepts for pitch and CHGO, $\rho_{T^\circ,pitch}$ and $\rho_{T^\circ,CHGO}$, were found based on the knowledge of their densities at 25°C. The parameters are summarized in Table 3.1 for pitch, CHGO, 52% wt. pitch blend, mineral oil from this work and Athabasca bitumen from Bulkowski and Prill (1978). The 95% confidence interval is given for the 52%wt. pitch mixture and for mineral oil. The densities of any blend of pitch and CHGO at a given temperature can then be estimated from the following mixing rule using Equation 3.3 for component densities:

$$\rho_{T,m} = x_p \cdot \rho_{T,p} + (1 - x_p) \cdot \rho_{T,CHGO} \tag{3.4}$$

For the 52%wt. pitch mixture, the deviation between the predicted and the measured densities is 1% over the temperature range 60–145°C.

Table 3.1: Summary of Parameters in Equation 3.3

Fluid	ρ_{T° (kg/m^3)	A (°C^{-1})	Source
Pitch	1086.8	0.62	Syncrude
CHGO	975.0	0.62	Syncrude
52%wt. pitch	1042.4±0.6	0.621±0.005	Present work
Mineral Oil	866.7±1.4	0.62±0.01	Present work
Athabasca	1025	0.62	Lu (1989)

3.3 Viscosity

Viscosity is the property of a fluid that measures resistance to movement of adjacent fluid layers (Miadonye and Puttagunta (1996)). For Newtonian fluids, viscosity is defined as the measure of the internal fluid friction, which is the constant of proportionality between the shear stress at any point and the velocity gradient (Tassios and Goletz Jr. (1977)). In the literature, absolute viscosity is generally symbolized by μ and kinematic viscosity is denoted by ν and this common practice has been adopted in this chapter. Conversion from one to the other is obtained through the following relation:

$$\nu = \frac{\mu}{\rho} \tag{3.5}$$

A knowledge of the viscosity is essential for fluid flow and heat transfer calculations inherent to this project. Although many calculation procedures for bitumen and heavy oil viscosity have been presented in the literature, most of them are not applicable to the fluids studied here. Some of them are based on parameters such as boiling points, molecular weight, specific gravity, and accentric factors which are not available for pitch and CHGO. Also, most of the available data used to derive or to evaluate these procedures have been measured at temperatures lower than 200°C on lighter fractions than CHGO and pitch. Therefore, given the very high sensitivity of the viscosity of heavy fractions of petroleum to temperature change, extremely large errors are bound to occur when extrapolating to temperatures in the range 300–350°C where the fouling runs were carried out.

Although measurements were obviously needed, the determination of viscosity of highly viscous materials handled at such high temperatures is difficult as explained by Miadonye and Puttagunta (1996). In Section 3.3.1, new data are presented for the effect of temperature on the viscosity of pitch, CHGO, and their blends in the temperature range of 80–340°C. Modeling of the data was attempted and the results are given and discussed in Section 3.4.

3.3.1 High Temperature Viscosity Measurements

The viscosity data were obtained at atmospheric pressure using a Rotovisco RV12 from Haake Co. using the viscosity sensor system MV 400 I. This sensor system was designed

for viscosity measurements from -60°C to 300°C and could be used with or without an inert gas cover. It consisted of a rotor and cup which were surrounded by an electronically controlled metal block heater, and temperature control was maintained by means of a thermistor control TP24 from Haake Co..

For a Newtonian fluid in the absence of turbulence, the rate of shear D (s^{-1}) is directly proportional to the shear stress τ (mPa) and the viscosity is defined by the Newton equation:

$$\mu = \frac{\tau}{D} = K\frac{S}{n} \tag{3.6}$$

During each test, the value of the torque S is plotted against a series of preset test rotational speeds n and the viscosity is obtained by multiplying the slope by an 'instrument factor' K, specific to each drive unit and sensor system. The calibration was carried out with a standard liquid of known viscosity and the factory calibration factor K=1374 (mPa·s/scale grad.·min.) was confirmed. More details on the equipment and proper measuring procedure can be found in the Haake Rotovisco Instruction Manual.

All measurements generated linear $n - S$ diagrams (see Figure 3.2), indicating Newtonian fluids. This result is consistent with the literature since bitumen is generally regarded

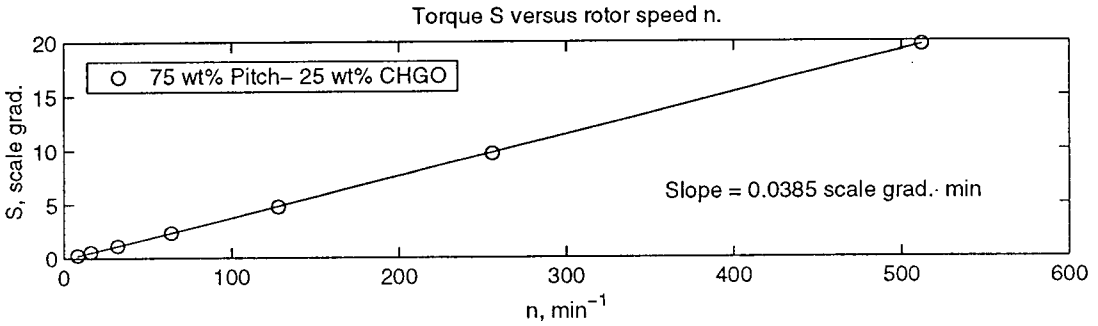

Figure 3.2: A Typical n-S Diagram (T = 190°C).

as a Newtonian fluid (Miadonye and Puttagunta (1996)). Table 3.2 contains the detailed viscosity-temperature data and all of the viscosities are plotted against temperature in Figure 3.3. The kinematic viscosities were obtained from Equation 3.5 by using density relationships established in Section 3.2.

Table 3.2: Dynamic viscosity (mPa·s)-temperature data for pitch, CHGO, and their blends.

Temperature	%wt. pitch				
°C	0	25	51.7	75	100
80.0	25.9	130.9	1187	19116	-
100.0	12.7	52.2	340.0	3429	-
110.0	-	-	-	-	43462
120.0	-	-	-	-	17727
128.0	6.1	-	-	-	-
130.0	-	18.6	85.0	519.6	7581
160.0	3.3	9.1	32.2	134.6	1129
190.0	2.9	5.1	16.3	52.6	300.9
220.0	-	3.2	9.6	24.9	106.5
250.0	-	2.9	6.7	14.6	49.1
260.0	2.4	-	-	-	-
280.0	-	2.6	4.9	9.3	27.4
290.0	2.1	-	-	-	-
310.0	-	2.4	3.9	6.5	15.9
340.0	-	-	-	4.0	10.4

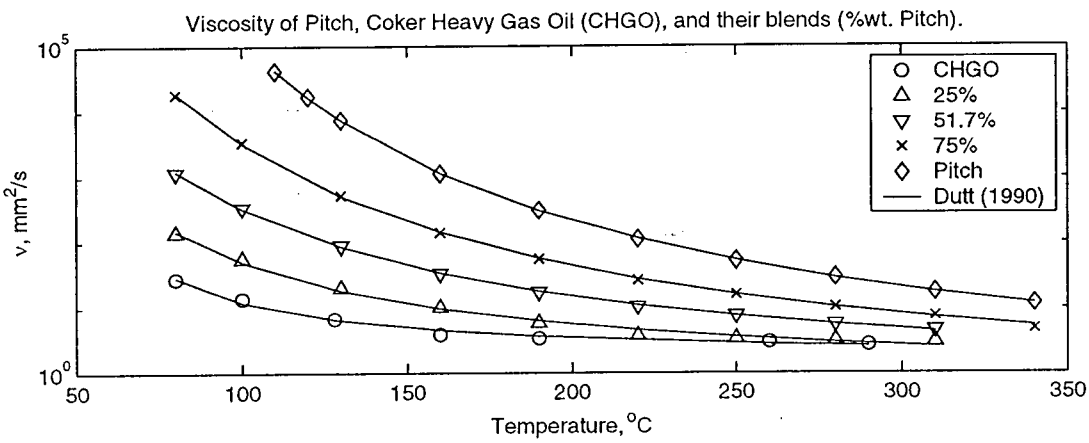

Figure 3.3: Kinematic viscosity-temperature data; fitted lines obtained using Dutt's (1990) equation and parameters given in Table 3.4.

3.4 Modelling Viscosity Data

The viscosity prediction of pitch, CHGO, and their blends based on some readily available characterization would be most convenient. Reviews of viscosity correlations and calculation methods for the viscosity of petroleum liquids have been given by Mehrotra et al. (1996) and Miadonye and Puttagunta (1996). Due to the complicated and undefined nature of heavy petroleum liquids, their viscosity is usually calculated from semi-empirical models or empirical equations. Most semi-theoretical models for liquid petroleums are based either on the corresponding state approach or on the modified Chapman-Enskog theory. These methods require boiling points and therefore can not be applied to heavy oils and pitch which, unlike light crude oils, cannot be distilled completely (Miadonye and Puttagunta (1996)). Also, in the corresponding state approach, the MW, SG, and NBP for each of the pseudo components characterizing the whole heavy petroleum liquid must be available for calculating critical parameters (T_c, P_c, V_c) and the accentric factor. This is not the case with CHGO and pitch.

Empirical methods make use of the many relationships that have been proposed to correlate viscosity and temperature and, in few cases, the parameters have been generalized. However, the parameters are essentially expressed in terms of average boiling points which are not available for pitch and blends with CHGO. This prevents the application of those methods or similar generalizations of parameters.

The objective of this work was to develop an estimation method for the correlation and prediction of the viscosity of the fluids studied based on the experimental data obtained and other available information.

3.4.1 Evaluating Empirical Equations

The first step in modeling was to find an equation that would correlate reasonably well the viscosity data over the whole measurement temperature range and for all the components and blends. For that purpose, several empirical equations previously used for viscosity modeling (Miadonye and Puttagunta (1996)) were tested and some of them are summarized in Table 3.3. The constants were regressed in all the equations and are listed

in Table 3.4.

Throughout the literature, the criterion for evaluating the adequacy of a viscosity calculation procedure is the average absolute deviation (AAD) defined as:

$$AAD = 100 \times \frac{1}{N} \sum_{i=1}^{N} \mid \mu_{exp} - \mu_{corr} \mid / \mu_{exp} \tag{3.7}$$

Table 3.3: Summary of Some of the Viscosity Correlations Tested

Author(s)	Equation	Comments
Dutt	$ln\nu = A + \frac{B}{T+C}$	ν is viscosity in mm^2/s, T in °C
Dutt Mixture	$ln\nu_m = \sum_{j=1}^{n} x_j \, ln\nu_j$	x_j is the mass fraction of component j
Herschel	$log\mu = A + B \, logT$	T in °F, μ in poise, A and B are constants
Litovitz	$\mu = A \, exp\left(\frac{a}{RT^3}\right)$	μ in mPa-s, T in K, A is a constant, R is the gas constant, a is activation energy
Mehrotra	$log \, log(\mu + 0.7) = b_1 + b_2 \, logT$	μ in mPa-s, T in K, b_1 and b_2 are constants
Mehrotra Mixture	$log(\mu_m + 0.7) = \sum_{j=1}^{n} x_j \, log(\mu_j + 0.7)$	x_j is the mass fraction of component j
Vogel	$ln\mu = A\left(\frac{-1}{B} + \frac{1}{T+C}\right)$	μ in mPa-s, T in K
Puttagunta	$log\mu = \frac{b}{\left(1+\frac{T-30}{303.15}\right)^s} + C$ C=-3.002; b=log$\mu_{30°C}$ - C s=0.0066940 b + 3.5364	μ in Pa-s, T in °C
Andrade	$ln\nu = lnA + \left(\frac{B}{T}\right)$	ν in mm^2/s, T in °C,
Andrade Gen.	A=-0.4004 $\%wt_p^2$ + 0.2699 $\%wt_p$ + 0.9204 B=803 $\%wt_p^2$ + 226.33 $\%wt_p$ + 287.86	$R^2 = 1$ $R^2 = 0.9937$

Table 3.4: Constants Regressed in the Viscosity Correlations Tested

	%wt. pitch	0	25	51.7	75	100
Vogel	A	185.6	279.3	488.5	671.5	863.9
	B	942341	942341	942341	942341	942341
	C	-296.8	-297.9	-286.1	-287.3	-304.4
Herschel	A	-2.099	-3.387	-4.924	-6.369	-8.094
	B	3.962	7.559	11.976	16.3	21.516
Litovitz	ln A	-0.255	-0.574	-0.389	-0.522	-0.390
	a	1.199E+09	194E+09	2.687E+09	3.75E+09	5.11E+09
Dutt	A	0.359	-0.597	-1.084	-1.840	-1.951
	B	147.2	475.1	851.7	1299.8	1565.0
	C	-31.267	5.087	23.802	30.872	13.870
Puttagunta	$\mu_{30°C}$ (Pa-s)	0.27067	4.44142	202.10	25312.95	63353826
Mehrotra	b_1	6.1121	8.1486	8.3472	8.9351	8.8042
	b_2	-2.3667	-3.0850	-3.0917	-3.2613	-3.1528
Andrade	ln A	-0.0831	-0.4896	-0.3937	-0.7095	-1.3843
	B	266.0	440.3	613.2	872.0	1337.0

The criterion was computed for all equations applied to each oil fraction. It is shown in Table 3.5 with the average deviation for each method. In the following paragraphs, each of them will be discussed.

- ASTM or Walther Equation

Mehrotra et al. (1989) applied the double-log equation to correlate the viscosity of Cold Lake bitumen and its fractions and the two parameters, b_1 and b_2, were related to the molar mass. They reported overall AADs within 6%. This is consistent with the AAD results for pitch and 75%wt. pitch mixture. Also, Mehrotra et al. (1989) applied a linear regression to their data for CL bitumen and the results are shown in Figure 3.4 along with the results obtained in this work. The measurement temperature range (°C) is indicated. Over the whole measurement temperature range for our results, the parameters obtained for pitch and 75%wt. pitch blend are close to the values they reported for Cut 5. However, as the pitch content decreases, the fit becomes unacceptable as indicated in Table 3.5 and

Table 3.5: Average Absolute Deviation (AAD) for Correlations Tested

Equation	%wt. pitch					Average
	0	25	51.7	75	100	
Vogel	7.7	18.6	19.1	34.9	23.6	20.8
Mehrotra	24.3	17.7	9.7	6.2	6.2	12.8
Mehrotra Mixture	n/a	69.4	57.7	60.8	n/a	62.6
Dutt	8.5	10.0	3.0	4.0	1.4	5.4
Generalization 1	29.0	36.4	18.1	7.3	12.3	20.6
Generalization 2	10.4	10.7	9.3	7.2	20.6	11.7
Generalization 3	12.3	17.8	4.0	8.6	3.8	9.3
Dutt Mixture	n/a	55.2	47.9	52.6	n/a	51.9
Puttagunta	19.2	13.9	8.7	14.4	22.3	15.7
Litovitz	18.5	12.6	7.6	7.9	7.6	10.8
Herschel	26.4	25.5	24.1	34.4	33.5	28.8
Andrade	12.7	10.4	8.8	16.5	4.7	10.6
Andrade Gen.	21.5	15.5	9.2	28.9	10.6	17.1

the parameters deviate significantly from the range of values they reported. Now, the maximum measurement temperature for their heaviest cut was 210°C and around 100°C for the lighter cuts. When the correlation is applied to our data up to 220°C for 52 and 25%wt. pitch mixtures and up to 160°C for CHGO, the AADs become within the values they reported. Also, all the regressed parameters become consistent with their results. It

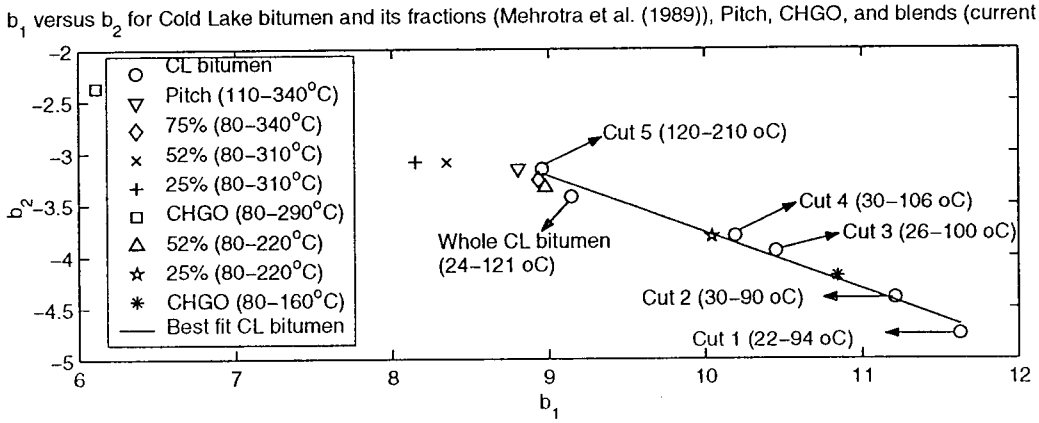

Figure 3.4: Parameters b_1 and b_2 from Mehrotra et al. (1989) and from this work.

is suggested that the double-log equation can only be applied to heavy cuts such as pitch and the 75%wt. pitch blend over the full temperature range involved; for lighter fractions, the correlation should not be used over the full temperature range and for extrapolation.

Puttagunta et al. (1993) proposed a correlation which was shown by Mehrotra (1994) to be essentially the Walther equation. The correlation requires one viscosity data point at 30°C and was found by iteration for each oil fraction. As shown in Table 3.4, the viscosity at this temperature is extremely high for fractions with high pitch content and the AADs show that the correlation is not well suited for the data. Furthermore, no compositional dependence or mixing rule is provided, implying that one viscosity datum is required for every new mixture (Mehrotra et al. (1996)).

• Andrade and Vogel Equations

Allan and Teja (1991) calculated the viscosity of several crude oil fractions with AADs of 5–15% by using their Effective Carbon Number (ECN) approach to estimate the coefficients in the Vogel equation. However, Gregory (1992) showed that the method gives an incorrect viscosity-temperature trend for ECN>22. Since the ECN values for the fluids studied were found greater than 22 and given the AADs obtained (see Table 3.5), this form of the Vogel equation should not be used.

The Andrade equation was applied to model the kinematic viscosity of several crude oil fractions by Amin and Maddox (1980) and Beg et al. (1988); overall AADs between 5.5% and 11.1% were obtained. An average AAD of 10.6% was obtained for our data but the parameters could not be generalized. Also, Mehrotra and Svrcek (1988) showed that an Andrade-type equation was inadequate to model the effect of temperature on the viscosity of bitumens.

Dutt (1990) applied the Vogel equation to model the kinematic viscosity of crude oil fractions using the 50% boiling point as the only input. With parameter C obtained as per Tassios and Goletz Jr. (1977) and parameters A and B generalized, overall AADs between 3.8% to 6.8% were obtained. The method was applied to CHGO using the SIMDIST curve (see Figure B.1), but the data could not be fitted linearly. Also, the regressed constant C for CHGO in Table 3.4 did not predict the 50% boiling point based on the Goletz-Tassios equation. Note that a SIMDIST curve was not available for pitch as is usually the case

for cuts having very few constituents with BP<550°C (Mehrotra et al. (1989)).

However, by fitting to the data the equation used by Dutt, the best average AAD of 5.4% was obtained with a maximum of 10% as indicated in Table 3.5. The parameters could also be generalized as will be shown later. The correlated viscosities are shown as smooth curves in Figure 3.3.

• Other Correlations

The correlations by Herschel (1922) and by Litovitz (1952) were not retained as suitable equations for modeling the viscosity of pitch, CHGO, and their blends. Although the Litovitz equation gave an average AAD of 10.8%, the parameters could not be generalized.

3.4.2 Mixture Viscosity Equations

Several liquid-mixture viscosity correlations are available for calculating the viscosity from the component viscosity data. Some of them require viscous interaction terms and are not applicable to bitumen fractions (Mehrotra et al. (1989)). Most of the simple correlations for liquid-mixture viscosity can be generalized (Reid et al. (1977)) as:

$$f(\mu_m) = \sum_{j=1}^{n} x_j f(\mu_j) \tag{3.8}$$

where $f(\mu)$ may be (μ), $(1/\mu)$, $ln(\mu)$, $log(\mu)$, etc., and x_j may be either of the liquid volume, mass or mole fraction.

An equation proposed by Mehrotra et al. (1989) was applied to the calculated viscosities from the double-log equation. A similar approach was used with the Vogel equation (Dutt (1990)). In both cases, the AADs were extremely high as seen in Table 3.5 and the approach was abandoned. The results achieved by Mehrotra et al. (1989) were also in that range.

3.4.3 Generalization of Parameters

A generalization of parameters was attempted with the Andrade and Dutt equations. The results were more successful with the correlation used by Dutt (1990) as shown in Table 3.5. Several generalizations were performed and they are summarized in Table 3.6.

The best fits for parameters B and C were obtained with linear and quadratic functions of the weight fraction of pitch, respectively. This was the only characterization parameter available for generalization. For parameter A, the lowest average AAD of 9.3% was achieved with the third generalization, although the second generalization gave slightly lower AADs for CHGO and the 25%wt. pitch blend. The following model is therefore recommended for the viscosity prediction of CHGO, pitch, and any blend of the two, especially for those with a high pitch content:

$$ln\nu = A + \frac{B}{T+C} \tag{3.9}$$

$$A = -0.1885 \cdot (lnB)^2 + 1.3342 \cdot lnB - 1.6161 \tag{3.10}$$

$$B = 1463.08 \cdot x_p + 131.2386 \tag{3.11}$$

$$C = -133.56 \cdot x_p^2 + 179.93 \cdot x_p - 31.56 \tag{3.12}$$

Here x_p refers to the weight fraction of pitch, T is in °C, and ν is in mm^2/s. This model covers a wide temperature range—up to 340°C—and accounts for the compositional effect. Figure 3.5 shows how well the data are fitted using these generalized parameters.

Table 3.6: Generalization of Parameters in Dutt Correlation.

Generalization	Equation	Comments
1	A=-2.3458·x_p+0.1584	R^2=0.950
	B=1463.08·x_p+131.2386	R^2=0.994
	C=-133.5612·x_p^2 +179.93·x_p -31.56	R^2=0.995
2	A=-0.9386·lnB+5.0524	R^2=0.958
3	A=-0.1885·(lnB)^2+1.3342·lnB-1.6101	R^2=0.993

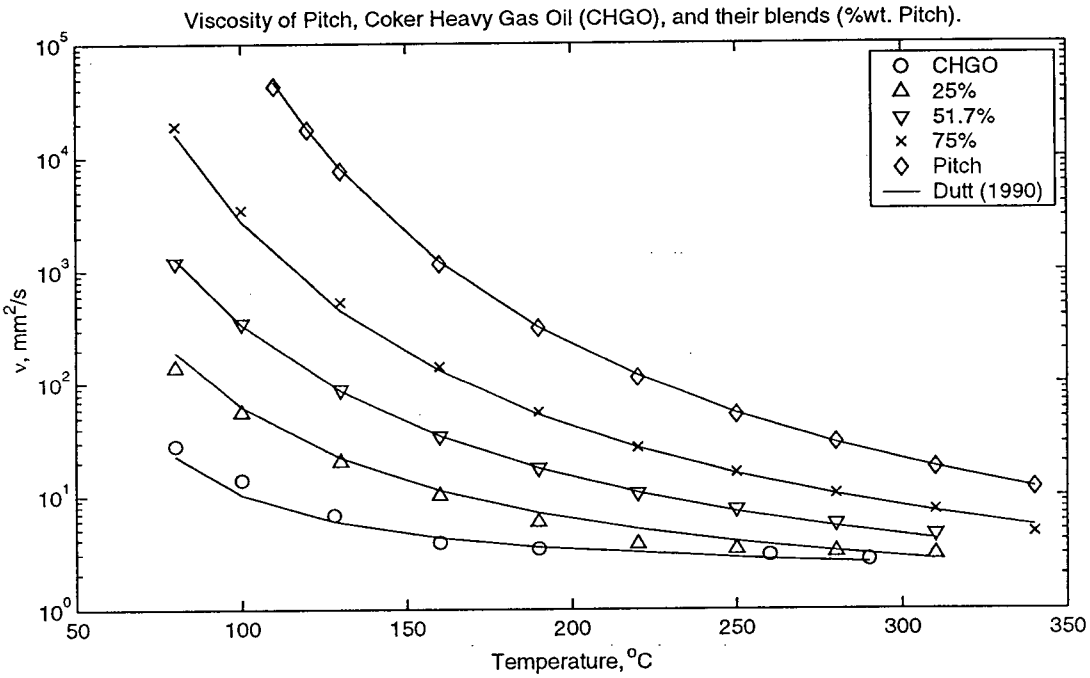

Figure 3.5: Kinematic viscosity-temperature data; fitted lines obtained with Equations 3.9 to 3.12.

Chapter 4

Development and Operation of the Fouling Unit

4.1 Original Apparatus

Initial experiments were performed with the recycle flow loop shown in Figure 4.1 which had been designed and installed by others (see Yue and Watkinson (1998)). The test fluid was kept at a constant temperature in a 2.5 L stainless steel stirred tank and heated by two ceramic elements. A gear pump for high temperature (Viking pump series 115, model G115, capacity of 1.8 USGPM at 20 psi) driven by a 1/2 HP, 1750 RPM electric motor pumped liquid through a test section consisting of a 1.10 m long vertically mounted 1/4 in. O.D. stainless steel tube (0.5334 mm I.D.). The test section was heated externally over 0.46 m of its length by a quartz sand fluidized bed surrounded by two ceramic heaters. After being heated during upflow in the test section, the test fluid returned to the tank supply. When necessary, a water cooler was used to avoid temperature build-up, and an in-line filter could be used for suspended solids removal. The first bypass configuration included a pressure relief valve and a needle valve in series to prevent eventual pressure build up (e.g. in case of blockage) and to allow the excess flow to return to the tank.

The first tests and experiments carried out made it clear that the original design could not properly handle the viscous fluids studied nor reach the desired temperature conditions, and it exhibited several fluctuations that made the analysis of the results difficult. Also, the design did not permit convenient verification of the flowrate and, given the nature of these experiments, safety and data monitoring were inadequate.

Therefore, instead of studying the effect of process variables on fouling, most of the experimental work in this project has been devoted to improving the unit and evaluating its ability to generate fouling results. Several equipment malfunctions such as two pump failures and breakage of the fluidized bed heating system required rebuilding of parts of

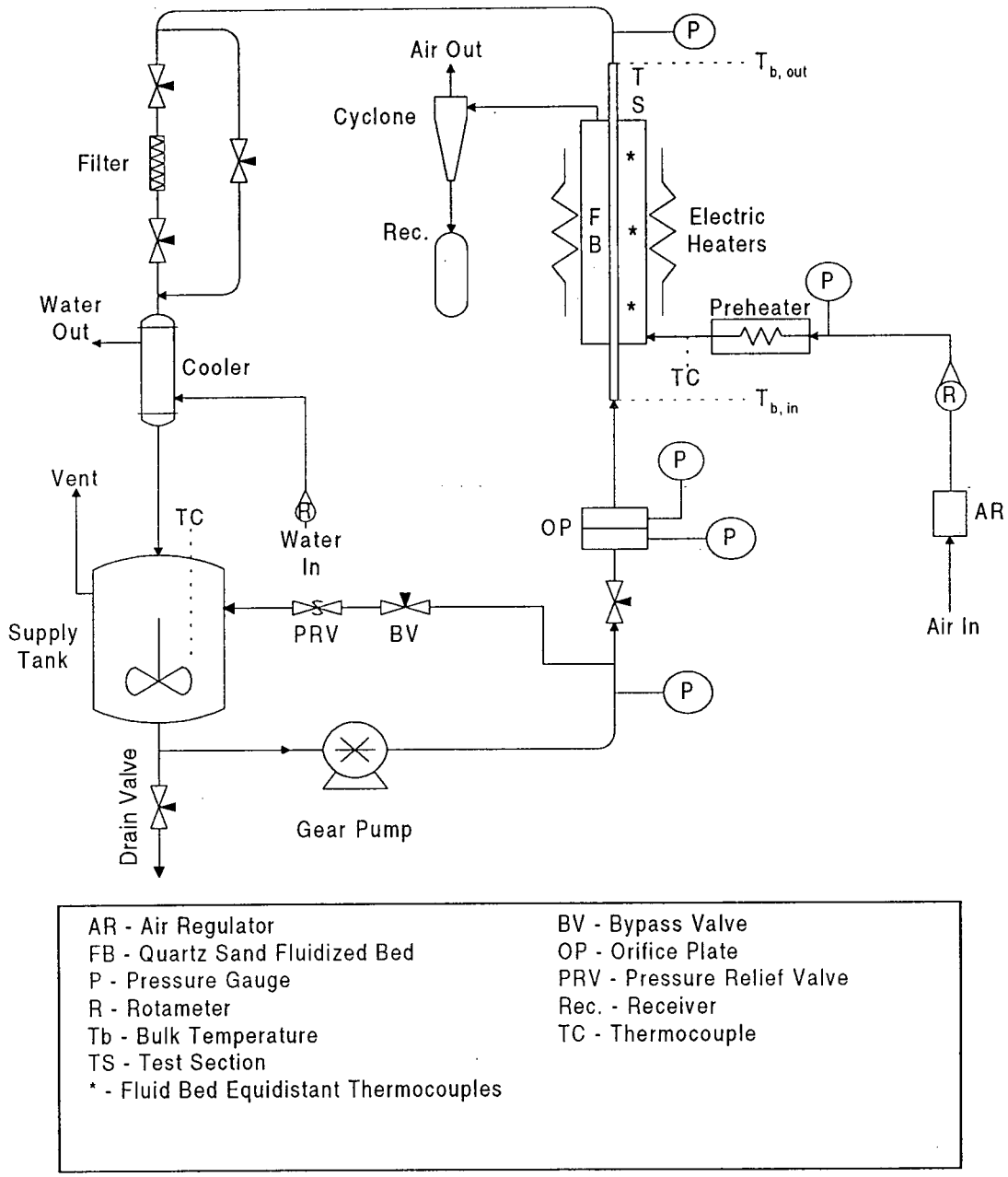

Figure 4.1: Original Apparatus

the unit, and hindered the course of this project. This chapter describes the unit in detail and discusses the modifications made over the duration of the project. It ends with a diagram representing the final state of the loop which summarizes all the changes made.

4.2 Liquid Flowrate Measurement

To provide a measure of the liquid flowrate in the test section which could verify the actual flowrate, a high temperature three-way valve (Swagelok, model# SS-63XTS8-F8) was inserted downstream of the test section. At the end of each run or during calibration of the orifice, the flow was diverted into a 1 L pyrex beaker. Initially, only a volumetric flowrate could be measured; since the quantity of liquid available is small, this leads to important inaccuracies in the time and volume measured. Also, the flowrate measured in this manner would have to be corrected to give the true flowrate, since the temperature in the test section was higher than the temperature in the beaker.

These problems were solved when a digital balance (A & D Co., ser.# J8003182) connected to a computer was used to record the mass collected versus time; the mass flowrate measurement was obtained from the slope of a plot of weight versus time and required a small amount of liquid. The data acquisition was done using LabTech Notebook version 5.0.

4.3 Pressure Drop Measurement

Initially, the pressure drop across the orifice plate was measured by two silicone filled pressure gauges. However, due to the high viscosity of the fluid studied, the gauges were often blocked preventing pressure drop measurements to be obtained for flowrate estimation and monitoring. A new scheme involving a differential pressure transducer (DPT) was designed and implemented successfully.

4.3.1 Differential Pressure Transducer Design, Operation, and Calibration

The DPT (Omega Eng., model# PX771-025DI) was connected to the orifice plate via two 1/4 in. tubes which were wrapped with heating tape to reduce the viscosity of the

fluid during the startup period. Zero differential pressure was set from the ball valve (Swagelok, model# SS-4P4T) connecting both lines, while the two remaining ball valves allowed air removal through the sampling valves and prevented possible damage to the DPT from excess pressure. Since the DPT was incompatible with the highly viscous fluids involved, the lines were filled with coker heavy gas oil which is less viscous than the test fluid. During filling, traces of air were removed using the DPT purge valve.

The DPT was factory calibrated and a linear relationship was used to convert the 4-20 mV output to 0-25 psid. The readings were confirmed by applying known pressure loads to the cell between 0 to 25 psid.

4.4 Liquid Flowrate Estimation

Combining the techniques described in the last two sections provided a method to estimate the flowrate that proved reliable and accurate. A relationship between mass flowrate and pressure drop was obtained. During calibration, care was taken to ensure that the temperature conditions remained constant.

During the course of this study, two orifice plates were used. The first eleven experiments were done with a 1/8 in. diam. orifice plate (β=0.2); however, as no fouling seemed to form in the test section, lower flowrates were studied, requiring a 1/16 in. diam. orifice plate (β=0.1) to be used for the remainder of the project. Both orifice plates were calibrated under the conditions of their use and the calibration curves are shown in Figures A.2 and A.3. As seen on Figure A.2, the larger orifice plate gave two curves for the same temperature conditions. The upper curve was discarded as measurements done at the end of some runs showed that the other was more consistent. The smaller orifice plate was calibrated under two operating temperature conditions and measurements at the end of some runs also revealed that both curves were constant.

4.5 Test Section and Fluidized Bed

The test section was a 1/4 in. O.D. stainless steel tube 1.10 m long (0.01 in. wall thickness TP 316/316 L Seamless, 0.5334 mm I.D.) heated by quartz sand particles (d_p=349 μm,

density=2631 kg/m^3) contained in a 0.46 m long×0.05 m I.D. stainless steel cylinder. Figure 4.2 shows the details of the fluidized bed and test section. The test section was replaced with a new one for each experiment. Operating temperatures were obtained from two ceramic heating elements surrounding the cylinder and by preheating the air upstream of the air distributor. Air flowrates were measured using a calibrated rotameter (Porter Instrument Co., model# B-250-6) which has the calibration curve shown in Figure A.1, and a pressure gauge was used to correct for the bed back pressure. A pressure regulator (Bellofram Co., part# 241-960-068, range 0–60 psi) was used to maintain a constant air pressure to the rotameter.

4.5.1 Air Distributor

Four 1/8 in. O.D. stainless steel tubes having two 0.6 mm diam. holes were used to introduce the fluidizing air into the bed (see Figure 4.2). The pressure drop across the distributor was estimated using the following equation Kunii and Levenspiel (1991) based on orifice theory:

$$\Delta P_{dist} = \left(\frac{U_{or}}{C_{or}}\right)^2 \frac{\rho_g}{2} \tag{4.1}$$

where the orifice coefficient, C_{or}, is selected from a table as a function of the vessel Reynolds number, $Re_v = D_v U \rho_g / \mu_g$ for the total flow approaching the distributor. The results of these calculations are shown in Table 4.1 for different air flowrates, $\dot{m}_{air}$. ΔP_{dist} represents a significant portion of the total pressure drop, or $\Delta P_t = \Delta P_v + \Delta P_{cyclone}$. According to Zuiderweg (1967), in the early years of fluidization engineering, rules of

Table 4.1: Estimation of Pressure Drop Across Air Distributor

$\dot{m}_{air}$ (g/s)	ΔP_t (psid)	U_{or} (m/s)	ΔP_{dist} (psid)	$\Delta P_{dist}/\Delta P_t$ (%)
0.206	5.7	97.3	1.39	24.4
0.297	8.1	125.3	2.58	31.8
0.484	12.8	169.5	5.69	44.4
0.526	13.7	178.4	6.51	47.5
0.663	17.0	201.4	9.26	54.5

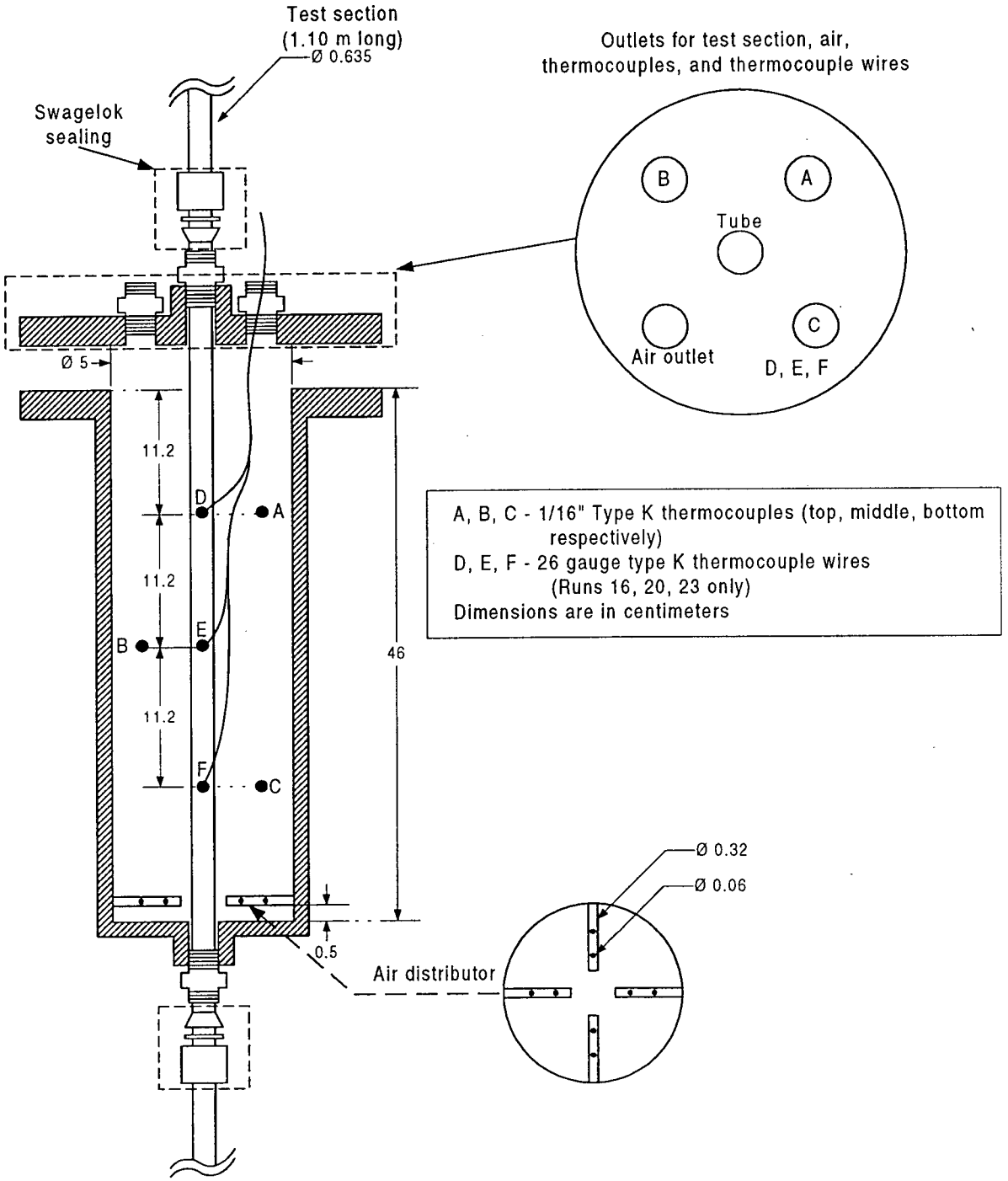

Figure 4.2: Test section, fluidized bed, and air distributor.

thumbs were followed, such as:

$$\Delta P_{dist} = (0.2 - 0.4) \cdot \Delta P_v \tag{4.2}$$

The current distributor clearly exceeds the design recommendation and the gas velocity at the nozzle, U_{or}, also exceeds the jet velocity from orifices in commercial distributors (up to 30–40 m/s). This may result in erosion and breakage of particles and an undesirable shift in size distribution—see Chapter 4 of Kunii and Levenspiel (1991)—, which in turn affects the heat transfer (Molerus et al. (1995)).

4.5.2 Temperature Measurement and Control

For all experiments the temperature of the bed was measured by three 1/16 in. chromel-alumel thermocouples equally spaced (11.2 cm apart) in the axial direction—see Figure 4.2. The uppermost thermocouple was 11.2 cm from the top of the bed. Also, each thermocouple was approximately 1.2 cm away from the test section, although vibrations of the thermocouples due to fluidization of the sand may have affected this distance. Moreover, for Runs 16, 20, and 23, three additional thermocouples were silver soldered on the outside wall of the test section at the same axial positions as the three others to provide a measure of the wall temperature. They consisted of 26 gauge type K thermocouple wires. The temperature of the air entering the bed was also measured.

The bulk inlet and outlet oil temperatures were measured by type K thermocouples located at each end of the test section. An entrance length of 40 cm was provided to ensure a fully developed velocity profile in the heated section. The bulk inlet temperature was controlled by keeping constant the temperature in the supply tank using an analog proportioning controller with a 5°C display resolution (Omega Eng., model 49 controller). The fluidized bed temperature was controlled by the middle thermocouple with the same kind of device which had a 10°C display resolution.

4.5.3 Modifications

As will be discussed in Chapter 6, evidence was obtained that a significant amount of deposit is formed when the flow of liquid is stopped at the end of a run, if the fluidized

bed is at a temperature at which batch coking is believed to occur. A successful technique used to avoid this problem has been to cool the bed with air before shutting down the pump. To shorten the cooling period, thereby reducing the chances of disturbing possible fouling deposits, a sand discharge was installed. It consisted of a stainless steel cylinder connected via a 1/2 in. tube to a 1/3 in. NPT hole drilled at the bottom of the bed. The container was also provided with an air outlet consisting of a piece of tube filled with stainless steel wool. This prevented ejection of hot sand dust from the sand discharge. The choice of the valve separating the sand discharge from the bed was complicated by the high temperatures involved (500-600°C). The difficulty was resolved by using a gas cock valve made of brass which had no plastic seal.

Finally, since the temperature of the air entering the fluidized bed was found to fluctuate, an air mass flow meter (Matheson Co., model 8160) was added for closer monitoring of the flowrate and to identify the cause(s) of the fluctuations. A voltage regulator (SL Waber, type PC2400) was used after it was found that some of the fluctuations were caused by variations in the power supplied.

4.6 Data Collection and Loop Monitoring

Given the length of these experiments (24–60 hr), the addition of a data acquisition system to the original setup was clearly needed. To this end, temperature, differential pressure and mass flow meter measurements were sent to a Digitrend 235 datalogger (Doric Scientific) that converted analog signals from the measuring devices into digital signals. These signals were then transmitted to a personal computer to be displayed and saved at any specified time interval on the hard disk. All the measurements were also displayed on a local instrumentation panel that consisted of digital meters, selector switches, and pressure gauges.

Due to the nature of these experiments and to an inadequate automatic safety system, during operation an operator was always present to monitor the apparatus. To improve the safety of the unit, an alarm device was designed, implemented, and tested. It consisted of a controller (Omega Eng., model# CN76130-PV) which received an output from the differential pressure transducer. An output from this controller was sent to a magnetic

relay switch which controlled power to the entire system except the controller itself. When the pressure drop across the orifice plate exceeds the low and high alarm setpoints on the controller, the magnetic relay switch is opened and all power to the system is shut down. This protects the unit from overheating in case of pump failure or oil line blockage. If desired, the alarm can be bypassed.

4.7 Other Modifications and Final Apparatus

4.7.1 Initial Unsteady-State Period

One primary objective of the fouling experiments was to measure initial fouling rates. Since meaningful values can only be determined when the system is essentially at themal steady-state, care must be taken to reduce the initial unsteady-state period when the temperature set points have not been reached. This is especially valid for this unit with constant surface temperature operation since the temperature of the deposit in contact with the liquid is decreasing as fouling forms.

At several times during this project, the insulation of the loop was improved to reduce the start-up period. Also, the amount of liquid added to the tank was increased from 2 to 2.5 L. The initial unsteady-state period was further reduced by pumping the stream in the bypass circuit only and diverting the flow in the loop once the setpoint was reached. These changes caused the initial unsteady-state period to drop from 200 minutes to reach 284°C to less than 50 minutes to achieve 300°C.

4.7.2 Liquid Flowrate Fluctuations

Throughout this project, a major and persistent problem has been to explain and eliminate important fluctuations in the liquid flowrate which confound the heat transfer measurements. First, an air chamber was installed in the bypass circuit to reduce the effect of pulsations caused by the pump on the pressure drop measurement across the orifice plate and to provide a readable measurement. Also, the original bypass design included a pressure relief valve (Swagelok, model# SS-4R3A5-A) and a needle valve (Swagelok, model# SS-6NBS8-G) in series as shown in Figure 4.1. The first pressure relief valve

(nominal cracking pressure range 50–350 psig) resulted in pressures higher than what the pump could handle so that the excess flow from the pump could not return to the tank and damage was actually done to the pump. A more appropriate relief valve (Swagelok, model# SS-RL3M4-F4, cracking range 10–225 psig) was therefore installed allowing the excess flow to return to the tank and lowering the operating pressure in the bypass circuit.

In order to reduce the fluctuations in the liquid flowrate, the bypass circuit was completely redesigned. The pressure relief valve and the needle valve were installed in parallel. The effect of this modification on the results will be discussed in Chapter 6.

4.7.3 Viscosity Reduction

On several occasions, the pump could not be started due to the high viscosity of the test fluid involved. Heating tapes were installed around the bypass circuit and the tubing upstream and downstream of the pump. This section of the loop could be heated before starting the pump to reduce the viscosity of test liquid trapped in this section of the loop which would otherwise prevent the pump from starting.

4.7.4 Volatilization

Finally, as higher feed temperatures were studied, a significant amount of initial feed was volatilized from the tank vent. This phenomenon led to an insufficient amount of liquid left in the loop and certainly changed the properties of the test liquid over the duration of the run. In order to minimize this effect, a water condenser consisting of a 3/8 in. tube in a 1.5 in. pipe (shell) was installed vertically on the supply tank. The volatiles condensed on the wall and returned to the tank by gravity.

All the modifications and additions to the loop described in the preceding sections are summarized in the diagram shown in Figure 4.3, which represents the final state of the apparatus.

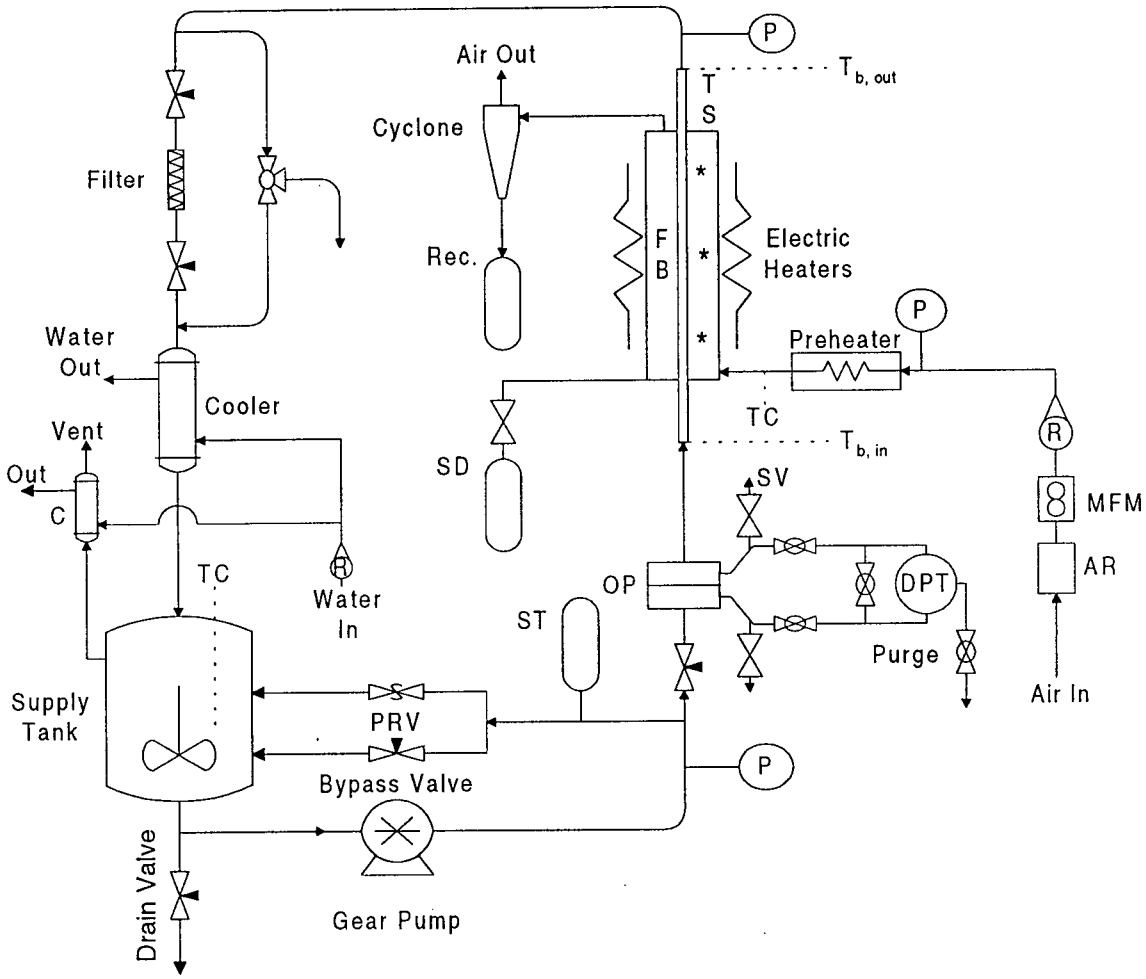

AR - Air Regulator
DPT - Differential Pressure Transducer
MFM - Mass Flow Meter
P - Pressure Gauge
R - Rotameter
SD - Sand Discharge
SV - Sampling Valve
TC - Thermocouple
* - Fluid Bed Equidistant Thermocouples

C - Condenser
FB - Quartz Sand Fluidized Bed
OP - Orifice Plate
PRV - Pressure Relief Valve
Rec. - Receiver
ST - Surge Tank
Tb - Bulk Temperature
TS - Test Section

Figure 4.3: Final Apparatus

Chapter 5

Experimental Procedures

5.1 Thermal Fouling Measurements

A fouling experiment involves three major steps which are: the preparation of the test fluid, the acquisition of thermal fouling measurements, and the cleaning and preparation of the fouling unit for the next fouling test.

For each fouling experiment, 2.5 L of test fluid is prepared; for obtaining the 50:50%vol. pitch-CHGO blend, 1339 g of pitch is broken in small pieces and 1252 g of CHGO pre-warmed on heating plates is poured on top of the pitch. The blending is perfomed in pyrex beakers placed under a fume hood on heating plates. The mixture is made homogeneous by stirring and when it is fluid, it is then poured into the feed tank of the fouling unit.

The next morning, in order to lower the viscosity of the test fluid, the feed tank heaters are turned on, the feed tank stirrer is set to low speed (percent speed=20), and the feed tank temperature controller is set to the desired setpoint. The speed of the feed tank stirrer is subsequently increased to 60 when the viscosity is reduced to facilitate heating of the test fluid. While the mixture is being heated, the power to the air preheater is turned on and the air flowrate to the fluidized bed is set to a suitable value which depends on the bed temperature. The power to the fluid bed heaters is also turned on and the temperature controller is set to the desired value. At the same time, the power to the heating tape surrounding the tubing located between the feed tank and the bypass circuit is turned on in order to lower the viscosity of the test fluid trapped in this section of the loop. It is heated for one hour allowing the temperature to reach 150°C. The power to the heating tape is controlled via a variable autotransformer which is adjusted manually.

Then, the data logging system is started and sampling of all the measurements is made every five minutes. When the bulk temperature in the feed tank has reached the setpoint,

the pump is started with both the needle valve in the bypass circuit and the needle valve upstream of the orifice plate completely opened. The power to the heating tape discussed above is turned off and the power to the heating tape surrounding the tubing to the DP cell is turned on. A temperature of about 100°C is maintained by means of the same variable autotransformer. Then, the ball valve connecting the two DP cell lines is opened and closed to obtain a value of 0 psid across the orifice plate. When the liquid mixture trapped in the DP cell lines is fluid, each of the two purge valves between the orifice plate and the transducer is opened in turn to remove traces of air, and then closed. At that point, about 200 mL of test fluid is taken from either of these purge valves which will constitute the 'initial sample'. Then, the two ball valves between the purge valves and the DP cell are opened for the rest of the run in order to create a pressure drop signal. Once a reading is obtained, the needle valve upstream of the orifice plate is then adjusted to get the desired pressure drop across the orifice plate which corresponds to a known liquid flowrate according to a calibration curve (see Figures A.2 and A.3). From that moment, the test fluid circulates in the unit for 24 hours on average while the process variables are maintained constant. Towards the end of the run, a digital balance covered with a sheet of asbestos wrapped in aluminum foil is placed under the three-way valve of the unit. The balance is connected to the computer and the software Labtech Notebook 5.0 is used to record the weight collected every second. This requires the data logging program for the thermal measurements to be stopped first since each program uses a different operating system. Then, a 1 L pyrex beaker is placed on the balance, the flow is diverted from the three-way valve until about 300 mL of liquid has been collected, and the data are saved in an ASCII file.

After that, the fluidized bed and the feed tank heaters are turned off. When the fluid bed temperature has dropped below 260°C, the pump is shut down. It should be mentioned that for the first seven experiments, the pump was shut down at the same time as the fluid bed and the feed tank heaters. From Run 22 onwards, the hot sand was dumped into a sand discharge to improve the cooling process. Finally, the power to the unit is shut off and the air flowrate to the fluid bed is closed. Approximately 200 mL of test fluid (the 'final sample') is taken from the feed tank through the needle valve located

below the tank and the rest is discharged into pyrex containers. The fouling data are saved in an ASCII file.

In the next stage, the test section is removed and replaced by a new one. Also, the sand left in the fluidized bed and collected in the bin below the cyclone is removed and 1000 g of sand are added to the fluidized bed. The unit is then re-insulated and is ready for the next fouling experiment. The spent sample collected in pyrex beakers is disposed in suitable containers and the pyrex beakers are washed with solvents under the fume hood. When a different test fluid is to be studied, the unit is washed with toluene and subsequently dried with ambient air.

5.2 Toluene Insoluble Formation and Deposition Measurements

A clean glass liner is weighed and then about 1.5 g of the initial sample is placed in the glass liner. The glass liner with its sample is then weighed again and submerged in a sealed flask with 100 mL toluene without agitation for 16 hours. The resulting suspension is filtered through a 0.2 μm Gelman Science TF-200 (Teflon) filter at room temperature using a vacuum provided by a water aspirator as described by Sanaie (1998). The glass liner and flask container are then flushed with 50 mL toluene in order to remove any possible adhering insolubles, and the resulting suspension is also filtered through the same filter. The wall of the glass funnel containing the suspension is also flushed with toluene and the residue on the filter is washed with toluene until the filtrate becomes clear. Then the filter and its residue are removed from the filtration system into a watch glass using a forceps, and dried for 16 hours at 90°C in air at atmospheric pressure before weighing. Also, after removing the filter from the filtration system, any possible residue stuck to the glass funnel is scraped and added to the residue on the filter in the watch glass prior to drying. These precautions ensure that all the solids precipitated by the toluene are collected on the filter. The solids left on the filter are termed the toluene insolubles (TI), or coke. The same procedure is applied to the final sample.

Following a fouling experiment, the inside of the test section is soaked in toluene for about 16 hours and the suspension is then filtered according to the same procedure as given above. When the test section is dried, the inside of the test section is scraped with

stainless steel wool to collect any possible residue stuck to the wall of the test section. This material is added to the residue on the filter used to filter the suspension from the test section. The solids thus obtained are termed w_c and represent the amount of coke present at the end of a run in the whole test section, which includes both a heated and a non-heated portions. Note that the insolubles obtained in the runs perfomed with the 75 wt.% FO-10 wt.% HO-15 wt.% DAO blend were measured according to the same method except that varsol was used instead of toluene. This is because the deposits obtained with such a mixture are of asphaltene-type, which are soluble in toluene, not in varsol. After draining the varsol from the test section, it was flushed with acetone.

Chapter 6

Results and Discussion

Throughout this project, twenty fouling experiments were performed in which the coke formation and deposition tendencies of a mixture of pitch and coker heavy gas oil (50:50% vol.) were investigated by changing the surface temperature of the test section, the bulk temperature of the test fluid, the fluid velocity, and the recirculation time.

For each run, the fouling process was measured by thermal measurements and the final amount of deposit was evaluated by weighing the mass deposited inside the test section; the change in the toluene insolubles content of the test fluid, which represents the coke precursor concentration, was also measured. The results will be presented in the first section.

In several runs, interpretation of the thermal fouling measurements was confounded by the sensitivity of the measurements to fluctuations in process variables. An analysis of the variations in the latter will be given to provide an understanding of the unit behavior, and to eliminate their effects on the thermal fouling data. The effects of a series of improvements to the high temperature fouling unit are also illustrated.

The effect of the air flowrate and temperature on the heat transfer coefficient in the fluidized bed was also investigated. The data obtained will be compared to different semi-empirical models taken from the associated literature in order to discuss the possible factors that may have affected the heat transfer during the experiments. Also, the heat transfer coefficient on the liquid side was calculated in order to check the consistency in the measurements and will be compared to predictions from available correlations.

Finally, to assess the ability of the unit to detect fouling by thermal measurement, three experiments were carried out with a known fouling fluid. The results will be given and discussed.

6.1 Fouling Tendency of 50:50%vol. Pitch and CHGO Blend

6.1.1 Summary of Fouling Runs

The conditions of temperature, mass flowrate ($\dot{m}_{cb}$), fluid velocity in the test section (v_{cb}), recirculation time (t_r) and flow regime investigated (Re_{cb}) are summarized in Table 6.1.

Table 6.1: Summary of variables investigated in fouling experiments with a 50:50%vol. blend of pitch and CHGO and with FO-HO-DAO blend[‡].

Run no.	$\overline{T}_{fb}$ (°C)	$\overline{T}_{in}$ (°C)	$\overline{\Delta T}_b$ (°C)	$\overline{T}_b$ (°C)	v_{cb} (m/s)	t_r (min)	$\dot{m}_{cb}$ (g/s)	Re_{cb}	S.S. (min)	$\overline{Q}$ (kW)	$\overline{1/U_o}$ (m^2-K/kW)	$\overline{\Delta T}_{lm}$ (°C)
1	520	196	7.0	198	1.61	1560	33.1	559	85	0.64	4.4	311
2	514	277	7.7	280	1.09	730	21.1	1039	200	0.40	5.3	233
3	503	245	4.5	247	1.70	740	33.8	1159	265	0.36	6.3	246
4	507	286	9.5	290	0.81	1070	15.6	849	216	0.40	4.1	180
5	499	288	4.1	291	2.31	972	44.5	2395	55	0.46	4.2	208
6	503	290	3.9	292	2.36	1057	44.5	2490	75	0.45	4.4	212
7	507	277	14.7	285	0.63	887	12.2	632	100	0.48	4.3	226
8	498	291	4.4	293	1.57	646	30.2	1690	100	0.34	5.7	203
9	503	284	13.1	291	0.69	917	13.3	731	75	0.42	4.7	215
10	502	277	19.9	287	0.48	762	9.2	487	55	0.43	4.6	216
11	502	281	16.3	289	0.48	1085	9.2	522	85	0.42	4.7	214
12	501	286	19.0	295	0.43	762	8.3	469	70	0.39	4.8	207
13	600	289	18.8	298	0.83	1123	16.0	935	120	0.75	3.7	304
14	598	282	34.1	300	0.41	1148	7.9	470	200	0.63	4.4	299
15	508	199	15.4	207	0.79	2009	16.1	311	200	0.56	4.9	299
16	615	286	33.8	302	0.40	1122	7.7	465	355	0.62	4.7	313
17	601	286	31.2	302	0.40	3359	7.7	472	300	0.59	4.6	300
18	596	329	31.0	346	0.36	3353	6.6	563	300	0.51	4.5	250
19	236	87	16.6	95	0.31	1304	5.8	206	166	0.19	6.8	139
20	449	95	73.4	132	0.17	1889	3.2	266	300	0.50	5.9	317
21	444	107	25.4	120	0.68	2019	12.7	813	200	0.66	4.5	323
22	612	348	25.6	358	0.45	2059	8.3	762	200	0.50	4.4	240
23	615	363	25.3	375	0.44	1720	8.0	824	200	0.51	4.3	238

[‡]Only Runs 19, 20, and 21 were performed with the 15% DAO-10% HO-75% FO blend.

The fluidized bed temperature reported, $\overline{T}_{fb}$, refers to the temperature in the sand which is not the same as the wall temperature. This fluidized bed temperature is the average of the three axial temperature measurements described in Section 4.5.2 and is calculated after the time the system takes to achieve thermal steady-state (S.S.). The average bulk temperatures of the test fluid entering and leaving the test section, $\overline{T}_{in}$ and $\overline{T}_{out}$, are also calculated at steady-state and $\overline{T}_b$ represents the bulk average temperature in the test section, which is the average of $\overline{T}_{in}$ and $\overline{T}_{out}$. $\overline{\Delta T}_b$ is the average bulk temperature difference across the test section, calculated at steady-state. The average heat flow, $\overline{Q}$, the average inverse overall heat transfer coefficient, $\overline{1/U_o}$, and the average log mean temperature difference, $\overline{\Delta T}_{lm}$, are also calculated at steady-state. The equations used to calculate these parameters are given in Appendix D.6. Finally, the mass flowrate, the fluid velocity, and the Reynolds number in the test section are based on the calibration measurement performed at the end of each experiment.

Since one of the objectives was to establish the conditions at which significant fouling is formed, the approach adopted in the experiments was to vary the process variables in the direction in which fouling formation is believed to increase. As a result, the fluid bed temperature, the bulk temperature and the recirculation time were increased, while the velocity was decreased. For the first experiments, the average fluid bed temperature was around 500°C. As no significant fouling was observed, the temperature was increased to its maximum value of 600°C for most of the remaining runs. The average bulk temperature in the test section was set initially at 198°C and was subsequently increased to around 290°C for the majority of the runs. Since no significant fouling was detected, it was further increased reaching 375°C in the last experiment. Moreover, the velocity in the test section was varied from 0.2 to 2.2 m/s and the flow regime was laminar for all runs. Since Q was determined from the temperature rise of the oil, ΔT_b, if flowrates were too high, and ΔT_b was too low, then Q would be subject to significant error. As shown for Run 6, at Re=2490, ΔT_b was around 3.9°C. Higher velocities (turbulent flow) would have resulted in an even smaller ΔT_b which might not have been accurately measured, given a resolution of one decimal place. It is also generally accepted that reducing the fluid velocity increases the fouling tendency (see Chapter 2), hence reducing velocity was

desirable for detecting fouling.

6.1.2 Toluene Insolubles Measurements

For fouling involving coking reactions, the amount of coke precursor in the test fluid and its change with recirculation time may provide clues for an understanding. For each run, the coke precursor content in the initial and final sample was measured as explained in Chapter 5. From the knowledge of the weight of the sample and that of the coke, the concentration of coke is expressed as

$$TI = \frac{Weight\ of\ coke\ recovered}{Sample\ weight} * 100 \tag{6.1}$$

Inorganic mineral matter in the fluid will contribute to the toluene insolubles as defined above. The yield of coke is then given by $(TI - TI_0)$, where TI_0 is the value of TI at time zero. Upon heating of these blends, a fraction of the initial test fluid is lost due to a combination of evaporation and bond-breaking with volatilization of light fragments, this effect increasing with the severity of conditions. This weight loss, or volatile yield, is calculated as

$$V = \frac{Initial\ total\ weight\ -\ Final\ total\ weight}{Initial\ total\ weight} * 100 \tag{6.2}$$

For the heavy gas oils, evaporation is expected to be a major factor, given the boiling curves shown in Figure B.1. For pitch, little evaporation is expected at the temperatures investigated, and volatilization of light reaction products will dominate.

Watkinson et al. (1998) carried out batch heating experiments on 50:50% vol. pitch-virgin gas oil blends in order to determine the kinetics of coke precursor formation. Their TI and weight loss results are reproduced in Figure 6.1 to show how those important parameters are affected by temperature and reaction time. For all runs in the present work, except one, the amount of volatile matter released was not measured and, as a result, the toluene insolubles are given in terms of the weight of the final sample. To provide a more suitable basis for comparison, the toluene insoluble results of Figure 6.1 are also shown on the basis of the final sample weight. Note that from Figure 6.1c, 250

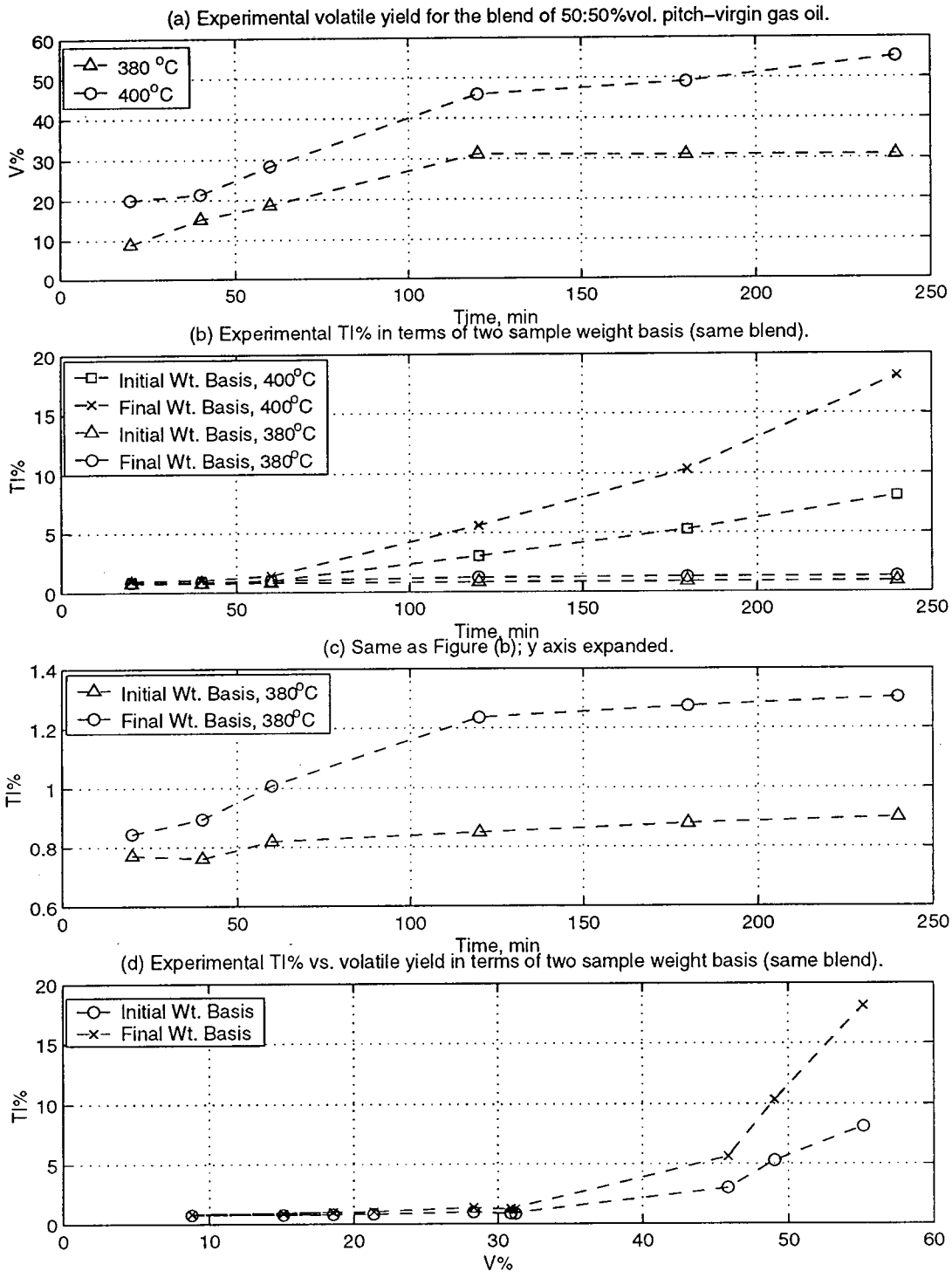

Figure 6.1: Batch coking experiments of 50:50%vol. Pitch and Virgin Gas Oil Blend—Expts. Yue (1998).

minutes of heating at 380°C results in TI=0.90% and, with TI_0=0.77%, a coke yield of about 0.12%.

When the toluene insolubles are plotted against volatile yield in Figure 6.1d, all data calculated on the same sample weight basis collapse to a single curve. Similar results were also observed for gas oils, pitch, and other mixtures of gas oils and pitch in the range 360–400°C. For pitch, it was noted that toluene insolubles formation only starts after a 23%wt. loss has been reached for any of the reaction times and temperatures investigated. For the 50:50%vol. pitch-VGO mixture, the TI appears to increase when about 30%wt. loss has been reached, as shown on Figure 6.1d.

Table 6.2 contains the toluene insoluble weight percent for the initial and final test fluid samples for all runs performed as part of this thesis. The same results are shown in Figure 6.2 as a function of recirculation time, t_r. The outliers are attributed to difficulties in the filtration procedure or contamination of the unit with toluene. The 95% confidence

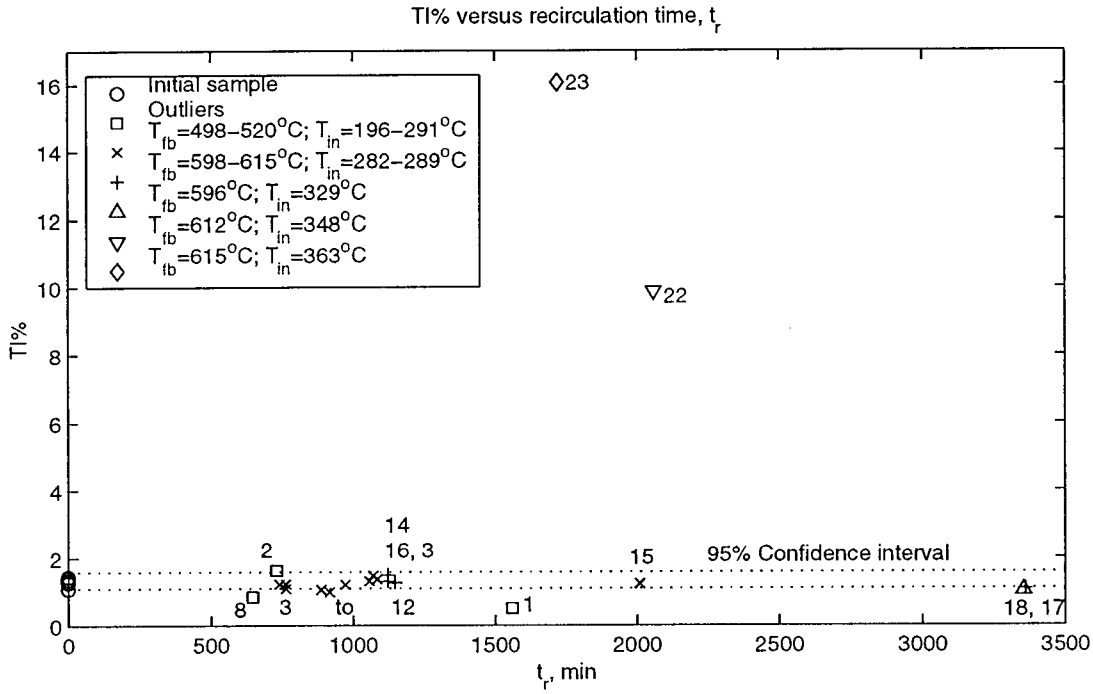

Figure 6.2: Toluene insolubles content based on actual sample weight versus recirculation time for all runs (50:50%vol. pitch and CHGO blend).

interval on the average initial TI content is given where the errors were assumed $N(0, \sigma^2)$. The batch coking data of Figure 6.1 did not permit prediction of the volatile yields in the current work in order to present the toluene insoluble results for the final sample on the basis of the weight of the initial sample. For that reason, the confidence interval given cannot be directly applied to the data of the final sample. However, it can be expected that the TI in final sample would be lower if they were reported in terms of the weight of the initial test fluid sample.

Table 6.2: Toluene insolubles content in the initial and final test fluid for all runs.

Run no.	$^{\ddagger}TI_{initial}$ (%wt.)	$^{\ddagger}TI_{final}$ (%wt.)	Run no.	$^{\ddagger}TI_{initial}$ (%wt.)	$^{\ddagger}TI_{final}$ (%wt.)
1	†n.m.	0.50	11	1.44	1.36
2	n.m.	1.62	12	1.35	1.21
3	n.m.	1.21	13	1.27	1.49
4	n.m.	1.46	14	1.25	1.26
5	n.m.	1.20	15	1.44	1.22
6	n.m.	1.30	16	1.27	1.30
7	n.m.	1.05	17	1.45	1.07
8	n.m.	0.84	18	1.29	1.02
9	1.36	0.98	22	1.46	9.87
10	1.29	1.08	23	1.08	16.07

†n.m.:not measured; ‡calculated based on actual sample weight.

The TI measurements in the present work are consistent with the experimental data given previously in Figure 6.1d. The recirculation times were 3 to 14 times longer than the maximum reaction time of four hours in the batch coking experiments, however the bulk temperatures were markedly lower. In Run 22, 23%wt. of the initial test fluid weight was recovered by condensation. This amount is lower than the total volatiles actually released since part of it could not be condensed. The data therefore suggest that substantial toluene insolubles formation only starts after a critical volatile yield close to 30%wt. has been reached for any reaction time and temperature. As long as a lesser amount of volatiles has been released, no significant increase in the toluene insolubles will occur. Finally, in 7 cases out of 10, a small decrease in TI was observed (see Table 6.2). So far, a reasonable account for this has not been found.

6.1.3 Mass Deposition Measurements

The total amount of coke left in the test section (heated and non-heated sections) at the end of a run, w_c, was measured for each run as explained in Chapter 5. This amount comes from any coke present in the oil residue left on the wall of the tube, and any solid or semi-solid coke-like material formed as a result of fouling.

For the first seven runs, the fluidized bed was not cooled down before shutting down the pump. Also, for Runs 9 and 14, the pump was stopped during the run for a few minutes because of problems with the pump or the fluidized bed. From Run 8 onwards, the fluidized bed was cooled down to approximately 260°C before shutting down the pump; to further help the cooling process, a sand discharge was added from Run 22. The results, shown in Table 6.3, are therefore separated according to the fluid bed cooling procedure used.

Table 6.3: Coke collected in test section and equivalent liquid thickness which would give rise to w_c.

No cooling			Cooling		
Run no.	w_c (mg)	x_{res} (μm)	Run no.	w_c (mg)	x_{res} (μm)
1	49	516	8	2	13
2	13	42	10	6	29
3	63	274	11	5	19
4	392	414	12	18	78
5	58	255	13	10	35
6	34	138	15	18	78
7	185	928	16	14	56
9	237	1274	17	10	51
14	684	2859	18	3	16
			22	67	36
			23	262	86

Except for the last two runs, the major difference in the magnitude of the amounts of coke collected appears to be explained in terms of the fluid bed cooling procedure used. The data suggest that a significant amount of coke is formed if the fluid bed is not cooled

down properly when the flow of oil has stopped. From the batch coking experiments (see Watkinson et al. (1998)) and from the knowledge that there is always a certain amount of residue left in the test section once the pump is stopped, it is concluded that most of the amounts of coke shown in the left hand side of Table 6.3 come from batch coking reactions in the residue left on the tube wall. Therefore, these results cannot be attributed to fouling and will be discarded for the rest of the analysis.

In order to evaluate the amount of coke formed as a result of fouling in the remaining runs it is useful to take into account the toluene insolubles in the final sample. If we assume that w_c comes exclusively from the residue left on the tube wall, an equivalent liquid thickness which would give rise to w_c mg of coke may be calculated:

$$x_{res} = \frac{w_c}{TI_{final} \cdot \rho_{res} \pi D_i L} \tag{6.3}$$

where ρ_{res} is the density of the liquid residue which was calculated at 20°C from Equation 3.2 and L is the test section length (=1.10 m). The values of w_c and x_{res} on the right side of Table 6.3 are shown in Figures 6.3a and 6.3b as a function of total recirculation time. It can be observed that no significant increasing trend in w_c exists. For fixed $\overline{T}_b$, $\overline{T}_{fb}$, v, etc., it can be expected that a longer recirculation time would result in a higher amount of coke accumulated on the surface. Runs 16 and 17 differ only by their recirculation time as shown in Table 6.1 but show no significant difference in their w_c values. Also, Figure 6.3a indicates that, except for the last two experiments, all runs resulted in approximately the same low w_c value. As for x_{res}, the values shown on the right hand side of Table 6.3 are reasonable when compared to the tube diameter (D_i=0.533 cm) and do not differ significantly from run to run as shown in Figure 6.3b. If the residue layers present on the tubes at the end of the runs had such thicknesses, then the higher w_c values of Runs 22 and 23 were due to the TI content in the final sample and not to a larger amount of fouling. This idea is consistent with the correlation found between w_c and TI_{final} shown in Figure 6.3c. One could argue that Figure 6.3c may also suggest that the higher concentration of coke precursor in the fluid explains the higher amount of deposit on the surface. However, this would imply for Runs 22 and 23 a different (thinner) residue layer on the tube, which is not reasonable. In addition, the small values of x_{res} and the fact that they are scattered with t_r suggest that the assumption behind x_{res} is realistic.

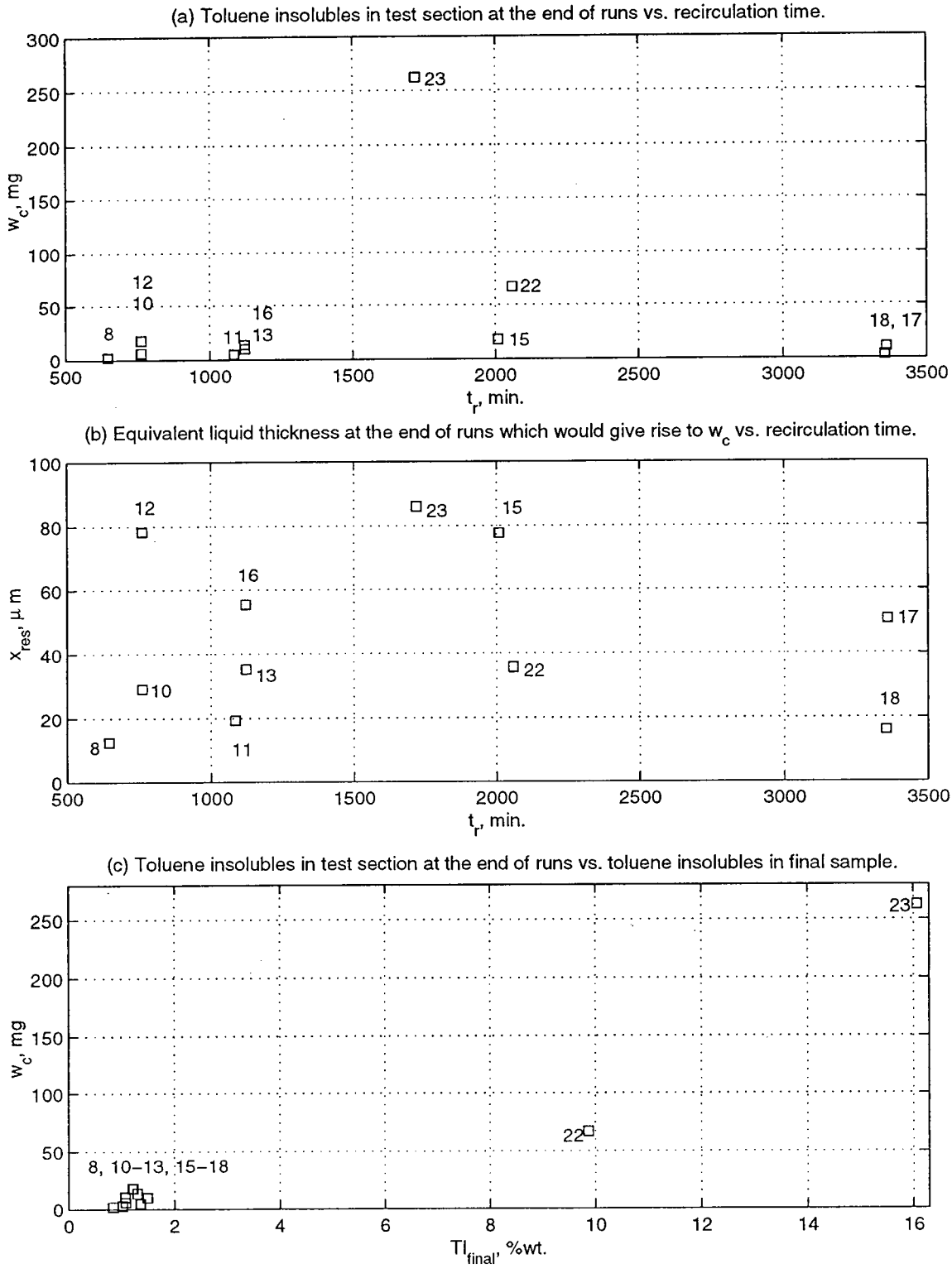

Figure 6.3: Mass deposition measurement analysis; run number shown besides symbol.

Consequently, these numbers suggest very little coke formation during recirculation. As a consequence, no substantial effect of fluid velocity, bulk fluid temperature, fluidized bed temperature and recirculation time was observed. This conclusion is consistent with the thermal fouling measurements which indicated no significant fouling.

6.2 Analysis of Variations in Liquid Flowrate

6.2.1 Experiments with Pressure Drop Measurement

Ideally, the temperature difference across the test section, ΔT_b, should remain constant as long as no fouling has been formed. However, for several runs, this parameter exhibited severe fluctuations and most of these variations were caused by fluctuations in mass flowrate. Evidence of this was obtained by inspecting both measurements as shown in Figure 6.4 for Run 9 and from the relationship between $\overline{\Delta T_b}$ and $\overline{\dot{m}}$ which is shown in Figure 6.5 for several runs; $\overline{\Delta T_b}$ and $\overline{\dot{m}}$ are average values of ΔT_b and $\dot{m}$ which are calculated, for a given run, over the same time interval. The results of Figure 6.5 are expected since for small changes in $\dot{m}$, with U_o little affected, $\dot{m}\overline{C_p}\Delta T_b$ is constant and therefore $\Delta T_b \propto (1/\dot{m})$. Figure 6.4 reveals that the change in both measurements occurs at the same time and according to an inverse relationship which is consistent with the results of Figure 6.5.

The concept of cross-correlation can be used to measure linear dependence between two trends (time series). The cross-correlation function between two time series $\{Y_t\}$ and $\{Z_t\}$ at lag k is given by

$$\begin{aligned} r_k &= xcorr(Y_t, Z_{t-k}) = \frac{cov(Y_t, Z_{t-k})}{var(Y_t)var(Z_{t-k})} \\ &= \frac{\sum_{t=1}^{n-k}(Y_t - \overline{Y})(Z_{t-k} - \overline{Z})}{\left[\sum_{t=1}^{n}(Y_t - \overline{Y})^2 \sum_{t=1}^{n}(Z_t - \overline{Z})^2\right]^{1/2}} \end{aligned} \tag{6.4}$$

where n is the number of data points and $\overline{Y}$ and $\overline{Z}$ are mean functions. Values of r_k near ± 1 indicate strong (linear) dependence. If r_k=0, then Y_t and Z_{t-k} are said to be

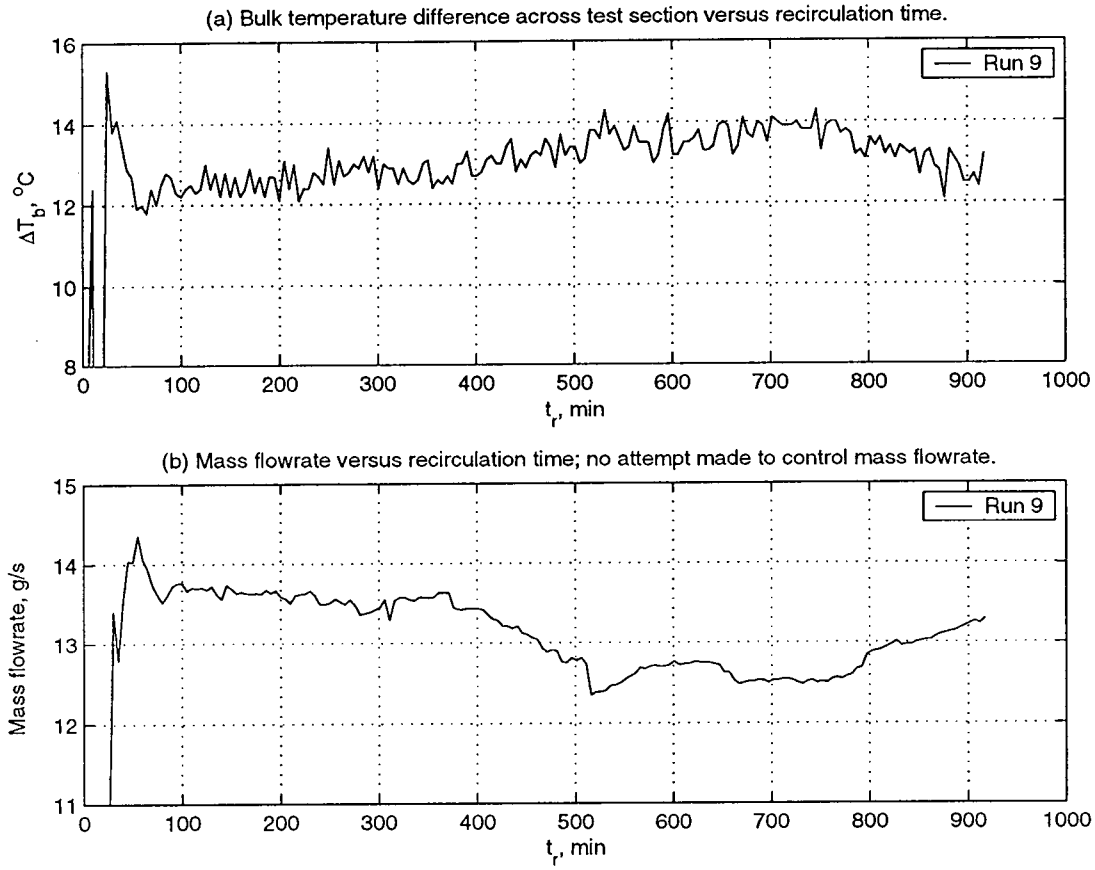

Figure 6.4: Fluctuations in ΔT_b caused by variations in mass flowrate in Run 9.

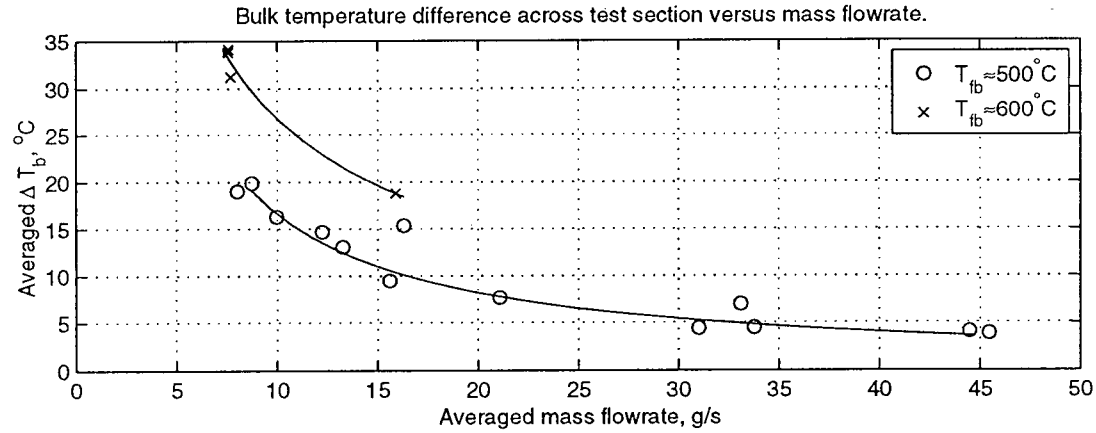

Figure 6.5: Relationship between $\overline{\Delta T_b}$ and $\overline{\dot{m}}$; lines from Equations 6.6 and 6.7.

uncorrelated. In order to apply this concept to the data, the assumption of stationarity needs to be reasonable. A time series $\{Z_t\}$ is said to be stationary if the mean function and the variance are constant for all time. An example of a non-stationary time series is given in Figure 6.4. A common approach used to transform a non-stationary time series into a stationary one is to use the following transformation—called differencing:

$$\Delta Z_t = Z_t - Z_{t-1} \text{ for } t = 2, 3, \cdots, n \tag{6.5}$$

The cross-correlation function was calculated between ΔT_b and $\dot{m}$ and the above transformation was used when necessary. The results are given in Table 6.4 with the 95% confidence interval and Figure 6.6 illustrates typical results for a correlated and an uncorrelated time series. For the correlated cases, the negative value and the fact that

Table 6.4: Cross-correlation between ΔT_b and $\dot{m}$ at lag zero.

Run no.	r_0	95% CI	Run no.	r_0	95% CI
8	-0.01	0.19	16	-0.81	0.16
9	-0.10	0.15	17	-0.01	0.08
10	-0.45	0.17	18	-0.12	0.08
11	-0.88	0.14	19	-0.12	0.19
12	-0.91	0.17	20	0.03	0.19
13	-0.26	0.14	21	-0.61	0.19
14	-0.93	0.14	22b	-0.82	0.11
15	0.01	0.10	23	-0.56	0.14

it is only significant at lag 0 is clearly consistent with Figure 6.5 which shows an inverse relationship and emphasizes the above observation that the change in both measurements occurs at the same time. The large negative cross-correlation values obtained in some runs, such as 11, 12, and 14, are attributed to larger and/or more variations in liquid flowrate. It was observed that when attempts were made to control the flowrate, variations in liquid flowrate were more important and more frequent than when no attempts were made. Attempts to control the flowrate were done in Runs 11, 12, 14, 16, and 22b. On the other hand, when the variation in flowrate was too small, no correlation was found.

In order to see whether the changes in ΔT_b with respect to $\dot{m}$ observed in each run are consistent with the results of Figure 6.5, the run average values of ΔT_b and $\dot{m}$ were

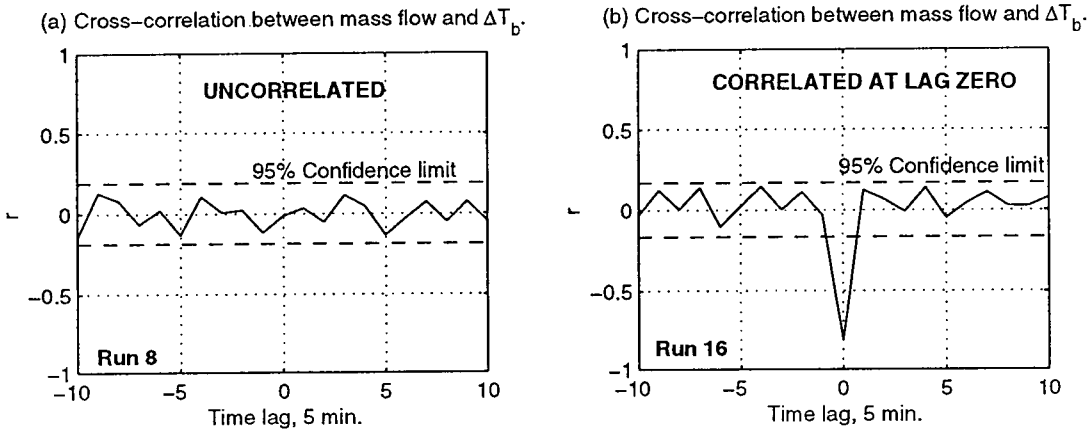

Figure 6.6: Cross-correlation function between ΔT_b and $\dot{m}$ for Runs 8 and 16.

fitted to the following equations which are shown as lines in the same figure for the two fluidized bed temperatures:

$$\overline{\Delta T}_{b,500°C} = 173.1 \cdot \overline{\dot{m}}^{-1.02} \tag{6.6}$$

$$\overline{\Delta T}_{b,600°C} = 156.0 \cdot \overline{\dot{m}}^{-0.77} \tag{6.7}$$

The power-law equation was chosen since $\dot{m} \cdot \Delta T_b$ is expected to be approximately constant. The temperature difference, ΔT_b, and $\dot{m}$ were plotted against each other as shown in Figure 6.7 and the slope was compared to the first derivative—with respect to $\overline{\dot{m}}$—of Equation 6.6 or 6.7. The results are shown in Figure 6.8. For both bed temperatures, the results are quite consistent given the errors in the fitted curves and in the individual runs. It must be taken into account that it was not the purpose of these experiments to

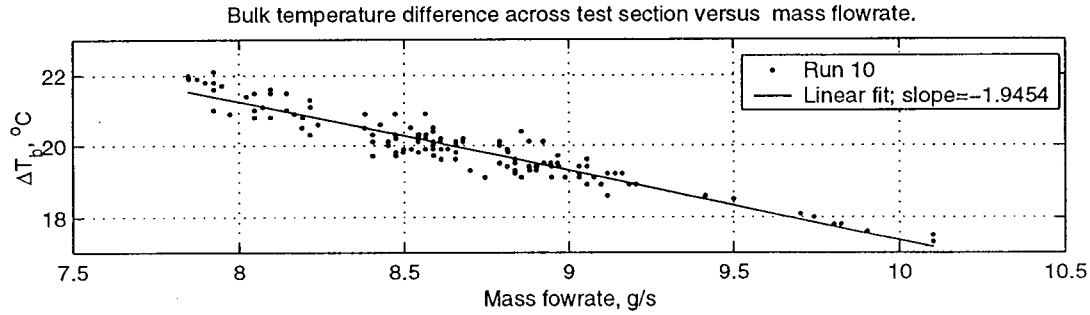

Figure 6.7: Linear correlation found between ΔT_b and $\dot{m}$.

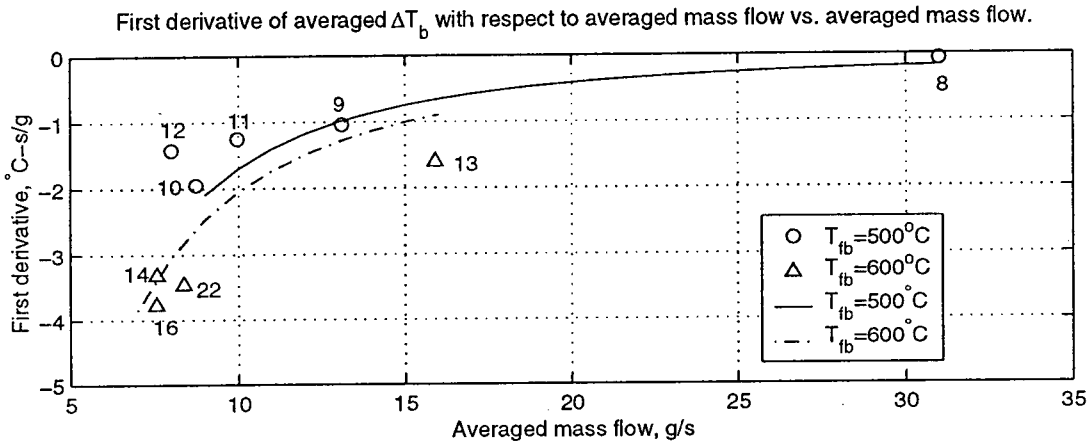

Figure 6.8: Slopes of Equations 6.6 and 6.7 (lines) versus corresponding slope in individual runs (symbols).

obtain such relationships and therefore the data was not taken under perfectly controlled conditions. Based on these results, it appears that the variation in ΔT_b observed in these runs may have been caused by flowrate variations.

6.2.2 Initial Experiments

In the early experiments (Runs 1–7), the flowrate was determined only by bourdon pressure gauges which measured ΔP across the orifice plate. Subsequently the DP cell was used. Because of frequent blockage in the gauges and other problems, the flowrate was uncertain in Runs 1–7. The available pressure drop measurements in Run 1 revealed that the observed drop in ΔT_b had been caused by an increase in flowrate, as shown in Figure 6.9. Hence it was concluded that in spite of the apparent increase in the fouling resistance, R_{fc}, no fouling had occurred. However, for Runs 4–7, no pressure drop measurements could be made due to blockage of the pressure gauges. In order to recover useful data from these runs, attempts were made to correlate ΔT_b with other parameters which could be related to the flowrate, $\dot{m}$.

A measurement which was affected by the flowrate was the temperature difference between the temperature of the test fluid in the tank and the bulk inlet temperature caused by heat losses, ΔT_{loss}. Hence an attempt was made to relate $\overline{\Delta T}_{loss}$ to the mass

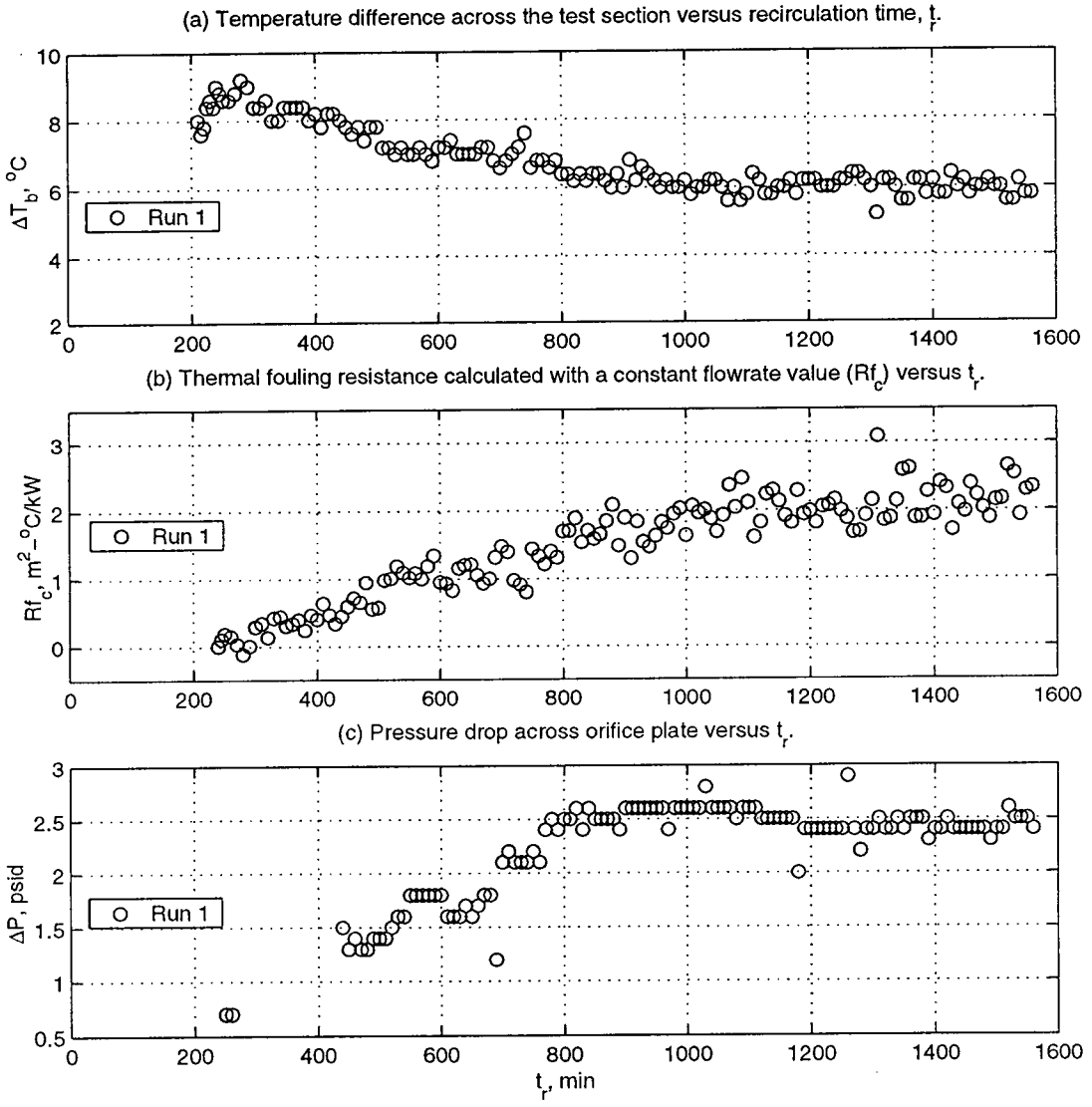

Figure 6.9: Drop in ΔT_b in Run 1 caused by a flowrate increase.

flow and to $\overline{\Delta T_b}$ in order to determine whether fouling or mass flow variations were the cause of the observed changes in ΔT_b. $\overline{\Delta T_{loss}}$ is the average value of ΔT_{loss} which is calculated, for a given run, over the same time interval as $\overline{\dot{m}}$. A correlation was found between $\overline{\Delta T_{loss}}$ and $\overline{\dot{m}}$, as shown in Figure 6.10a for a bulk inlet temperature of about 290°C. Figures 6.5 and 6.10a were then combined to provide a correlation between $\overline{\Delta T_b}$ and $\overline{\Delta T_{loss}}$ caused by the same underlying variation in flowrate; the result is shown in

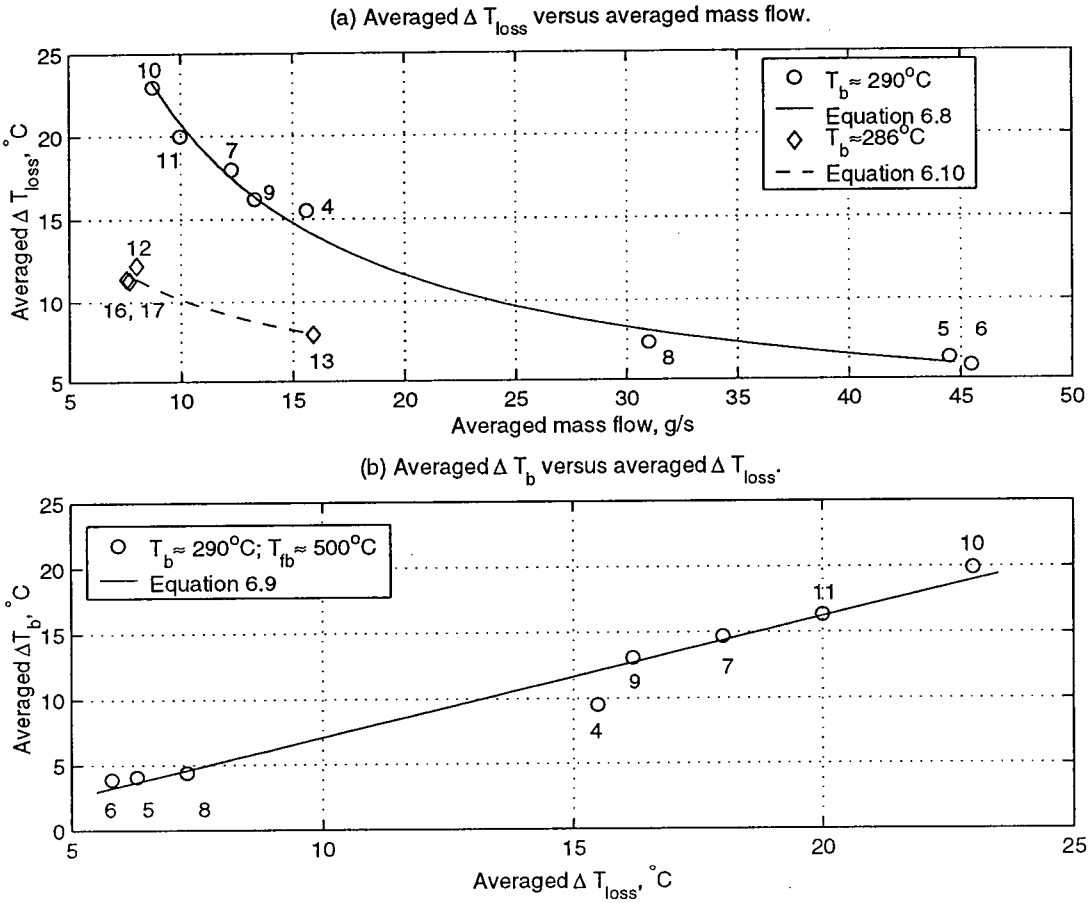

Figure 6.10: Correlations found between ΔT_{loss}, ΔT_b, and $\dot{m}$ for Runs 4–11.

Figure 6.10b. Hence, the following equations were fitted to the data of Figure 6.10:

$$\overline{\Delta T}_{loss} = 142.21 \cdot \overline{\dot{m}}^{-0.84} \tag{6.8}$$

$$\overline{\Delta T}_b = 0.91 \cdot \overline{\Delta T}_{loss} - 2.07 \tag{6.9}$$

$$\overline{\Delta T}_{loss,I} = 30.9 \cdot \overline{\dot{m}}^{-0.49} \tag{6.10}$$

Equations 6.8 and 6.9 are valid for some of the runs performed with the unit having its original insulation. The insulation of the unit was improved after Run 11. Equation 6.10 applies for some of the runs done after Run 11. ΔT_{loss} was plotted versus the mass flowrate and ΔT_b for each individual run as shown in Figure 6.11. The slopes obtained were compared to the first derivative of the above equations and the results are given in Figure 6.12. The slopes measured in the individual runs appear consistent with the

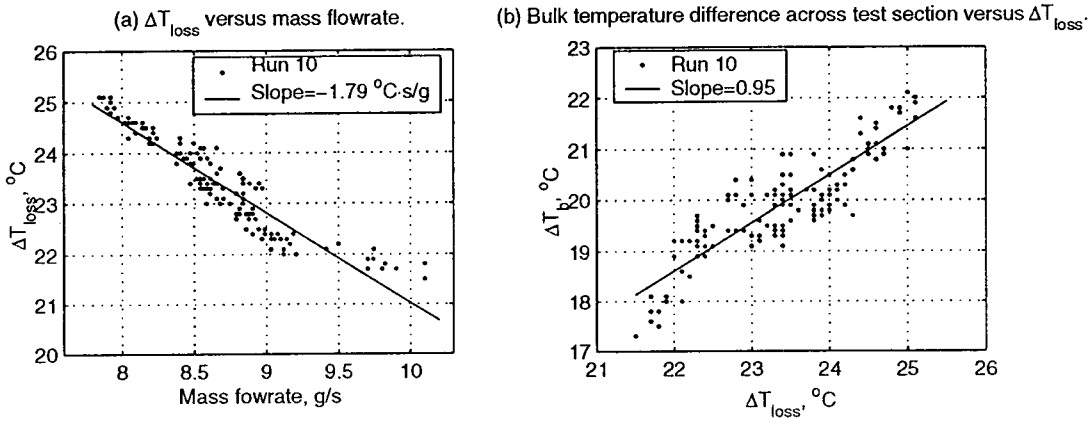

Figure 6.11: Correlations observed between ΔT_{loss} and $\dot{m}$ and between ΔT_b and ΔT_{loss}.

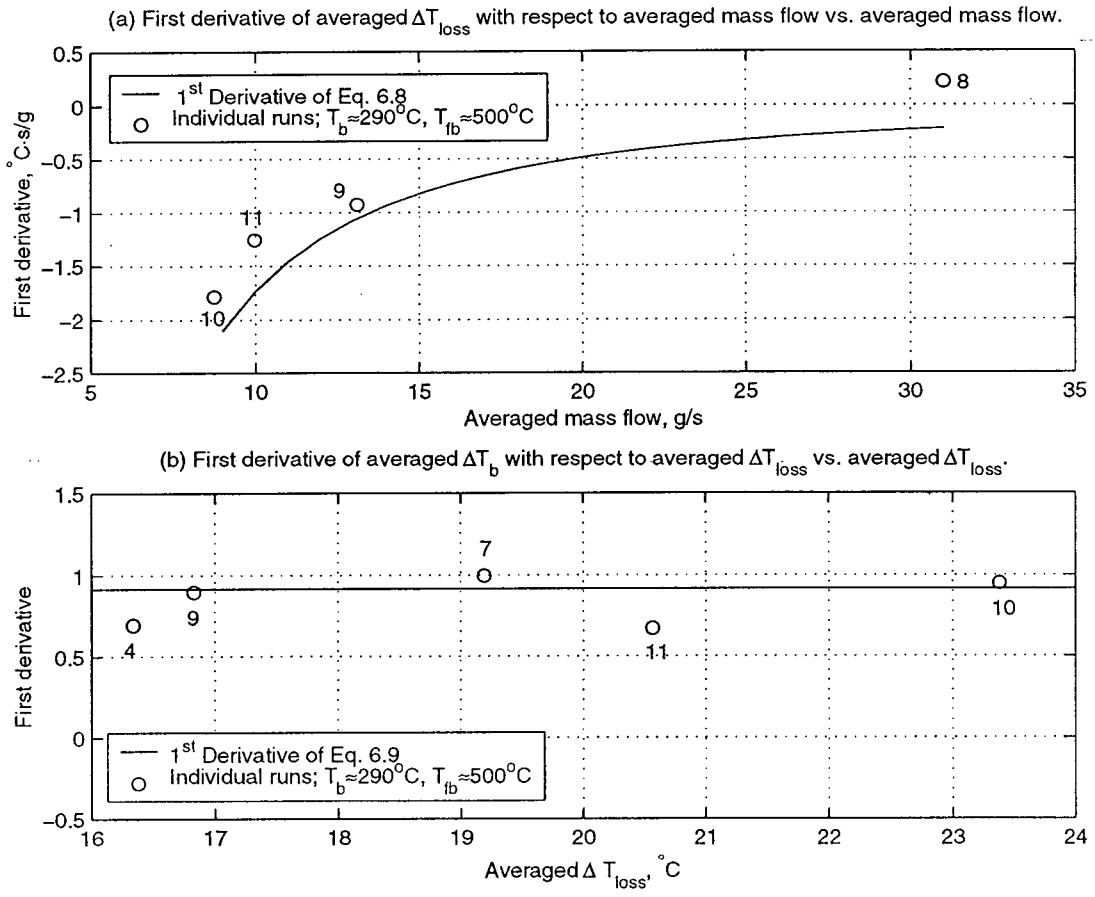

Figure 6.12: Slopes of Equations 6.8 and 6.9 vs. corresponding slopes in individual runs.

corresponding relationship. This suggests that the drop in ΔT_b observed in runs such as 4 and 7 were caused by an increase in flowrate. Figure 6.13 shows both temperature differences versus time for Runs 4, 7 and 10. The preceding discussion revealed that in Run 10, the variation in ΔT_b was caused by a flowrate variation and Figures 6.13e and 6.13f indicate that this variation produced a similar effect on ΔT_{loss}. The fact that the change in both measurements for Runs 4 and 7 occurs at the same time and given the above comparison of slopes suggest that the variation in ΔT_b in those experiments was also caused by a variation in flowrate.

6.2.3 ARMA Model and Variable Flowrate Approach

In order to distinguish fouling from flowrate variations effects, a procedure was developed in which two different techniques were applied to the data.

Once pressure drop measurements were available, the natural way to distinguish fouling from flowrate effects, which was applied to the data as a regular part of the work, was to calculate the heat flow (Equation 2.1) based on the actual flowrate. The effect of this approach is shown in Figure 6.14. This approach works as long as the change in flowrate is such that $\dot{m} \cdot \overline{C_p} \Delta T_b$ is approximately constant. When the variation in flowrate is too large, a significant change in the heat flow occurs; an example of this is shown in Figure 6.15 which is a plot of the average heat flow, $\overline{Q}$, versus the average mass flowrate, $\overline{\dot{m}}$. The increase in heat flow with mass flowrate shown for different fluid bed temperatures and two test fluids, is consistent with the fact that the heat transfer coefficient (oil side) also increases with the mass flowrate. This phenomenon is believed to be responsible for the poor results of using a variable flowrate obtained in Run 10. Figure 6.16 suggests that the drop in flowrate (Figure 6.13f) was large enough to cause a significant drop in heat flow.

Another technique used to distinguish fouling from flowrate variations consisted of modeling the temperature difference across the test section as a function of the pressure drop across the orifice plate, ΔP, and then using the model to compare the predicted ΔT_b with the true ΔT_b. Assuming that the variations in ΔT_b were only caused by the flowrate, a significant deviation between the prediction and the data would indicate fouling. Since

the model represents the process under clean conditions, the modeling step was done with the initial data where fouling had not yet occurred. A block diagram illustrating

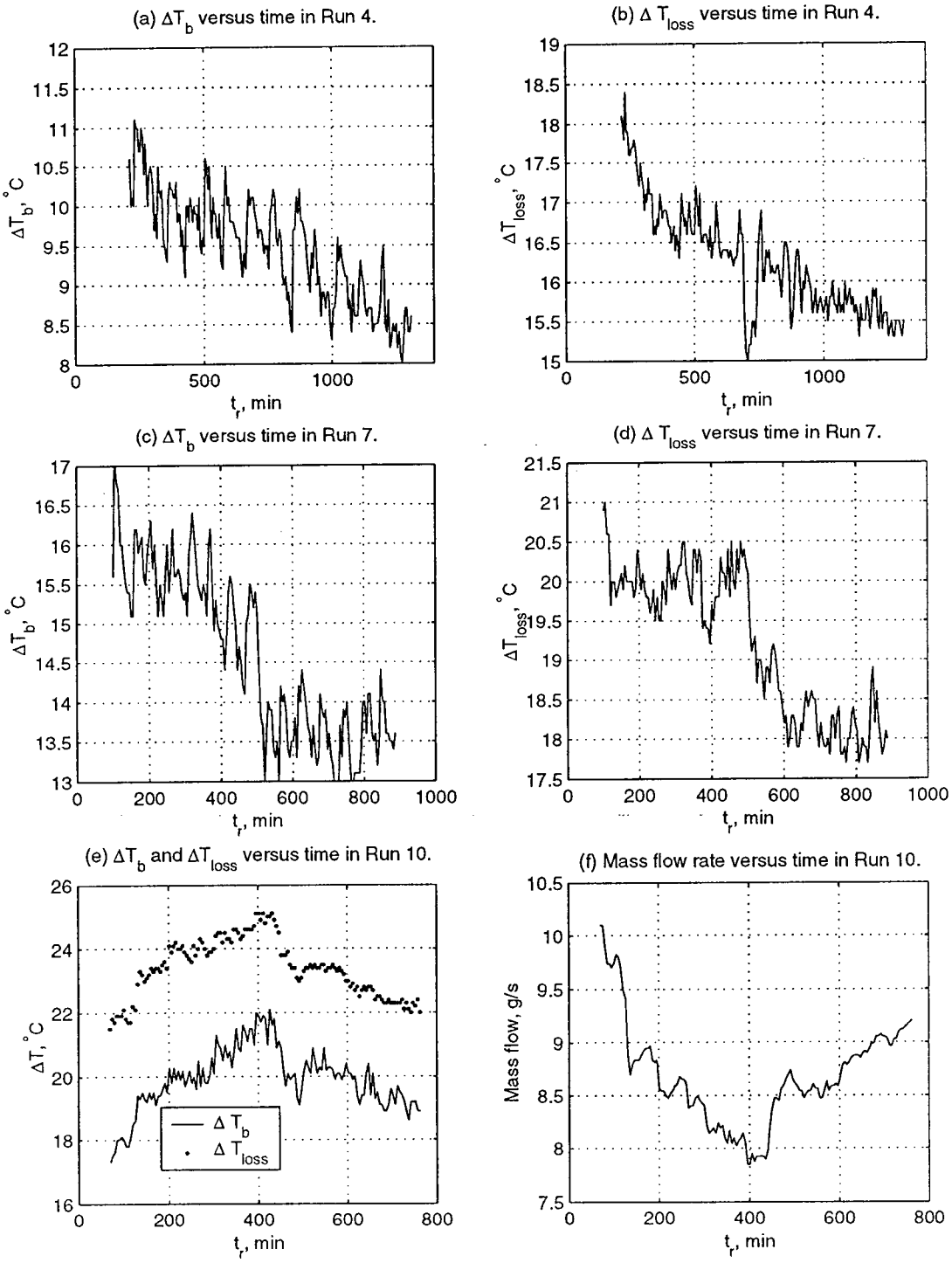

Figure 6.13: Similarity of patterns in ΔT_b, ΔT_{loss} and $\dot{m}$ for Runs 4, 7, and 10.

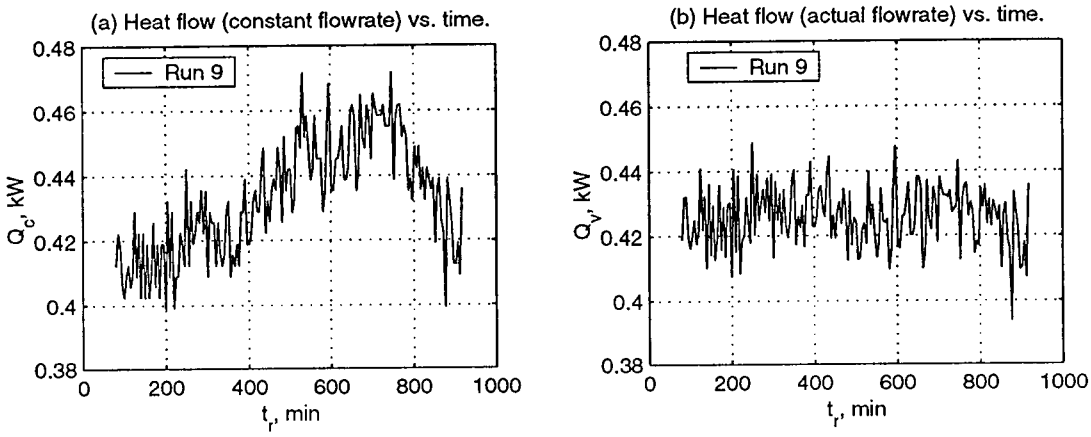

Figure 6.14: Use of variable flowrate approach to reduce the effects of flowrate on Q; for Q_c, the flowrate value measured at the end of the run was is always assumed.

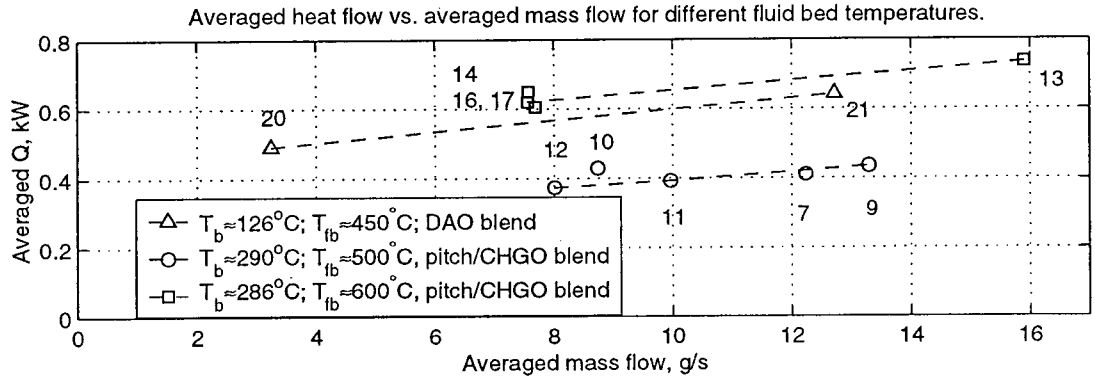

Figure 6.15: Relationship between the heat flow to the test section and the mass flowrate.

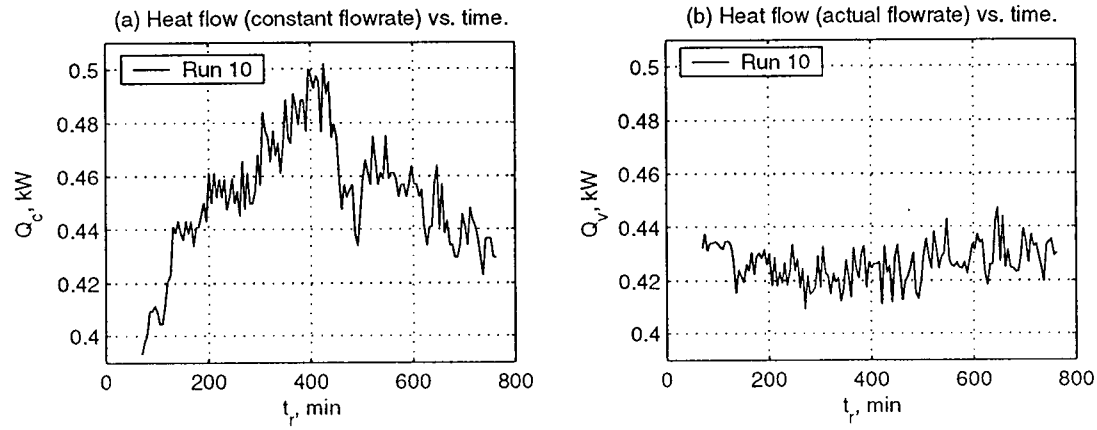

Figure 6.16: Use of variable flowrate approach to reduce the effects of flowrate on Q.

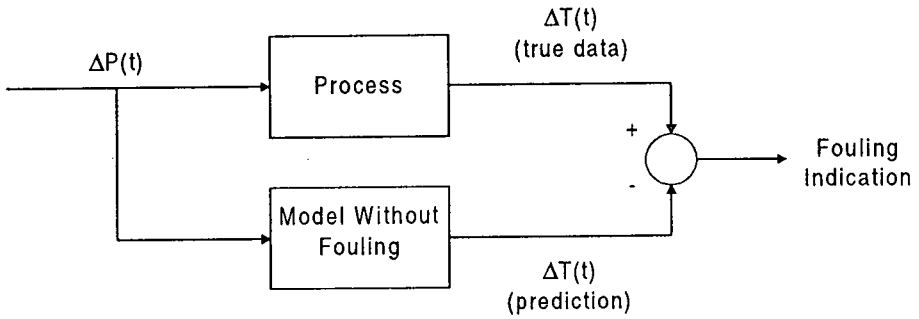

Figure 6.17: Block diagram of principle used to distinguish fouling from flowrate effects.

this principle is shown in Figure 6.17.

The process was modeled according to an output error model structure (ARMA) which belongs to the category of black-box models (see e.g. Box and Jenkins (1970) for more background):

$$\begin{aligned} \Delta T_b(t) &= \frac{B(q)}{F(q)}\Delta P(t) + e(t) \\ F(q) &= 1 + f_1 q^{-1} + \cdots + f_{n_f} q^{-n_f} \\ B(q) &= b_1 q^{-1} + b_2 q^{-2} + \cdots + b_{n_b} q^{-n_b} \end{aligned} \tag{6.11}$$

This model is a representation of linear time-invariant systems and was chosen for simplicity of identification and in the absence of a well-founded physically parametrized model. The purpose of this model was to predict changes in ΔT_b that occur over a relatively long period of time which are signals of low frequency. Therefore, n_b and n_f were taken as one. The parameters are given in Table 6.5 and the application of the model is displayed in Figure 6.18 for three runs. The parameters were determined using a function called 'bj' in Matlab©. The modeling data were taken up to 300 minutes where it was assumed that no fouling had occurred. The negative value of b_1 indicates an inverse relationship between the flowrate and ΔT_b which is consistent with Equations 6.6 and 6.7. Figures 6.18a and 6.18c clearly show that the variation in ΔT_b in Runs 9 and 13 can be predicted from the pressure drop data only; as a result, it can be said that no significant fouling occurred in these experiments. This procedure gave excellent results for these runs, but for some others such as 10, 11, and 12, the predictions were less satisfying (see

Table 6.5: Parameters regressed in Equation 6.11 for some experiments.

Run no.	Modeling Data (min)	Parameters	Standard Error
9	45 – 301	b_1 = -5.3926	1.8
		f_1 = -0.6307	0.15
10	35 – 301	b_1 = -22.1685	3.01
		f_1 = -0.0202	0.13
11	40 – 301	b_1 = -11.2571	1.23
		f_1 = 0.1601	0.11
12	100 – 300	b_1 = -1.2107	0.09
		f_1 = -0.041	0.07
13	75 – 301	b_1 = -0.1161	0.04
		f_1 = -0.9132	0.05

Figure 6.18e). The poor quality of initial data can give rise to incorrect predictions of ΔT_b although no fouling is formed. If initially the data are not rich enough to cause significant changes in ΔT_b, the resulting model will be inacurate and uncertain. This is often the case in fouling experiments since stability of variables is crucial. The greater uncertainty in parameter f_1 in Table 6.5 for Runs 10 to 12 than for the other runs seems to explain the poor predictions obtained. Another factor that can cause poor predictions may be non-linearities between ΔT_b and ΔP especially when large flowrate variations occur. The largest deviation between the predicted and measured ΔT_b in Run 10 (see Figure 6.18e) at 400 minutes is attributed to this. The relationship between ΔT_b and ΔP observed in the modeling data does not represent the data properly outside the range of modeling data.

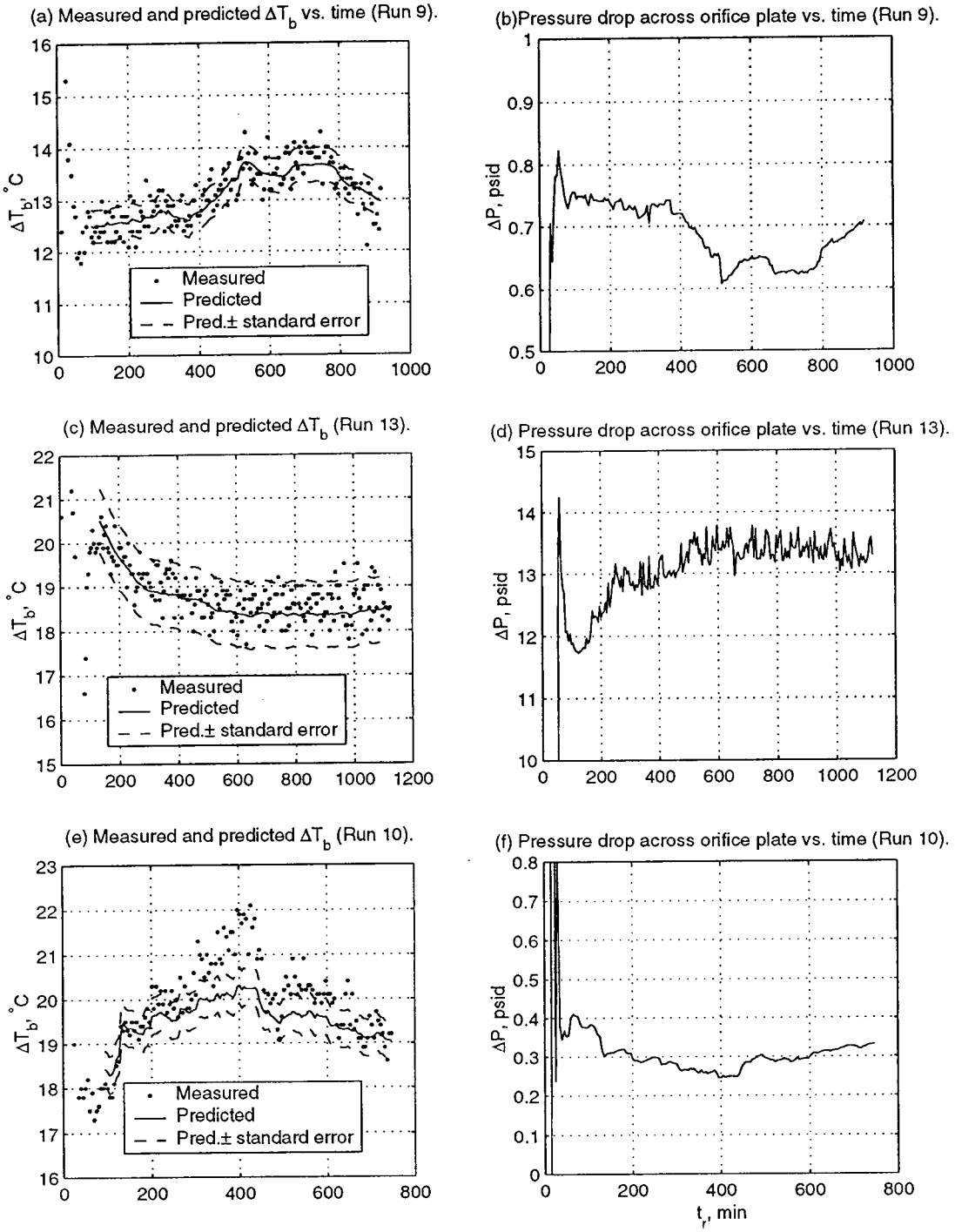

Figure 6.18: Application of ARMA model to predict ΔT_b based on ΔP.

6.2.4 Elimination of Fluctuations

Finding the source of the fluctuations in flowrate discussed in this section has not been straightforward. Several hypotheses were made as to what was causing them and several changes to the fouling unit were implemented to verify those hypotheses. For example, after observing a significant hysteresis problem, the orifice plate and the needle valve used to control the flowrate were replaced after Run 11.

The first bypass design consisted of a needle valve in series with a spring loaded pressure relief valve. During operation of the unit, a fraction of the total flowrate delivered from the pump circulated in the bypass line through the pressure relief valve. The fluctuations in the flowrate were clearly related to the stability of the split fraction of the flowrate between the test section and the bypass. This split fraction depends on the resistance to flow in both sections. After several runs with this bypass configuration, it was postulated that the flowrate fluctuations may be caused by oscillations in the spring of the pressure relief valve causing changes in the resistance to flow in the bypass section. Concerns about the design of the bypass circuit were also raised since liquid was not supposed to flow in the pressure relief valve except under pressure surges (e.g. in case of a test section blockage). In Run 17, in order to test this hypothesis, the needle valve and the pressure relief valve were therefore assembled in parallel as described in Chapter 4 so that no flow would circulate in the relief valve under normal conditions and the excess flow would only return to the tank via the needle valve.

In order to evaluate the change in the stability of the flowrate after modifying the design of the bypass circuit, the standard deviation of the flowrate measurement was calculated for all experiments and the results are shown in Figure 6.19. It can be seen from these results that for the first bypass design, the flowrate was more unstable in experiments with lower flowrates. Also, except for the last two runs, it is clear that the new bypass configuration greatly decreased the flowrate variations and, as a result, the quality of the data was significantly improved. The improvement obtained supports the hypothesis formulated. For the last two runs, it is believed that the poorer stability of the flowrate was again caused by the pressure relief valve. The seals in the pressure relief valve were made of viton which is rated for 204°C maximum and this was the highest

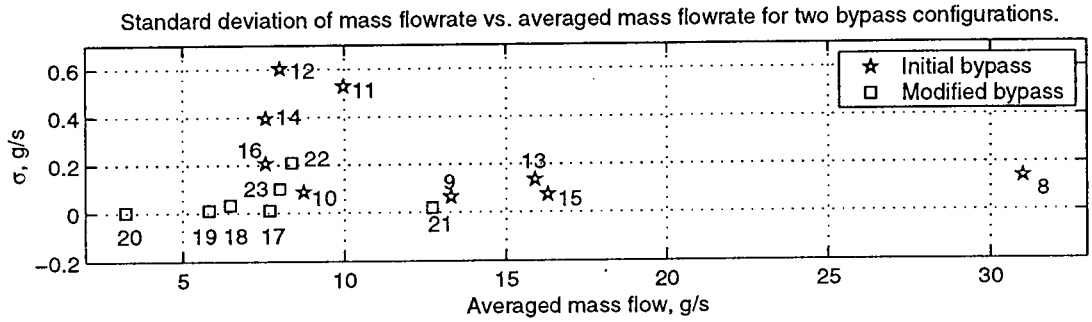

Figure 6.19: Standard deviation of flowrate versus flowrate for two bypass configurations.

rating available from the manufacturer. Now, the last two runs were done under the highest bulk temperatures ever studied (358 and 375°C). It is therefore possible, in those two runs, that the seals had reached a degradation state which allowed liquid to flow through the valve, therefore causing the flowrate variations observed in these runs.

6.2.5 Viscosity Effect

It has been shown in Section 6.2.1 that a relationship exists between the temperature difference between the tank and the test section inlet temperature, ΔT_{loss}, and $\dot{m}$ as shown in Figure 6.10a. Now, Runs 17 and 18 did not exhibit any correlation between ΔT_{loss} and $\dot{m}$ (see Figure 6.20). Although the data for these two runs indicate an increase

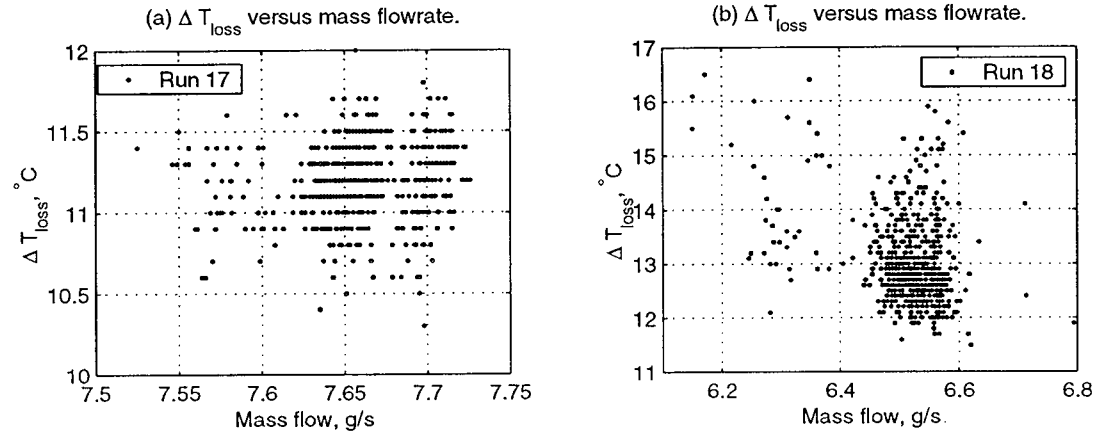

Figure 6.20: Test for correlation between ΔT_{loss} and $\dot{m}$ for Runs 17 and 18.

in ΔT_{loss}, which suggests a decrease in flowrate, the flowrate measurement appeared to be relatively constant, as shown in Figure 6.21.

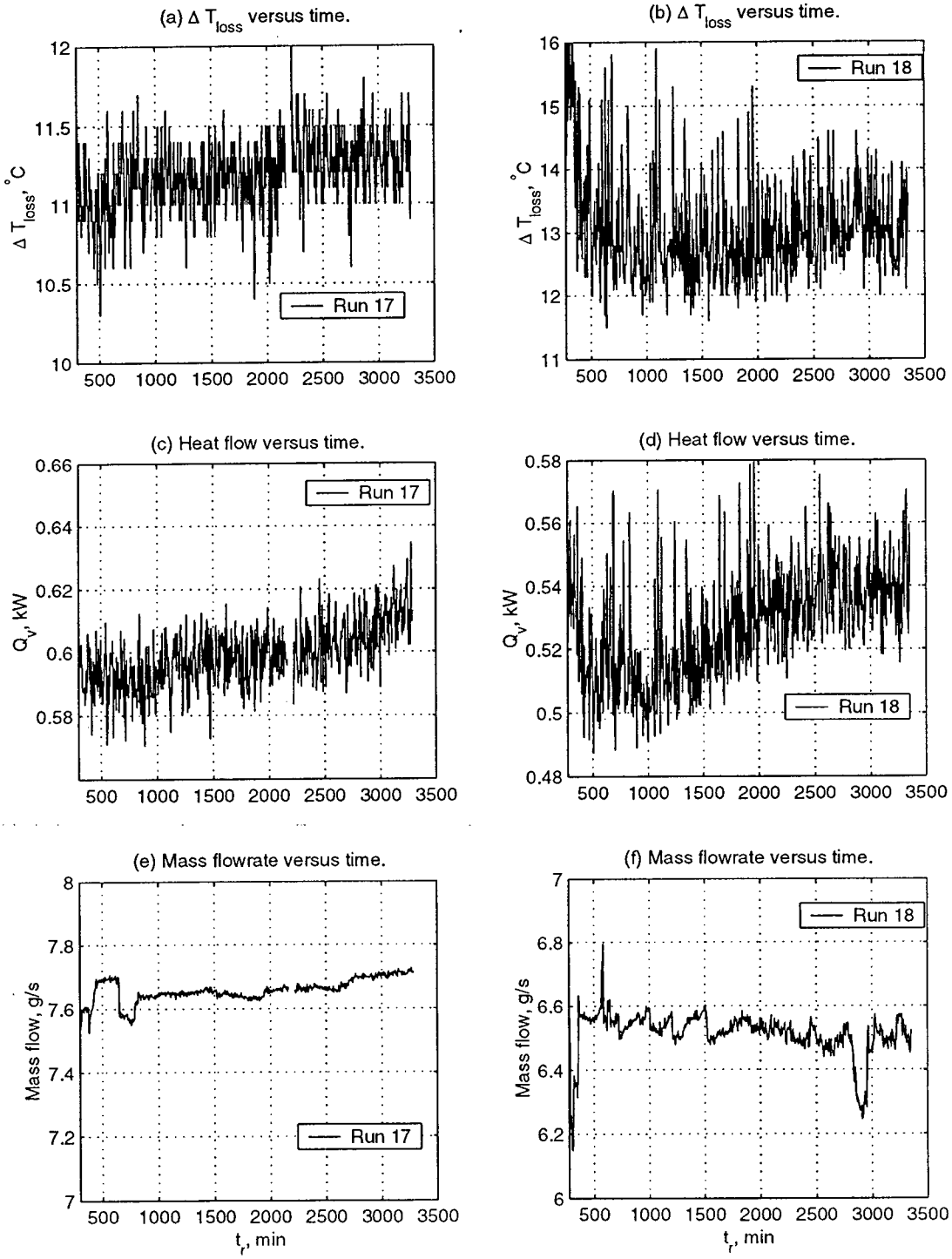

Figure 6.21: ΔT_{loss}, heat flow and mass flow measurements for Runs 17 and 18.

Now, the viscosity measurement for the initial and final samples obtained at 80.4°C for several experiments indicates that these two runs experienced the greatest drop in viscosity as shown in Figure 6.22. This viscosity reduction may be due to chemical

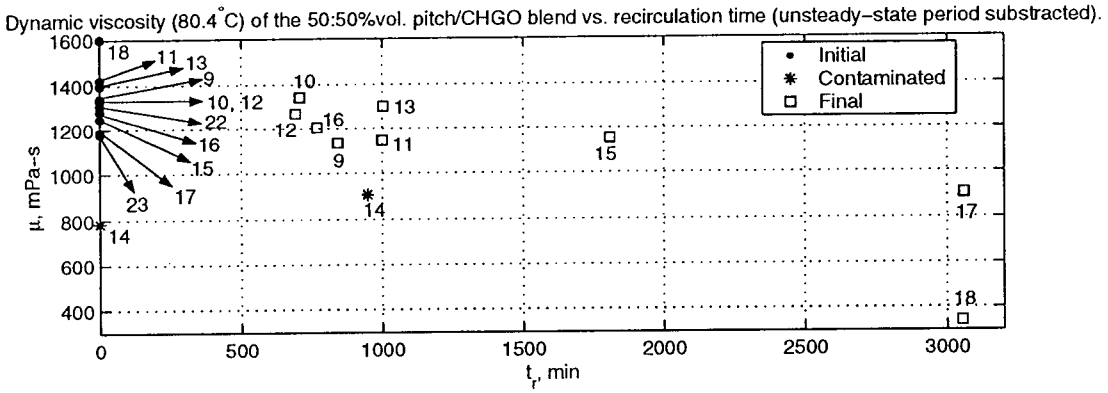

Figure 6.22: Viscosity drop during recirculation of test fluid.

changes in the liquid, called visbreaking (see Gray (1994)). The mass flowrates were calculated from the orifice plate equation:

$$\dot{m} = C \cdot \frac{\pi D_{th}^2}{4} \cdot \left(\frac{2\rho \Delta P}{1 - \beta^4} \right)^{1/2} \tag{6.12}$$

where C is the discharge coefficient, D_{th} is the diameter of the orifice throat ($= 1.588 \times 10^{-3}$ m), ρ is the density of the test fluid, ΔP is the pressure drop, and β is a diameter ratio ($= 0.1$). The discharge coefficient was measured and the results are shown in Figure 6.23. The data suggest a slightly decreasing trend with Reynolds number and this is consistent with the data reported in Perry and Green (1984) for this range of Reynolds number. During an experiment, all parameters in Equation 6.12 are expected to be constant such that the mass flowrate will be constant too. However, if the viscosity drops during recirculation of the fluid, Figure 6.23 predicts that the discharge coefficient would decrease, thereby causing a drop in the flowrate if the ΔP was held constant. This effect is in agreement with the observed increases in ΔT_{loss} in experiments 17 and 18 (Figure 6.21) which suggest a decrease in flowrate.

Since C is a non-linear function of Re_{th}, as shown in Perry and Green (1984), the data of Figure 6.23 were fitted to the following equation shown as a line in the same figure

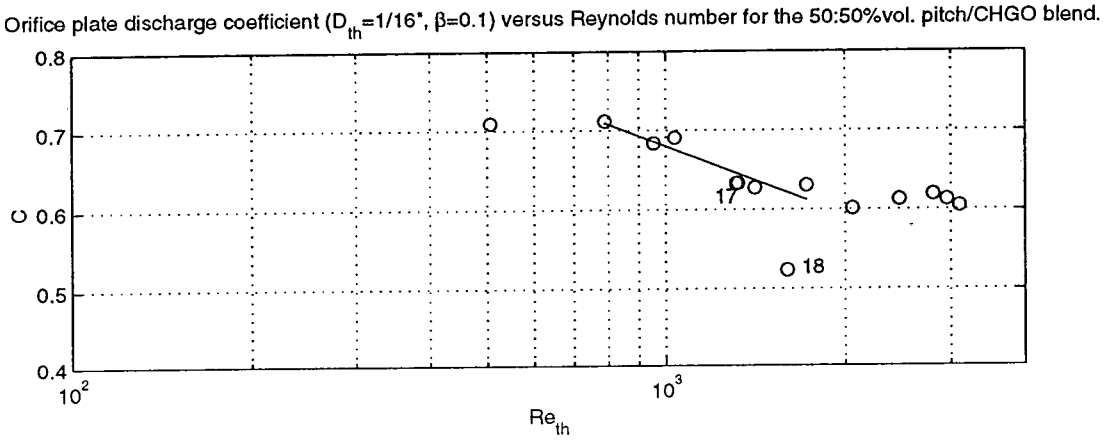

Figure 6.23: Discharge coefficient vs. Reynolds number for the 1/16" diam. orifice plate.

only over the narrow range of Reynolds number that included these two experiments:

$$\begin{aligned} C &= -0.287 \cdot log(Re_{th}) + 1.542 \\ Re_{th} &= \frac{4\dot{m}}{\pi \rho D_{th} \nu} \end{aligned} \tag{6.13}$$

Equation 6.12 can now be rearranged as:

$$\dot{m} = \left[-0.287 \cdot log \frac{4\dot{m}}{\pi \rho D_{th} \nu} + 1.542 \right] \cdot \left(\frac{\pi D_{th}^2}{4} \right) \cdot \left(\frac{2\rho \Delta P}{1 - \beta^4} \right)^{1/2} \tag{6.14}$$

The relative change in $\dot{m}$ during a run can be expressed as:

$$\left(\frac{\dot{m}_f - \dot{m}_0}{\dot{m}_f} \right) = \frac{-0.287 \cdot log \left(\frac{\dot{m}_f \cdot \nu_0}{\dot{m}_0 \cdot \nu_f} \right)}{-0.287 \cdot log \left(\frac{4\dot{m}_f}{\pi \rho D_{th} \nu_0} \right) + 1.542} \tag{6.15}$$

where the subscripts 0 and f refer to initial and final respectively, and where ρ is given by Equation 3.2 and ν_0 by Equation 3.9 in which A, B, and C are given in Table 3.4 for the 50:50%vol. blend (Dutt equation). The corrected initial viscosity at T_{in}, $\nu_{0,cc}$, was calculated by correcting the calculated initial viscosity at T_{in}, $\nu_{0,c}$, by a percentage obtained from the calculated and measured initial viscosities at 80.4°C, $Change_{cm}$. The corrected final viscosity at T_{in}, $\nu_{f,cc}$, was calculated by correcting the corrected initial viscosity at T_{in}, $\nu_{0,cc}$, by a percentage obtained from the measured initial and final viscosities at 80.4°C, $Change_{0f}$. The results are given in Table 6.6.

Table 6.6: Measured and calculated initial and final viscosities for Runs 17 and 18.

		80.4°C					T_{in}	
Run no.	T_{in} (°C)	†$\nu_{0,m}$ (mm²/s)	$\nu_{0,c}$ (mm²/s)	$Change_{cm}$ (%)	$\nu_{f,m}$ (mm²/s)	$Change_{0f}$ (%)	$\nu_{0,cc}$ (mm²/s)	$\nu_{f,cc}$ (mm²/s)
17	286	1196	1199	0.3	911	23.8	5.27	4.02
18	329	1611	1199	-34.4	345	78.6	5.08	1.09

†m: measured; c: calculated; cm: calculated to measured; 0: initial; f: final; $0f$: initial to final; cc: corrected.

The value of the initial flowrate, $\dot{m}_0$, was searched by trial and error and a satisfactory value was obtained by minimizing the absolute value of the difference between the left and the right hand sides of Equation 6.15. The value of the final flowrate was measured at the end of each run. Table 6.7 gives the results of these calculations as well as the predicted change in $\dot{m}$ based on the change in ΔT_{loss}, which is based on Equation 6.10:

$$\Delta\dot{m}_{\Delta T_{loss}} = \left(\frac{\overline{\Delta T}_{loss,I}}{30.9}\right)_0^{-\frac{1}{0.49}} - \left(\frac{\overline{\Delta T}_{loss,I}}{30.9}\right)_f^{-\frac{1}{0.49}} \tag{6.16}$$

Table 6.7: Predicted decreases in flowrate in Runs 17 and 18 based on two approaches.

Run no.	LHS	RHS	|LHS-RHS|	$\dot{m}_f$ (g/s)	$\dot{m}_0$ (g/s)	$\Delta\dot{m}_\nu$ (g/s)	$\Delta\dot{m}_{\Delta T_{loss}}$ (g/s)
17	-0.044	-0.044	4.46×10^{-10}	7.69	8.03	0.34	0.23
18	-0.251	-0.251	8.66×10^{-10}	6.47	8.09	1.62	0.43

It can be observed that both methods predict a decrease in flowrate. The deviation between these predictions may be partly due to uncertainties in Equation 6.10 which arise from an insufficient number of data used to derive it. For Run 18, the greater deviation may be attributed to the fact that the data in Run 18 are more noisy as seen on Figure 6.21. Also, Equation 6.10 represents data obtained for a bulk temperature of around 286°C which is different from the bulk temperature in Run 18 (329°C). Moreover, the slope of the fitted line in Figure 6.23 may be higher than the actual slope since, under the Reynolds number of Run 18, the slope appears to be decreasing. This is consistent with the results reported in Perry and Green (1984) which also exhibit a decreasing slope. A smaller slope would have resulted in a smaller value of $\Delta\dot{m}_\nu$ for Run 18.

Based on these results, it is possible that the drops in viscosity in these two experiments have caused a slight decrease in flowrate and, as a result, the temperature difference across the test section increased. Since the flowrate is based on a pressure drop across an orifice plate, which was maintained constant, an apparent increase in the heat flow was observed for these runs. Consequently, it appears that monitoring and controlling the viscosity during recirculation of these heavy hydrocarbon streams may be crucial for the correct interpretation of the fouling data.

6.3 Heat Transfer in a Bubbling Fluidized Bed

As discussed in Chapter 2, in order to estimate the relative importance of the different resistances between the fluidized bed and the flow of liquid inside the test section, three tests were performed in which wall temperature measurements were made, as described in Chapter 4. In Runs 16 and 20, measurements were obtained for a series of gas flowrates, but for Run 23, only one gas flowrate was used. In this section, the experimental values of fluidized bed heat transfer coefficients obtained in these tests will be compared to the predictions of calculation methods introduced in Chapter 2. Also, the characterization of the test fluids of Chapter 3 allowed the use of different correlations available to estimate the clean heat transfer coefficient inside the test section.

6.3.1 Heat Transfer Coefficient Around an Immersed Tube

The measured heat transfer coefficients for the three tests are compared with the predictions of some of the correlations given in Chapter 2 in Figures 6.24 and 6.25. For Runs 16 and 23, only the correlation by Molerus et al. (1995) was tested. It is well known that in the intermediate range of $10^2 < Ar < 10^5$, h_o goes through a maximum at some intermediate gas velocity, which is consistent with our results (see e.g. Kunii and Levenspiel (1991) and Molerus et al. (1995)). The decreasing h_o at higher superficial gas velocities was attributed by Kunii and Levenspiel (1991) to more contact time with bubbles with their low h values.

The percentage deviation of the experimental h_o from the predicted values is given

in Table 6.8 for the three experiments. The correlation by Vreedenburg (1960) deviates

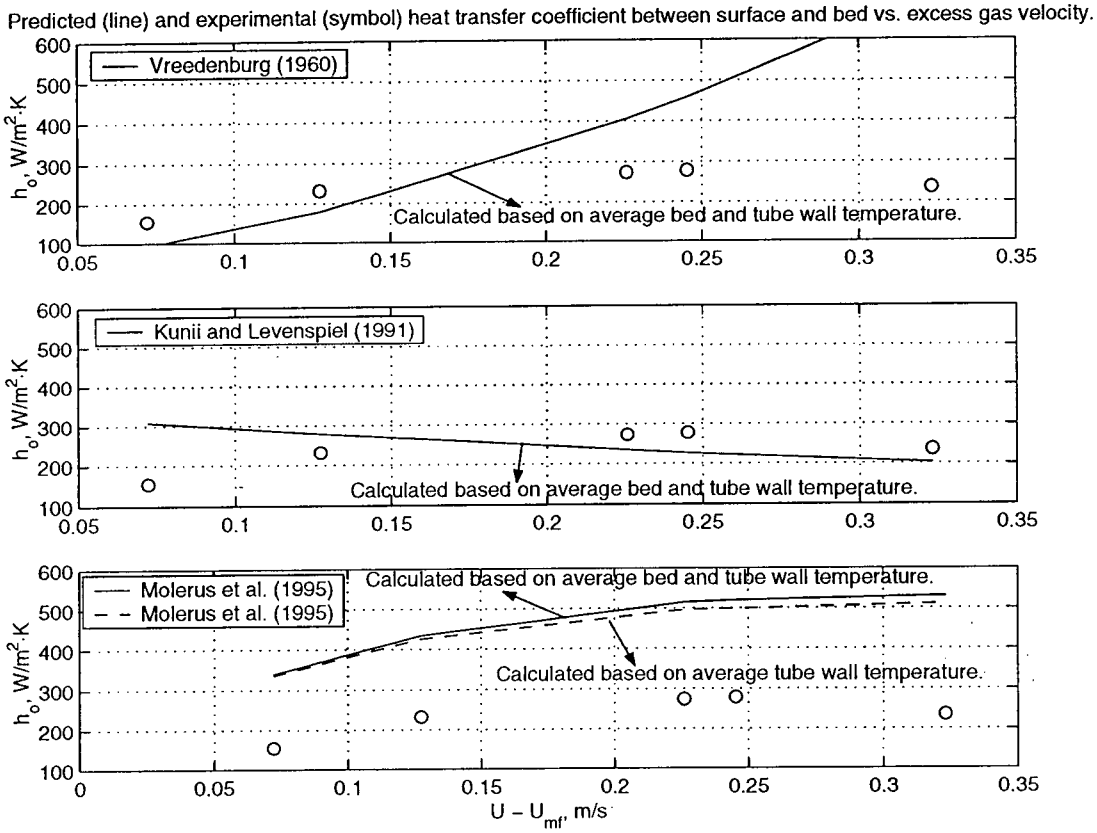

Figure 6.24: Measured and predicted h_o according to different methods for Run 20.

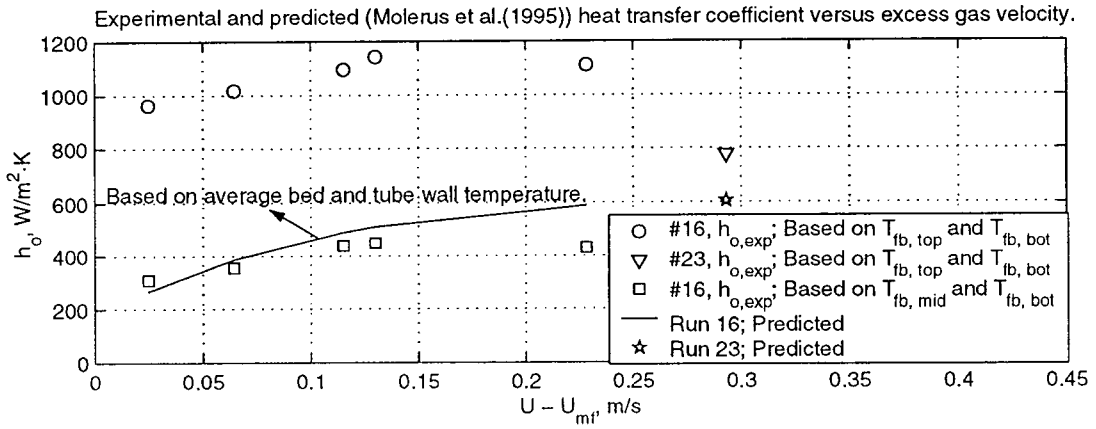

Figure 6.25: Measured and predicted h_o according to Equation 2.19 for Runs 16 and 23.

Table 6.8: Experimental and predicted h_o from various methods.

	Measured		Molerus et al. (1995)		Kunii and Levenspiel (1991)		Vreedenburg (1960)	
Run no.	U-U$^{\dagger}_{mf}$ (m/s)	h_o (W/m^2·K)	$\hat{h}_o$ (W/m^2·K)	‡Dev. (%)	$\hat{h}_o$ (W/m^2·K)	Dev. (%)	$\hat{h}_o$ (W/m^2·K)	Dev. (%)
20	0.0722	155	339	54	309	50	92	67
	0.1274	233	435	46	280	17	179	30
	0.2260	273	514	47	236	16	406	33
	0.2453	278	519	46	227	22	459	39
	0.3231	236	530	55	203	16	706	67
16	0.0248	309	266	16				
	0.0644	354	387	8				
	0.1152	438	489	10				
	0.1299	449	510	12				
	0.2282	430	589	27				
23	0.2931	776	606	28				

†U_{mf}: minimum fluidization velocity (see Appendix D.3); U-U_{mf} is excess gas velocity. ‡Dev. is deviation.

significantly from the data and does not predict a maximum as found in their experimental data. Saxena (1989) attributed this deficiency of the correlation to an absence of a particle concentration term $(1 - \epsilon)$. The correlations of Vreedenburg (1960) underestimated the data of Verma and Saxena (1983), the experimental values being about three times the calculated values. This is not the case for the data of Run 20. Note that the correlation by Wender and Cooper (1958), which was found by Verma and Saxena (1983) to reproduce their data best, could not be tested here because of a lack of information for the bed voidage, ϵ. The deviations of experimental data from the model proposed by Kunii and Levenspiel (1991) were smaller, although a maximum could not be predicted. This may be attributed to the lack of data for the bubble frequency at various gas flowrates, n_w.

The correlation by Molerus et al. (1995) reproduced best the qualitative trend of the experimental data, although the values were significantly lower for Run 20. The agreement for Run 23 is much better. For Run 16, the experimental coefficient, h_o, was obtained using two different sets of wall temperatures. Usually, the log mean temperature difference, LMTD, involved in the calculation of h_o was based on the bulk inlet and outlet temperatures and on the wall and the sand temperatures at the top and bottom

axial positions described in Chapter 4. This was the case for Runs 20, 23, and 16 (circle symbol). However, the temperature difference between the sand and the tube wall of the top axial position in Run 16 appeared to be too small compared to the other temperature drops observed. This is shown in Table 6.9. For that reason, the heat transfer

Table 6.9: Bed-to-wall temperature difference at three axial positions (Runs 16, 20, 23).

Axial position	# 16	# 20	# 23
top	15	175	70
middle	180	210	40
bottom	100	220	84

coefficient in Run 16 was recalculated using the middle and bottom bed temperatures measurements. The results, shown as squares on Figure 6.25, are more consistent with the predicted coefficient, $\hat{h}_o$. The deviations now range from -6% to +27% which is quite resonable given the accuracy of the available correlations. This suggests that the wall temperature measurement at the top of the bed in Run 16 was not correct. The h_o values for Run 16 marked with a circle are clearly too high. From these results, it is suspected that the wall temperature measurement may not necessarily give the actual wall temperature. Three new thermocouple wires were silver-soldered for each test, resulting in three welding "lumps" on the test section. It is likely that the variability in the position of the thermocouple tip in this spot will cause some error in the measurement. In some cases, the thermocouple tip was just on the top of the lump while sometimes it was deeper in the test section. Also, in each test, the spot was covered with sintered quartz sand. This may have increased the thermal resistance between the fluidized bed and the wall.

The significantly higher temperature gradients measured in Run 20 may have been caused by this phenomenon, therefore causing the measured h_o to be lower than the prediction. Usually, $\hat{h}_o$ is calculated under the conditions of an average fluid bed temperature between the wall and the bed temperatures. For Run 20, $\hat{h}_o$ was also calculated assuming the bed to be under the conditions of the average wall temperature only. The results are shown as a dashed line in Figure 6.24. This clearly does not account for the discrepancy

between the experimental and the predicted values. The accuracy of the correlations by Molerus and Mattmann (1992) and Molerus et al. (1995) was also tested with a set of independent data obtained by Makhorin and Kharchenko (1964) with a spherical probe immersed in 80-cm deep and 22-cm diameter air fluidized bed of quartz sand ($d_p = 0.34$ mm). The results are shown in Figure 6.26 and illustrate the accuracy of both correlations. Note that the diameter of particles was between 0.25 and 0.50 mm, which is considered a narrow size distribution. Based on these results, it seems reasonable to expect our data

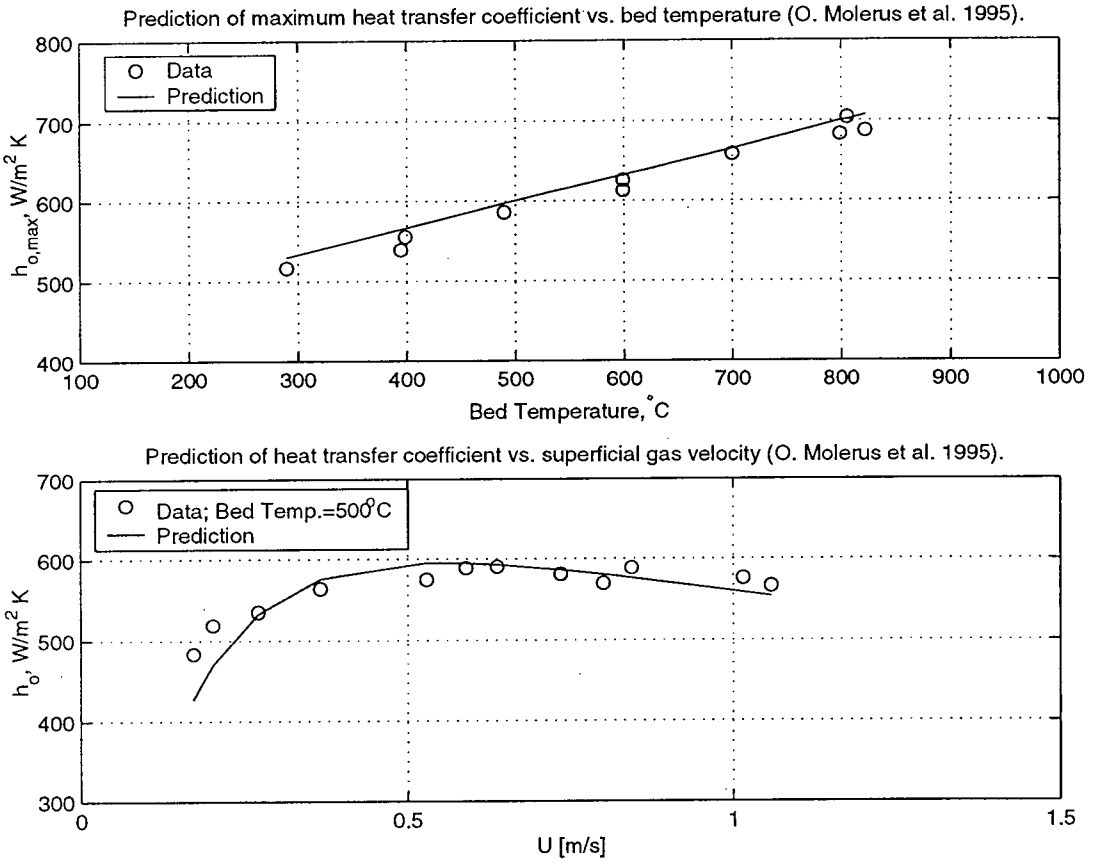

Figure 6.26: Fit by Equations 2.19 and 2.24; data from Makhorin and Kharchenko (1964).

for Run 20 to be lying somewhere between the data for 300°C and 500°C.

Molerus and Wirth (1997) have used data from Janssen (1973) obtained with quartz sand ($d_p = 0.58$mm) in air (horizontal tube) to illustrate the accuracy of their correlation 2.19. The results are shown in Figure 6.27 for various bed temperatures. As can be seen, at a 400 °C bed temperature and a particle size of $d_p = 0.58$ mm, a maximum heat

transfer coefficient close to h_o=400 W/m^2·K has been measured. Now, it is well known that the heat transfer coefficient decreases with particle size in the regime of $d_p \approx 100$ μm

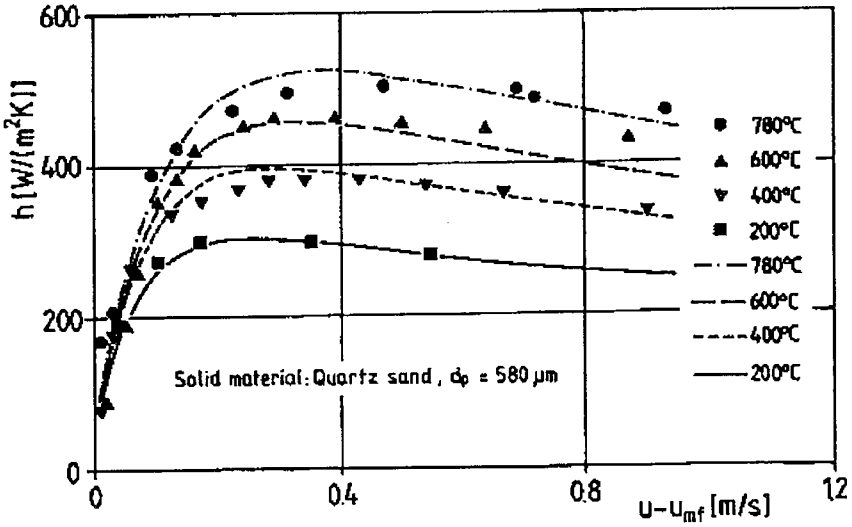

Figure 6.27: Experimental (symbols) with air at varying bed temperatures and predicted h_o (Equation 2.19); reproduced from Molerus and Wirth (1997) with permission.

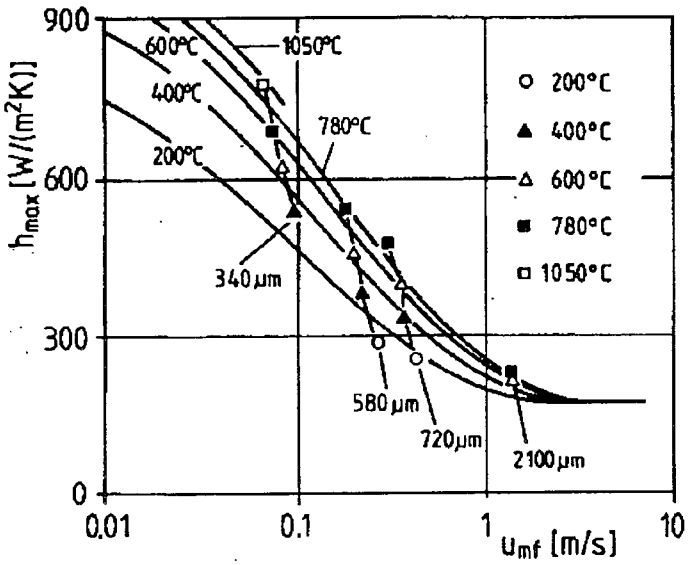

Figure 6.28: Experimental and predicted $h_{o,max}$ (Equation 2.24) at different levels of temperature; reproduced from Molerus and Wirth (1997) with permission.

up to 1 mm. Figure 6.28 shows measured maximum heat transfer coefficients at 400°C for a particle size of d_p=0.34 mm in the order of $h_{o,max}$ ≈500 W/m^2·K. This suggests that our results for Run 20 may be too low.

Moreover, as seen in Figures 6.24 and 6.25, the predicted maximum coefficient does not occur at the same gas velocity as for the experimental data. The prediction is still increasing while the data is decreasing. Now, in both tests a loss of sand from the bed was observed for the highest gas flowrate. The premature decrease in h_o may be attributed to a reduction in the heat flow caused by this loss of sand. This behavior may not occur when using a more narrow particle size range as is generally the case for the data used to derive such correlations. With a wide particle distribution such as used here (Figure C.1), the fine particles may be entrained while this is not the case with a narrow size range.

Table 6.10 contains the measured and predicted maximum heat transfer coefficient, $h_{o,max}$ and $\hat{h}_{o,max}$ respectively, using the correlations given in Chapter 2. It can be seen that all correlations point to the fact that a higher value for $h_{o,max}$ would have been expected for both runs. This may be partly attributed to some error in the temperature measurement as explained above. Also, according to Figures 6.24 and 6.25 it is clear that $\hat{h}_{o,max}$ occurs at a higher gas velocity than in the measurements. This may be due to the loss of sand during the measurement which may not occur when a narrow size distribution is used.

Table 6.10: Measured, and predicted $h_{o,max}$ from various correlations for Runs 16 and 20.

Run no.	Measured	Zabrodsky	Varygin et al.	Grewal and Saxena	Molerus
16	449	641	572	698	651
20	336	518	464	568	531

Finally, it is interesting to consider the instantaneous heat transfer coefficient, h_{inst}. Mickley et al. (1961) reported values at a point on a 6.35-mm tube located along the axis of a 0.1-m fluidized bed of 43–320 μm particles and found sharply varying values, as shown in Figure 6.29. Baskakov et al. (1973) also obtained similar data. Kunii and Levenspiel (1991) saw this behavior as evidence for the fact that the exchanger surface is

bathed alternately by gas bubbles (very low h_{inst} values) and by emulsion packets (high h_{inst} values). The relatively high magnitude of the noise in our thermal fouling data may be attributed to this phenomenon.

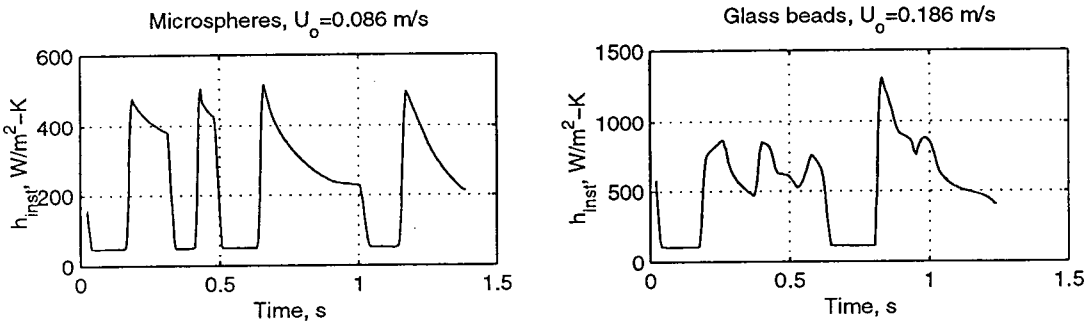

Figure 6.29: Instantaneous h on a vertical tube; adapted from Mickley et al.(1961).

6.3.2 Clean Coefficient For The Oil

The heat transfer between a pipe and the fluid flowing within it is determined either singly or in combination by two mechanisms, namely, forced convection and natural convection. In most process plant heat exchangers where the fluid is pumped through the system at relatively high velocity, the effects of natural convection are, therefore, insignificant.

In laminar flow, the distances required to attain the fully developed thermal boundary layer (thermal entry length, L_{e_T}) and hydrodynamic boundary layer (hydrodynamic entry length, L_e) are given by:

$$\left(\frac{x_{fd,T}}{D_i}\right)_{lam} = L_{e_T} \approx 0.05RePr \tag{6.17}$$

$$\left(\frac{x_{fd,H}}{D_i}\right)_{lam} = L_e \approx 0.05Re \tag{6.18}$$

For our test section with a non-heated entry length of about 40 cm, it was possible to treat the velocity profile as fully developed throughout the thermally developing region. Moreover, the Graetz number, defined as

$$Gz = \frac{D_i}{x}RePr \tag{6.19}$$

is an important parameter in the analysis of developing boundary layer phenomena. The thermal boundary layer is fully developed when Gz^{-1} has a value of about 0.05, which is the origin of Equation 6.17. Correlations with a fully established velocity profile for a developing temperature boundary layer ($Gz^{-1} < 0.05$) were compared with our experimental results obtained in Runs 16, 20, and 23. These correlations have usually been derived on the basis of constant fluid properties and the mean fluid temperature, $\overline{T}_b = (T_{b,in} + T_{b,out})/2$, was used in calculating the nondimensional parameters.

Gnielinski (1983) proposed the following Nusselt number ($\overline{Nu} = h_i \cdot D_i/k_l$) based on the average heat transfer coefficient over the length 0 to x for a uniform wall temperature

$$\overline{Nu} = 1.61 Gz^{1/3} \qquad Gz > 10^3 \tag{6.20}$$

For the constant surface temperature condition, Kays (1955) presents a correlation which presumes a thermal entry length and is of the form

$$\overline{Nu} = 3.66 + \frac{0.0668(D_i/L)RePr}{1 + 0.04[(D_i/L)RePr]^{2/3}} \tag{6.21}$$

where L is the heated length of the test section. The best results were obtained from a correlation proposed by Obot et al. (1997) who reported heat transfer data in laminar flow for the 0.7 to 126 Prandtl number range:

$$\overline{Nu} = 0.0086 Re^{3/2} \left(\frac{16}{Re}\right) Pr^{0.4} \tag{6.22}$$

From the knowledge of the measured heat transfer coefficient in the fluidized bed, h_o, of the wall resistance, and of the overall coefficient, U_o, the inside heat transfer coefficient, h_i, was calculated. Equation 6.22 was used to predict the average heat transfer coefficient inside the tube, $\hat{h}_i$, and the results are given in Tables 6.11 and 6.12. The values of heat capacity and thermal conductivity required in the calculation of the Prandtl number were obtained from Cassis et al. (1985) and Perry and Green (1984) respectively. It is shown that the flow is laminar and there is a fully developed hydrodynamic boundary layer with a developing temperature boundary layer over the whole length of the 46-cm heated section. Table 6.12 indicates that there is a significant deviation between experimental and predicted h_i, especially for Run 20. Now, if we use the correlation 2.19 proposed by Molerus et al. (1995) to calculate h_o, we can deduce the heat transfer inside the tube, $h_{i,M}$,

Table 6.11: Parameters involved in the calculation of $\hat{h}_i$.

Run no.	$\overline{T}_b$ (°C)	$x_{fd,T}$ (cm)	$x_{fd,H}$ (cm)	Re	Pr	$Gz^{-1} \times 10^3$
16	303	934	12	465	78	2.43
20	132	326	7	266	47	6.96
23	376	1073	22	824	49	2.26

Table 6.12: Measured (h_i), and predicted ($\hat{h}_i$) coefficient from Equation 6.22.

Run no.	h_i (W/m^2·K)	$\hat{h}_i$ (W/m^2·K)	Dev. (%)	$h_{i,M}$ (W/m^2·K)	Dev. (%)
16	498	408	22	451	11
20	530	252	110	293	16
23	407	444	-8	460	3

knowing the overall heat transfer coefficient U_o. The results, given in Table 6.12, become much more consistent with the predicted h_i. This reinforces the validity of Molerus's correlation and the possibility of an error in the wall temperature measurement.

Finally, Table 6.13 gives the inverse overall heat transfer coefficient based on the external surface area of the test section, $1/U_o$, and the relative importance of each of the individual resistances with respect to the total resistance. The relatively high resistance from the fluidized bed (average=38% of the total) may reduce the sensitivity of the fouling unit to detect a change in the overall heat transfer coefficient that would result from fouling.

Table 6.13: Total, and fractional tube side and shell side resistances[‡].

Run no.	Total $^{\dagger}U_o^{-1} \times 10^3$	Tube/Total $A_o/(A_i h_{i,M} U_o^{-1})$	Shell/Total $1/(h_{o,M} U_o^{-1})$
16	4.703	0.56	0.43
20	6.024	0.67	0.32
23	4.258	0.61	0.39

†(W/m^2·K); ‡Tube wall resistance is less than 1% in these runs.

6.4 Analysis of Variations in Fluidized Bed

6.4.1 Power Spectral Density

In order to identify undesirable oscillations in process variables, their frequency, their relative importance, and their effects on the fouling data, the measurements were decomposed by using a Fourier method called Fourier transform (FT). For a signal that is both discrete and periodic, the appropriate transform is the discrete Fourier transform (DFT). The DFT of the sequence $\{x_t\}$, $t = 0, 1, \ldots, N-1$ is given by

$$X(n) = \sum_{t=0}^{N-1} x_t W_N^{-nt}, \qquad n = 0, 1, \ldots, N-1 \tag{6.23}$$

$$W_N = exp\left(j\frac{2\pi}{N}\right) \tag{6.24}$$

This material is covered in many textbooks on digital signal processing such as Roberts and Mullis (1987). The DFT was computed using a fast algorithm implemented in Matlab© called fast Fourier transform (FFT). The frequency content of a signal y_t can be estimated from a periodogram $\hat{S}_p(\theta)$ which is an estimate of the power spectral density $S_p(\theta)$. In practice, only a sample of the entire periodogram is computed. A set of equally spaced samples of $\hat{S}_p(\theta)$ can be obtained from the FFT algorithm for the DFT. Let $N \geq L$ be a power of two, and let $\theta_0 = 2\pi/N$.

Then

$$\hat{S}_p(n\theta_0) = \frac{1}{L}\left|\sum_{t=0}^{N-1} y_t w_t e^{-jtn\theta_0}\right|^2 = \frac{1}{L}\left|\sum_{t=0}^{N-1} x_t W_N^{-tn}\right|^2 = \frac{|X(n)|^2}{L} \tag{6.25}$$

where

$$\begin{aligned} x_t &= y_t w_t, \qquad 0 \leq t \leq L-1 \\ &= 0, \qquad L \leq t \leq N-1 \end{aligned} \tag{6.26}$$

$$\begin{aligned} w_t &= 1, \qquad 0 \leq t \leq L-1 \\ &= 0, \qquad \text{otherwise} \end{aligned} \tag{6.27}$$

This tool was applied to all experiments and the results for Run 5 are given in Figure 6.30 as an example, plotted up to the Nyquist frequency. In Runs 3 to 7, a periodic

variation in the air flowrate fluidizing the bed was observed, although its origin had not yet been identified. This resulted in oscillations of several process variables such as the temperature of the air entering the fluidized bed, T_{air}, the fluid bed temperatures, and the heat flow. This is shown in Figure 6.30 by the major peaks at around 0.1 and 0.2 rad/min. The period ($p = 2\pi/\theta$ min.) corresponding to the first and second peaks was calculated and the results are given in Table 6.14. It can be noticed that, for a given run, the major fluctuations all have the same period, whose origin was the air building compressor as will be shown later. Also, the air flowrate had at least two important oscillations whose frequency varied from run to run. The variation in the air flowrate caused a corresponding variation in the heat transfer coefficient in the fluidized bed as discussed in the last section and as a result, the heat flow fluctuated. The temperature measurements at the top and bottom of the fluid bed were usually more affected than

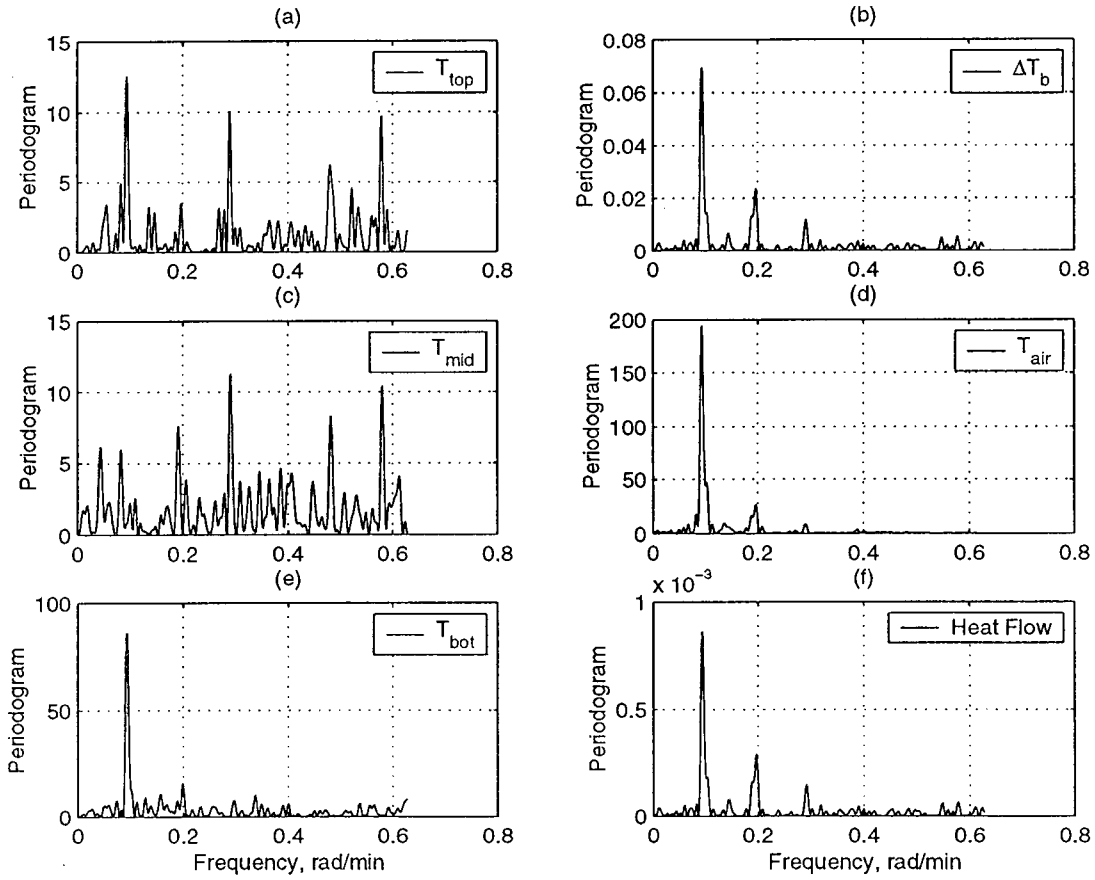

Figure 6.30: Samples of the periodogram obtained from the FFT (Data from Run 5).

Table 6.14: Magnitude and period of the peaks identified in Runs 3 to 7.

Run no.	T_{air}		Q		T_{top}		T_{mid}		T_{bot}	
	T (min)	Mag. ($°C^2$)	T (min)	Mag.$\times 10^4$ (kW^2)	T (min)	Mag. ($°C^2$)	T (min)	Mag. ($°C^2$)	T (min)	Mag. ($°C^2$)
3	37	92	38	1.05	37	31	26	3	36	22
4	73	352	72	4.56	71	5	22	4	73	319
	36	102	36	1.87	32	2	31	1	36	80
5	67	195	67	8.60	67	13	144	6	67	86
	32	26	32	2.83	32	3	33	8	31	15
6	66	212	66	9.90	66	8	65	6	65	45
	32	35	32	1.99	32	5	30	8	32	14
7	61	42	62	1.67	24	1	34	3	53	1
	53	74	53	1.26	-	-	-	-	-	-

the middle temperature as shown in Figure 6.30 and Table 6.14. Also, the second peak was not significant for all the runs. It is interesting to note that the fluctuation in heat flow may not be detected from the fluid bed temperature measurements as shown by Run 7 and others. Finally, after Run 8 the fluctuations in air flowrate were reduced and no other significant oscillations were detected.

6.4.2 Elimination of Fluctuations

To reduce the effect of air flow oscillations on fouling data, two approaches were taken. In the first one, a band-stop filter was designed specifically to remove the major oscillations from the data and in the other approach, the effect of the fluctuations was minimized.

In the discussion of filters, signals are viewed as a collection of signal components with different frequencies. A filter is designed to accept certain frequencies and reduce other frequencies. The Bodé diagram indicates which frequency components the filter reduces and how much each component is reduced. In this section, the design and application of a band-stop filter to eliminate the fluctuations discussed previously are demonstrated.

A band-stop filter has two frequency values, called the half-power frequencies, that are separated by a frequency range called the bandwidth of the filter. The band-stop filter

reduces all components of the signal between the two half-power frequencies and does not affect the components on either side. The maximum reduction of the signal occurs at the midpoint between the two half-power frequencies. A second order digital Butterworth filter is of the form

$$G_f(q) = \frac{b_1 + b_2 q^{-1} + b_3 q^{-2}}{1 + a_1 q^{-1} + a_2 q^{-2}} \tag{6.28}$$

where q^{-1} is the backward-shift operator and the parameters determine the frequency band to be attenuated and the attenuation. The function 'Butter' in Matlab© was used to design the filter; the inputs of the function were the order of the filter (=2) and the two half-power frequencies, whereas the outputs were the parameters a and b. To reduce the two significant components identified in last section, two band-stop filters were designed. The Bodé diagram for the digital filter used to minimize the component occurring at around 0.1 rad/min in Run 5 (see Figure 6.30) is shown in Figure 6.31. The filter produces -50.9 dB of attenuation at the desired frequency of 0.0939 rad/min. Table 6.15 contains

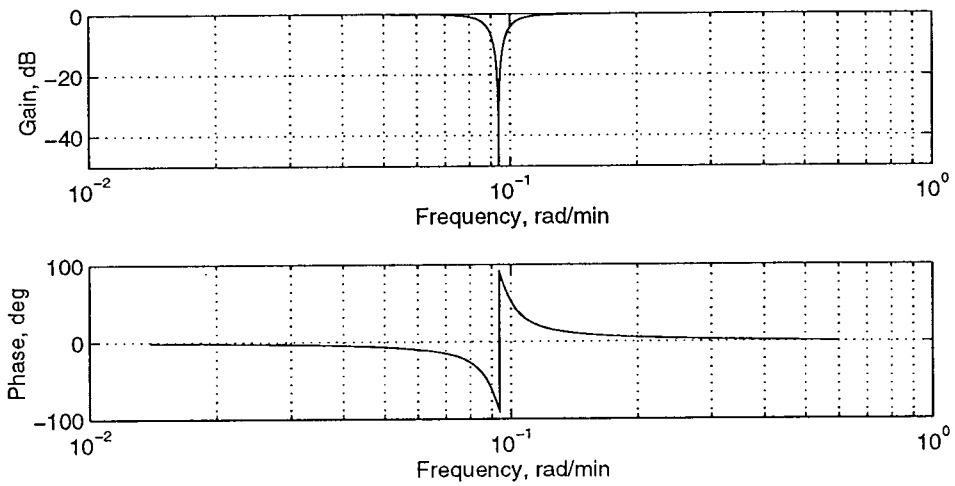

Figure 6.31: Bodé diagram of the band-stop filter used to reduce oscillations in Run 5.

the parameters a and b for the two filters used in Runs 5 and 6. The data for the temperature difference across the test section were filtered until sufficient attenuation of the desired components was obtained. The resulting power spectral density estimate for ΔT_b in Run 5 is shown in Figure 6.32 which clearly shows the attenuation of the two components. The heat flow was recalculated using the filtered data and the results are

Table 6.15: Parameters for the bandstop filters for Runs 5 and 6.

Run no.	b_1	b_2	b_3	a_1	a_2
	Filter 1				
5	0.9629	-1.7177	0.9629	-1.7177	0.9258
6	0.9651	-1.7149	0.9651	-1.7149	0.9302
	Filter 2				
5	0.8616	-0.9239	0.8616	-0.9239	0.7232
6	0.8632	-0.9351	0.8632	-0.9351	0.7263

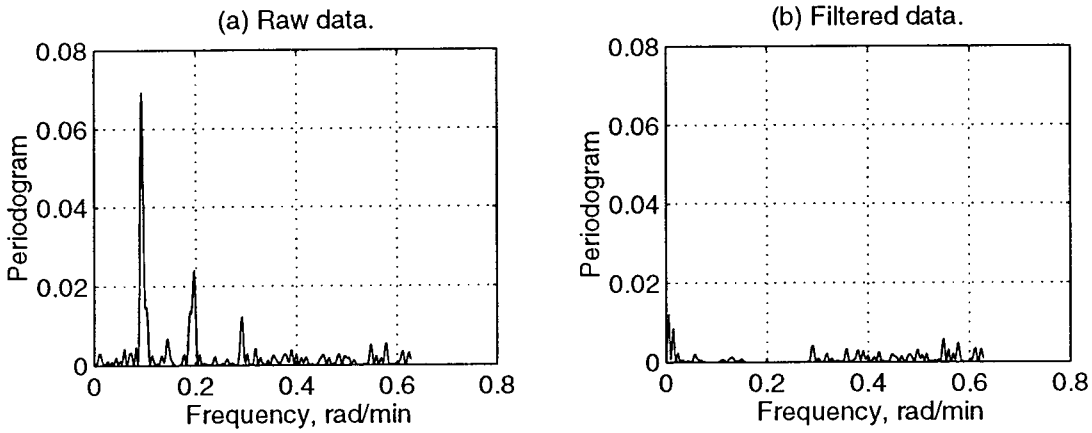

Figure 6.32: Samples of the periodogram for the raw and filtered ΔT_b for Run 5.

illustrated in Figure 6.33 for Runs 5 and 6. The attenuation of the two major oscillations has clearly improved the quality of the fouling data.

The air flowrate variations were caused by the periodic pressure increase and decrease of the air building compressor occurring at each cycle of the compressor. The variability in the frequency of this cycle observed in Table 6.14 depended on the demand of air at the time of the experiment and was sometimes decreasing during the night time within the same run. To minimize the effect of this cycle on the air flowrate, the pressure of the air regulator was reduced from 60 to 40 psig. A test revealed that when the pressure was set at 60 psig, the pressure varied between 50 to 60 psig within one cycle of the compressor. Because the compressor could not provide a constant pressure of 60 psig, the pressure of the air regulator was reduced to 40 psig. The effect of this change on the

air temperature entering the fluidized bed, which is directly related to the air flowrate, is shown in Figure 6.34. No significant oscillation in air flowrate was observed after implementing this change.

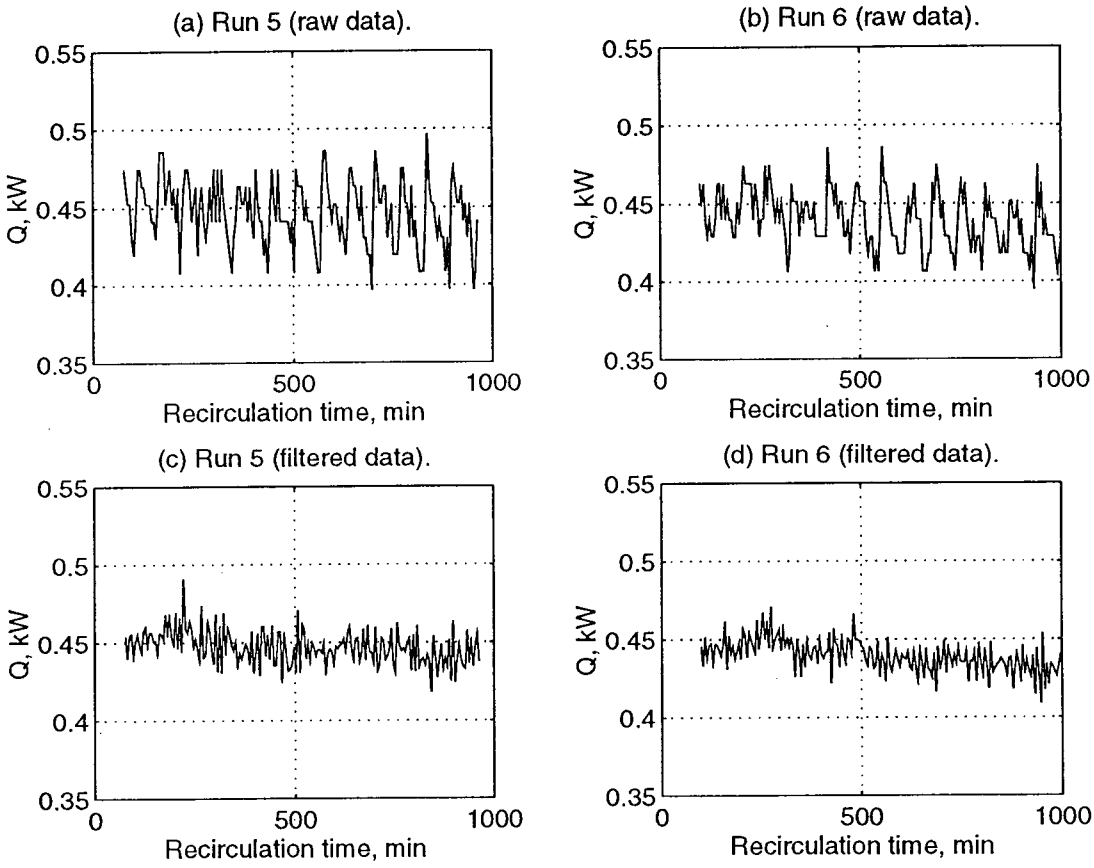

Figure 6.33: Raw and filtered heat flow for Runs 5 and 6.

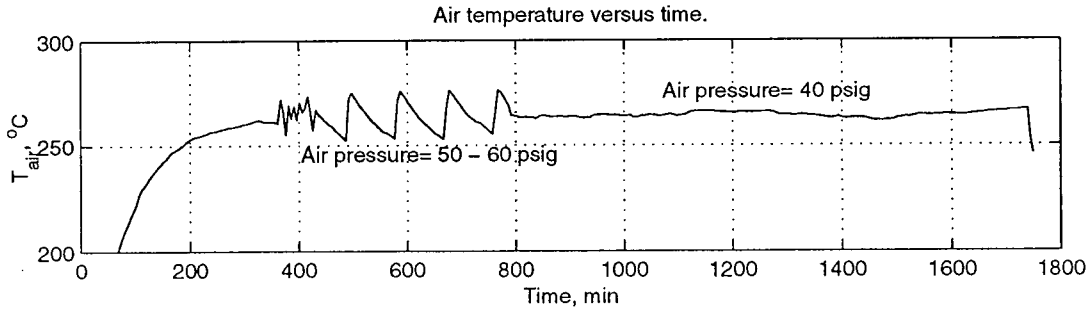

Figure 6.34: Test revealing the effect of air pressure on air temperature, T_{air}.

6.4.3 Sensitivity of U_o to Air Flow Variations

According to Equations 2.2 and 2.4, the heat flow and the overall heat transfer coefficient, U_o, share a similar dependency with the air flowrate as the heat transfer coefficient between the bed and the test section, h_o. The semi-empirical knowledge of h_o as a function of the superficial gas velocity described in Section 6.3.1 could be used to estimate changes in U_o resulting from air flowrate variations using Equation 2.4. Unfortunately, in none of the runs was a continuous measurement of the air flowrate recorded. Also, the correlations used in Section 6.3.1 could not predict the maximum in the curve h_o vs. excess gas velocity as observed experimentally. Concerning the experimental data for h_o obtained in Runs 16 and 20, they are valid only for the conditions under which they were obtained. The heat flow generated in each run depends on several factors as seen previously. Because the purpose of this work was not to study heat transfer in a fluidized bed, many of these parameters were not controlled from run to run. Nevertheless, in order to have an idea of the sensitivity of U_o to air flow variations, other empirical relationships between the experimental data were sought.

As seen previously, a relationship was observed between the air flowrate and the temperature of the air entering the fluidized bed, T_{air}. One approach considered was to estimate air flowrate variations based on this relationship and on the knowledge of T_{air}. Runs such as 5 and 6 would have provided a relationship between U_o and T_{air} and Run 20 would have given the link between T_{air} and air flowrate. However, this approach was not valid since it was found in Run 18 that T_{air} was also affected by variations in line voltage.

Another approach for evaluating the sensitivity U_o to air flowrate variations was to relate the fluid bed temperatures to U_o by using the data obtained in Run 20 as a result of step changes in air flowrate. The correlations found between U_o and the three fluid bed temperatures obtained in Run 20 are shown in Figure 6.35. The data indicate that an increase in air flowrate causes an increase in the temperature of the bed at the bottom and a decrease of the bed temperature at the top, but does not affect the temperature of the bed in the middle.

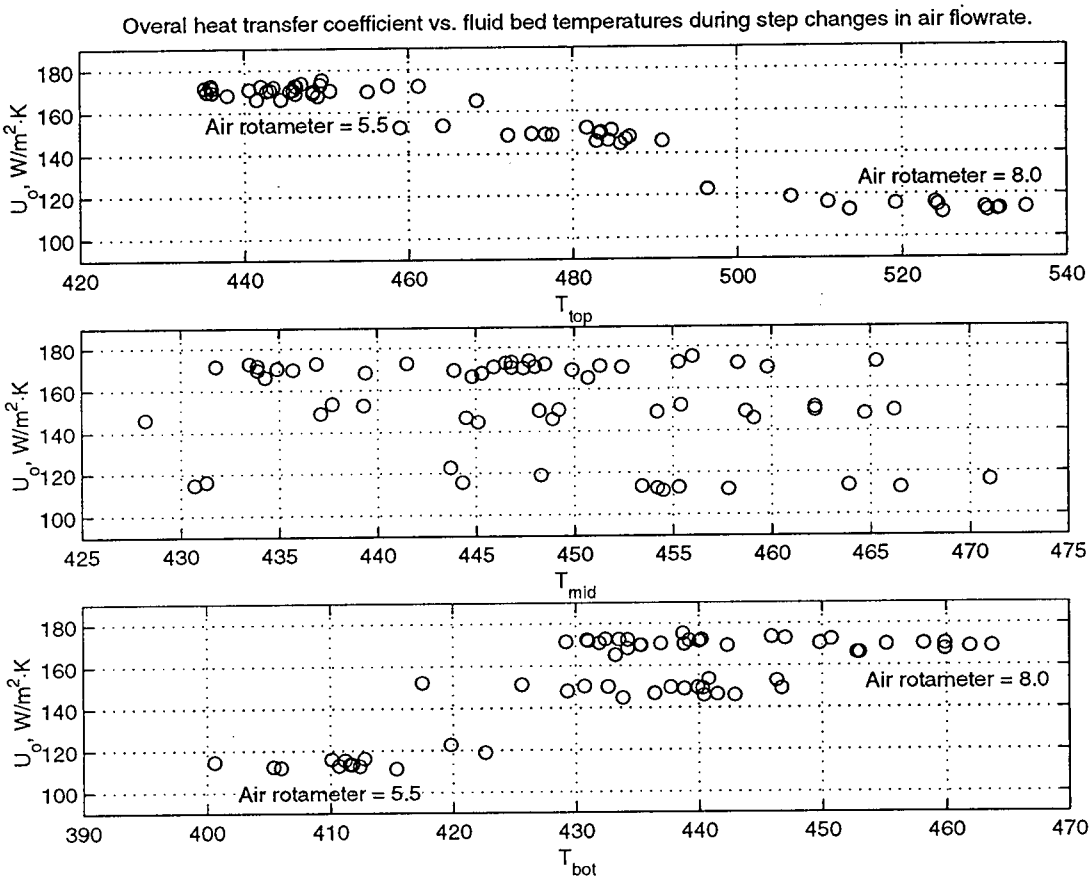

Figure 6.35: Correlation between U_o and the fluid bed temperatures in Run 20.

6.5 Tests With a Known Fouling Fluid

In order to evaluate the ability of the fouling unit to detect fouling, Runs 19 to 21 were performed using a mixture of fuel oil (75%wt.), heavy oil (10%wt.), and deasphalted oil—DAO—(15%wt.). This blend was selected because of the high fouling rates measured when used in another fouling unit (Al-Atar (2000)). The results obtained are discussed by taking into account all the fouling runs performed in the present work.

For each run, the initial and final values of the process variables believed to affect the heat flow to the test section were calculated by taking an average of twenty-one points. The initial value was calculated after a steady-state regime was achieved in all measured variables. In order to estimate the uncertainty in the measured and calculated variables, a linear regression (LS) was performed through these twenty-one points. Assuming the

prediction errors to be $N(0, \sigma^2)$, a 95% confidence interval was obtained as follows

$$\sigma_{pe} \cdot (t_{value}) \tag{6.29}$$

where σ_{pe} is the standard error of the prediction errors and (t_{value}) is obtained from a Student's t-distribution table. The results are given in Table 6.16 where the subscripts 0 and f refer to initial and final respectively and where N is the number of data points used to obtain the values.

Table 6.16: Initial and final values of measured and calculated variables for all runs with 95% confidence interval (CI).

Run no.	$data_0$ (min)	$data_f$ (min)	N	$1/U_{o,0}$ (m^2·K/kW)	CI	$1/U_{o,f}$ (m^2·K/kW)	CI	Q_0 (kW)	Q_f (kW)
1	240-400	1390-1560	18	4.4	0.3	6.8	0.6	0.64	0.45
2	200-300	630-730	12	5.3	0.7	5.4	0.3	0.40	0.39
3	270-370	671-770	21	6.3	0.6	6.3	0.6	0.36	0.36
4	216-316	1185-1305	21	4.1	0.2	4.9	0.2	0.40	0.33
5	101-201	862-962	21	4.2	0.3	4.3	0.4	0.46	0.44
6	125-225	957-1057	21	4.4	0.3	4.5	0.4	0.45	0.43
7	110-210	787-887	21	4.3	0.2	5.0	0.3	0.48	0.41
8	100-200	546-646	21	5.7	0.3	5.8	0.4	0.34	0.33
9	100-201	817-917	21	4.7	0.3	4.7	0.2	0.42	0.42
10	75-176	662-762	21	4.6	0.1	4.6	0.1	0.43	0.43
11	90-191	865-956	21	4.7	0.2	5.1	0.2	0.42	0.39
12	100-200	661-762	21	4.8	0.3	5.2	0.2	0.39	0.37
13	115-216	1023-1123	21	3.7	0.1	3.8	0.2	0.75	0.73
14	231-331	1048-1148	21	4.4	0.1	4.2	0.1	0.63	0.65
15	200-301	1909-2009	21	4.9	0.3	4.7	0.3	0.56	0.59
16	355-455	1022-1122	21	4.7	0.2	5.2	1.1	0.62	0.59
17	301-401	3186-3287	21	4.6	0.1	4.5	0.1	0.59	0.61
18	501-602	3253-3353	21	4.5	0.2	4.2	0.2	0.51	0.54
19	166-266	1203-1304	21	6.8	0.2	7.5	0.4	0.19	0.17
20	200-301	1788-1889	21	5.9	0.2	5.9	0.1	0.50	0.49
21	200-301	1919-2019	21	4.5	0.1	4.6	0.1	0.66	0.64
22	201-301	1654-1754	21	4.4	0.2	4.0	0.1	0.50	0.58
23	201-301	1153-1254	21	4.3	0.1	4.2	0.2	0.51	0.53

According to these results, the change in $(1/U_o)$ is significant for Runs 1, 4, 7, and 19. Section 6.2.3 has shown that for Runs 1, 4 and 7, the change in heat flow was mostly due to a variation in liquid flowrate. Runs 19, 20, and 21 were performed with the DAO mixture. For Run 19, there was no significant change in all the measured variables. This is the only run where both the increase in $(1/U_o)$ was significant and where there is no indication of significant changes in process variables. Figure 6.36e indicates that the mass flowrate during Run 19 was constant while the heat flow was slightly decreasing (see Figure 6.36a). The results of this run therefore suggest fouling formation. For Run 20,

Table 6.15: Continued.

Run no.	$T_{top,0}$ (°C)	CI (°C)	$T_{top,f}$ (°C)	CI (°C)	$T_{mid,0}$ (°C)	CI (°C)	$T_{mid,f}$ (°C)	CI (°C)	$T_{bot,0}$ (°C)	CI (°C)	$T_{bot,f}$ (°C)	CI (°C)
1	534	16	569	12	491	2	490	0	-	-	-	-
2	533	25	528	18	496	7	497	3	-	-	-	-
3	510	9	509	8	496	6	498	4	477	10	480	9
4	508	4	509	5	504	8	506	7	435	16	429	20
5	507	10	510	9	501	7	502	9	490	15	484	15
6	507	5	509	6	501	7	503	8	500	13	499	12
7	511	3	511	4	502	7	501	7	510	7	509	6
8	505	3	507	4	498	7	502	7	486	8	488	11
9	506	5	506	4	499	6	501	5	505	8	503	12
10	503	4	502	3	500	5	499	6	502	5	501	8
11	504	3	505	4	498	4	500	5	503	6	502	8
12	505	2	505	4	500	6	500	4	501	5	499	5
13	601	7	605	5	594	7	596	6	603	13	601	14
14	601	5	603	4	596	6	597	4	596	12	593	9
15	528	11	537	6	503	8	504	5	483	13	489	12
16	622	7	669	83	602	8	605	5	611	11	602	17
17	617	9	627	10	599	10	592	10	587	9	581	7
18	594	8	593	5	597	10	598	14	598	9	594	8
19	246	6	246	6	248	5	249	13	222	5	219	9
20	450	5	447	5	448	8	448	9	453	12	447	14
21	445	5	447	6	445	12	444	13	441	8	436	6
22	610	5	613	6	614	9	610	7	616	13	612	6
23	613	4	618	3	610	4	610	5	615	3	620	4

there is no significant change between the initial and final heat flow—this is also true for the flowrate as shown in Figure 6.36e—although some variations occurred during the run (see Figure 6.36a). The observed change in Q at around 700 min (Fig. 6.36a) is believed to have been caused by a decrease in bulk temperature which occurred at the same time; the bulk temperature came back to its original value at around 1000 min. Hence it was concluded that no fouling was detected in Run 20. For Run 21, the heat flow had an decreasing trend (Fig. 6.36b) although it was less pronounced than for Run 19. More fluctuations in flowrate were observed in Run 21 than in Runs 19 and 20 (Fig. 6.36f).

Table 6.15: Continued.

Run no.	m_0 (g/s)	CI (g/s)	m_f (g/s)	CI (g/s)	$T_{in,0}$ (°C)	CI (°C)	$T_{in,f}$ (°C)	CI (°C)
1	-	-	-	-	196.9	0.6	195.4	1.8
2	-	-	-	-	277.4	0.6	275.8	0.5
3	-	-	-	-	244.9	0.5	245.1	0.6
4	-	-	-	-	284.7	0.4	286.4	0.6
5	-	-	-	-	288.5	0.8	288.9	0.9
6	-	-	-	-	289.4	1.0	289.5	0.8
7	-	-	-	-	276.5	0.5	278.3	0.7
8	31.1	0.6	30.8	0.5	290.5	0.3	291.3	0.3
9	13.7	0.1	13.1	0.1	283.9	0.4	284.6	0.2
10	9.3	0.5	9.1	0.1	277.7	0.4	277.9	0.2
11	10.4	1.0	10.1	0.7	280.9	0.6	282.5	1.0
12	8.4	1.9	7.8	1.1	286.0	0.8	285.7	0.6
13	15.1	0.1	15.8	0.2	288.5	0.7	289.1	0.5
14	7.5	0.5	7.7	0.3	282.8	0.4	282.5	0.3
15	16.3	0.4	16.3	0.1	198.8	0.4	198.9	0.2
16	7.3	0.7	7.6	0.1	286.4	0.6	285.7	1.4
17	7.6	0.0	7.7	0.0	286.7	0.5	286.3	0.5
18	6.6	0.1	6.5	0.0	330.3	1.4	330.8	0.9
19	5.8	0.0	5.8	0.0	86.5	0.2	86.5	0.2
20	3.2	0.0	3.2	0.0	95.0	0.3	93.8	0.2
21	12.8	0.5	12.7	0.2	106.7	0.3	106.8	0.2
22	8.4	0.1	8.3	0.4	361.4	0.5	343.2	0.6
23	7.8	0.3	8.0	0.3	363.8	0.5	361.9	0.6

The test section used in Run 19 was cut axially in order to examine the inner surface of the tube by visual inspection. Only a layer of oil was observed; the layer was thin

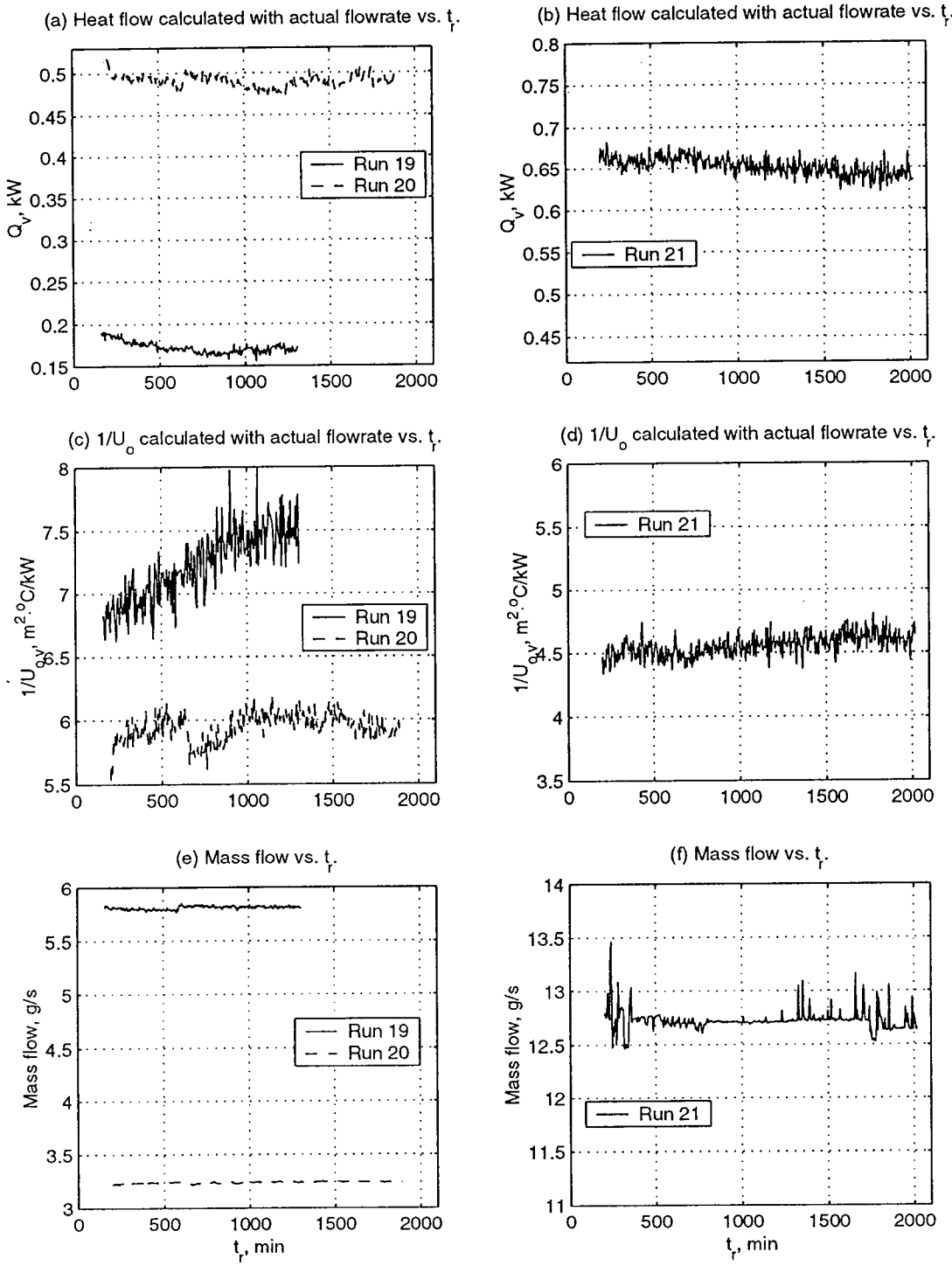

Figure 6.36: Heat flow, $(1/U_o)$, and mass flowrate in Runs 19 to 21.

enough such that the surface of the tube could still be seen. No black and thick deposit such as that obtained with the probe of the other unit when used with the same mixture was found. For Runs 20 and 21, the test section was washed with varsol according to the procedure described in Chapter 5 in order to measure w_c, the amount of coke in the test section at the end of a run. The results are given in Table 6.17. Note that w_c could

Table 6.17: Coke collected in test section at the end of Runs 20 and 21.

Run no.	w_c (mg)
19	-
20	41
21	18

not be measured in Run 19 because of the tube opening performed. Since the amount of insolubles in the DAO blend is probably negligible, the mass of coke for Runs 20 and 21 is therefore the result of fouling. However, based on the thermal measurements obtained in Runs 20 and 21, these deposits were apparently too small to be detected by the fouling unit. Note that the higher amount collected in Run 20 might have been caused by a lower liquid velocity, given that the other process variables and the total recirculation times were very similar (see Table 6.1), since fouling is often expected to increase when the velocity decreases.

The thermal measurements of Run 19 indicate fouling formation. Now, for the runs with pitch and CHGO, the mass deposition measurements have shown the absence of significant fouling under the conditions covered. However, in some of these runs, variations in $1/U_o$ were observed, although they could not be explained in terms of flowrate variations. Because of that, and since no mass deposition measurements were made in Run 19, which was the only run where fouling seems to have been detected, the evidence is judged insufficient to say whether fouling was actually formed in Run 19. For Runs 20 and 21, some fouling has occurred as shown by the measured deposits, but detection by thermal measurement may have been prevented by the small amounts measured, and by the noise level and variability of the fouling unit present in all the other experiments.

Chapter 7

Conclusions & Recommendations

7.1 Conclusions

The main objective of this study was to evaluate the tendency of the pitch-coker heavy gas oil stream to form coke as well as to assess the ability to detect it under the appropriate bulk and surface temperature conditions. To meet this objective, several fouling experiments were done by recirculating a 50:50%vol. pitch-heavy gas oil blend over 11–56 hour periods with bulk fluid temperatures of 200–375°C, tube side velocities of 0.3–2.2 m/s, and fluid bed temperatures in the range 500–615°C. Flow was generally laminar. Both the mass deposition and thermal measurements showed no significant fouling by coke formation. Interpretation of the thermal fouling data was sometimes made difficult by their sensitivity to variations in process variables. By the use of different data analysis techniques and of empirical correlations found between process variables, fouling was distinguished from other effects.

In order to see whether the absence of fouling observed was due to the fouling unit or could be attributed to the nature of the test fluid used, a series of fouling experiments were performed with a blend of de-asphalted oil known to give measurable fouling rates in turbulent flow and in similar periods of time as for the coking experiments.

Moreover, viscosity and density measurements were done to determine the flow regime in the fouling runs and to account for possible viscosity changes during the fouling experiments. Additional experiments were performed to monitor the viscosity change during recirculation of the test fluid and also the change in the amount of toluene insolubles in the 50:50%vol. pitch-heavy gas oil blend. Finally, measurements of heat transfer coefficients were also made to estimate the relative importance of the thermal resistances between the fluidized bed and the bulk liquid.

Based on these studies, the following conclusions can be drawn:

- An improved insulation of the fouling unit and the use of heating tapes increased the capability of the unit to handle viscous fluids and to reach the higher bulk temperatures required (see Sections 4.7.1 and 4.7.3).

- As described in Sections 4.2 to 4.4, the design and implementation of a pressure drop measuring system combined with a digital balance setup provided an accurate mass flowrate measurement of viscous fluids using a small amount of test fluid.

- An adjustment of the air pressure regulator reduced undesirable oscillations in air flowrate as shown in Section 6.4.2, thereby improving both the fluid bed temperature profile and the thermal fouling data. The data obtained prior to this adjustment were improved by filtering through a digital band-stop filter as demonstrated in Section 6.4.2. Oscillations in the voltage to the air preheater were also reduced by use of a voltage regulator.

- From the viscosity measurements reported in Chapter 3, viscosity-temperature correlations were developed over a wide range of temperatures for the viscosity prediction of any blend of pitch and CHGO. Density-temperature equations were also derived from the density data presented in the same chapter. Hence a laminar flow regime in all the fouling experiments performed could be determined.

- In some fouling runs a drop in viscosity was observed and a possible bias effect on the mass flowrate measurement was demonstrated in Section 6.2.5.

- For the runs with the 50:50%vol. pitch-CHGO blend, the TI measurements are consistent with the previous work of Watkinson et al. (1998) as discussed in Section 6.1.2; i.e. as long as a certain amount of volatiles has not been released, no significant change in the TI of the test fluid will occur.

- In Sections 6.2.1 and 6.2.2, the use of cross correlation analysis and empirical correlations found between process variables confirmed the effect of liquid flowrate variations on thermal measurements. An ARMA model and a variable flowrate approach were applied to the measurements which essentially eliminated the effect

of liquid flow variations as discussed in Section 6.2.3. Also, the configuration of the bypass circuit was modified thereby eliminating the variations in liquid flowrate (see Section 6.2.4).

- The tests for determining the heat transfer coefficient revealed the complexity of heat transfer in fluidized beds. Comparison of the data with predictions from correlations in Section 6.3.1 indicated that the wall temperature measurements may not always provide the actual wall temperature. Moreover, the loss of sand from the bed may explain the fact that the measured maximum heat transfer coefficent occurs at a lower gas velocity than for the predicted coefficient. The premature decrease in h_o may be attributed to the relatively large particle size range of the sand used.

- In Section 6.3.2 the measured and predicted heat transfer coefficients inside the test section have shown the relative importance of each of the individual resistances between the bed and the bulk fluid with respect to the total resistance. The resistance in the bed was as high as around 38% of the total resistance; this may reduce the sensitivity of the fouling unit to detect a change in the overall heat transfer coefficient that would result from coke deposition.

- Over the range of bulk fluid temperatures (200–375°C), fluid bed temperatures (500–615°C), and liquid velocities (0.3–2.2 m/s), no fouling was observed over recirculation periods of 11–56 hours. A statistical analysis of the thermal measurements on the 50:50% vol. pitch-CHGO blend presented in Section 6.5 showed that all the significant variations observed in the inverse overall heat transfer coefficient could be explained by variations in process variables. The analysis of the mass deposition measurements given in Section 6.1.3 also suggested evidence of very small coke formation over the range of conditions covered. Calculations of an equivalent liquid thickness of a residue layer presented in Section 6.1.3 revealed that the amounts of coke in the test section measured in the runs performed with adequate fluid bed cooling may have come exclusively from this residue layer. As for the other experiments, it was concluded that the coke collected was formed as a result of batch coking reactions in the residue left on the tube wall due to inadequate cooling of the fluid bed.

- For the tests with the DAO blend, the mass deposition measurements indicated that some fouling has taken place in Runs 20 and 21, although it was not detected from the thermal measurements. In Run 19 the thermal data indicated significant fouling. However, no mass deposition measurement were made, hence the evidence is judged insufficient to say whether fouling actually occurred. Nevertheless, based on the observed noise level and the variability in process variables, and the magnitude of the thermal resistance of the fluid bed, it is clear that the ability of the fouling unit to detect deposit formation must be improved.

7.2 Future Work

Based on the results obtained, the following recommendations are suggested to verify and ensure that the fouling unit is able to form and detect fouling and to provide more insights into the precipitation of carbon-rich material from heating heavy petroleum streams:

- As discussed in Section 6.3.2, the high thermal resistance due to the fluidized bed may be detrimental to the sensitivity of the fouling unit to detect coke formation. Also, the high level of noise observed in the thermal measurements deteriorates the quality of the data and appears to be due to the intrinsic nature of the fluid bed as suggested in Section 6.3.1. Moreover, the heat transfer between a fluidized bed and a vertical tube is extremely complex and the experiments revealed the difficulty of maintaining a constant heat flow to the test section, which is essential for a correct interpretation of the fouling data. Hence it seems appropriate to consider another heating method.

- It is recommended to use a 'Portable Fouling Research Unit (PFRU)' probe capable of reaching the desired surface temperatures and which is supplied by 'Heat Transfer Research Incorporated (HTRI)' because of the successful results obtained with this type of probe in an apparatus originally constructed by Fetissoff (1982). It has several advantages over the fluidized bed. The thermal resistance between the probe surface and the bulk liquid is usually the dominant resistance as opposed to the fluidized bed. Also, it is experimentally much simpler to use because of the fewer

operations required to replace the probe and because the heat flow is self-controlled. Due to its design the surface temperature is readily obtained and is likely to be more accurate than the more difficult measurements in a fluid bed. Furthermore, the evidence of coke formation is more obvious since fouling occurs on the outer surface of the probe.

- As explained in Section 6.1.2, the amount of toluene insolubles in the test fluid remains approximately constant as long as a critical yield of about 30% has not been reached. It is important to operate under this value to keep the properties of the test fluid constant. A water condenser has already been installed in the vent line of the feeder to return the condensates in the system.

- Because of the change in viscosity observed in the experiments and its possible bias effect on the flowrate, it is recommended to monitor the viscosity and to ensure it remains constant during recirculation.

- Due to the voltage variations observed, it is recommended to maintain the power to the unit constant by using voltage regulators when necessary.

- Due to the flammable and toxic nature of the fluids studied and the long periods of time required by the fouling experiments, it is recommended to implement all the necessary security devices. An alarm system relating the pressure drop across the orifice plate to the total power to the unit has been designed and is now being used. This system shuts off the power in case the pressure signal becomes outside a specified pressure band.

The above suggestions will help ensure that whatever change observed in the overall heat transfer coefficient is due to fouling not to variations in process variables, in fluid properties, or to a problem in the design of the fouling unit. Once the ability of the fouling unit has been confirmed—for example by repeating the tests with the DAO mixture—the coke forming tendency of various blends can be studied systematically by varying the fluid velocity, the bulk and surface temperatures, and the recirculation time.

Bibliography

Al-Atar, E. (2000). Effect of oil compatibility and resins/asphaltenes ratio on heat exchanger fouling of mixtures containing heavy oil. *M.A.Sc. Thesis*. University of British Columbia.

Albright, L. F., B. L. Crynes, and W. H. Corcoran (1983). *Pyrolysis: Theory and industrial practice*. New-York: Academic Press Inc.

Allan, J. M. and A. S. Teja (1991). Correlation and prediction of the viscosity of defined and undefined hydrocarbon liquids. *Can. J. Chem. Eng. 69*, 986–991.

Amin, M. B. and R. N. Maddox (1980). Estimate viscosity versus temperature. *Hydrocarbon Processing 59*, 131–135.

Asomaning, S. (1997). *Heat Exchanger Fouling by Petroleum Asphaltenes*. Ph. D. thesis, University of British Columbia.

Bach, G., G. Zimmermann, F. D. Kopinke, S. Barendregt, P. van den Oosterkamp, and H. Woerde (1995). Transfer-line heat exchanger fouling during pyrolysis of hydrocarbons I. *Ind. Eng. Chem. Res. 34*(4), 1132–1139.

Baskakov, A. P. (1985). Heat transfer in fluidized beds: Radiative heat transfer in fluidized beds. In J. F. Davidson, R. Clift, and D. Harrison (Eds.), *Fluidization* (2^{nd} ed.)., pp. 465–472. Orlando: Academic Press Inc.

Baskakov, A. P., B. V. Berg, O. K. Vitt, N. F. Filippovsky, V. A. Kirakosyan, J. M. Goldobin, and V. K. Maskaev (1973). Heat transfer to objects immersed in fluidized beds. *Powder Technol. 8*, 273.

Beg, S. A., M. B. Amin, and I. Hussain (1988). Generalized kinematic viscosity-temperature correlation for undefined petroleum fractions. *Chem. Eng. J. 38*, 123–136.

Bock, H. J. and O. Molerus (1983). Heat transfer in gas/solid fluidized beds. *German Chem. Eng. 6*, 57.

Borodulya, V. A., V. L. Ganzha, and A. I. Podberezsky (1980). Heat transfer in a fluidized bed at high pressure. In J. R. Grace and J. M. Matsen (Eds.), *Fluidization*, pp. 201–207. New-York: Plenum.

Bott, T. R. (1988). General fouling problems. In L. F. Melo, T. R. Bott, and C. A. Bernardo (Eds.), *Fouling Science and Technology*, Volume 145 of *NATO ASI Series*. Kluwer Academic Publishers.

Bott, T. R. (1995). *Fouling of Heat Exchangers*. The Netherlands: Elsevier.

Botterill, J. S. M. and G. D. Hawkes (1989). The influence of a substantial fines component on bed-to-tube heat transfer. In J. R. Grace, L. W. Schmidt, and M. A. Bergougnou (Eds.), *Fluidization VI*, pp. 661–668. New-York: Engineering Foundation.

Box, G. E. P. and G. M. Jenkins (1970). *Time Series Analysis, Forecasting and Control*. San Francisco: Holden-Day.

Braun, R. (1977). The nature of petroleum process fouling—results with a practical instrument. *Materials Performance 16*(11), 35–41.

Braun, R. and R. H. Hausler (1976). Contribution to understanding fouling phenomena in the petroleum industry. In *Paper 76-CSME/CSChE-23, 16th Nat'l Heat Transfer Conf.*

Bulkowski, P. and G. Prill (1978). Internal report of Alberta Research Council.

Cassis, R., N. Fuller, L. G. Hepler, R. J. C. McLean, A. Skauge, N. S. Srinivasan, and H. Yan (1985). Specific heat capacities of bitumens and heavy oils, reservoir minerals, clays, dehydrated clays, asphaltenes, and coke. *AOSTRA Journal of research 1*(3), 163–173.

Crittenden, B. D. (1988). Chemical reaction fouling of heat exchangers. In L. F. Melo, T. R. Bott, and C. A. Bernardo (Eds.), *Fouling Science and Technology*, Volume 145 of *NATO ASI Series*, pp. 315–332. Kluwer Academic Publishers.

Crittenden, B. D., S. A. Hout, and N. J. Alderman (1987). Model experiments of chemical reaction fouling. *Chem. Eng. Res. Des. 65*(2), 165–170.

Denloye, A. O. O. and J. S. M. Botterill (1978). Bed to surface heat transfer in a fluidized bed of large particles. *Powder Technol. 19*, 197–203.

Dickakian, G. B. and S. Seay (1988). Asphaltenes precipitation primary crude exchanger fouling mechanism. *Oil and Gas Journal 86*, 47–50.

Dutt, N. V. K. (1990). A simple method of estimating the viscosity of petroleum crude oil and fractions. *Chem. Eng. J. 45*, 86–83.

Eaton, P. and R. Lux (1984). Laboratory fouling test apparatus for hydrocarbon feestocks. *ASME HTD 35*, 33–42.

Epstein, N. (1983). Thinking about heat transfer fouling: a 5x5 matrix. *Heat transfer engineering 4*(1), 43–56.

Fetissoff, P. E. (1982). Comparison of two fouling probes. *M.A.Sc. Thesis*. University of British Columbia.

Fitzer, E., K. Mueller, and W. Shaefer (1971). The chemistry of pyrolytic conversion of organic compounds to carbon. *Chemistry and Physics of Carbon 7*, 237–376.

Froment, G. F. (1981). Fouling of heat transfer surfaces by coke formation in petrochemical reactors. In E. F. C. Somerscales and J. G. Knudsen (Eds.), *Fouling of Heat Transfer Equipment*, pp. 441–435. Hemisphere Publishing Co.

Geldart, D. (1973). Types of gas fluidization. *Powder Technol. 7*, 285–292.

Gelperin, N. I. and V. G. Einstein (1971). Heat transfer in fluidized beds. In J. F. Davidson and D. Harrison (Eds.), *Fluidization*, Chapter 10, pp. 471–540. New-York: Academic Press.

Gnielinski, V. (1983). *Heat exchanger design handbook*. Washington: Hemisphere Pub. Corp.

Grace, J. R. (1982). Fluidized-bed heat transfer. In G. Hetsroni (Ed.), *Handbook of Multi-Phase Systems*, Chapter 8.2, pp. 8.65–8.83. New-York: McGraw-Hill.

Gray, M. R. (1994). *Upgrading Petroleum Residues and Heavy Oils*. New York: Marcel Dekker.

Gregory, G. A. (1992). Letter to the Editor. *Can. J. Chem. Eng. 70*, 1037.

Grewal, N. S. and S. C. Saxena (1981). Maximum heat transfer coefficient between a horizontal tube and a gas-solid fluidized bed. *Ind. Eng. Chem. Process Des. Dev. 20*, 108.

Herschel, W. H. (1922). The change in viscosity of oils with temperature. *Ind. & Engr. Chem. 14*(8), 715–723.

Huntrods, R. S., J. A. Nighswander, A. K. Mehrotra, and L. A. Behie (1989). Modeling of coke formation in gas quenchers of industrial ethane cracking furnaces. *Chem. Eng. Res. Des. 67*, 632–638.

Incropera, F. and D. P. DeWitt (1996). *Fundamentals of Heat and Mass Transfer* (4^{th} ed.). New York: Wiley.

Janssen, K. (1973). *Dr-Ing. dissertation.* Ph. D. thesis, University of Bonn.

Kays, W. M. (1955). Numerical solutions for laminar-flow heat transfer in circular tubes. *Trans. ASME 77*, 1265.

Knudsen, J. F. (1981). Apparatus and techniques for measurement of fouling of heat transfer surfaces. In E. F. C. Somerscales and J. G. Knudsen (Eds.), *Fouling of Heat Transfer Equipment*, pp. 57–81. Hemisphere Publishing Co.

Kopinke, F. D., G. Zimmermann, G. C. Reyniers, S. Barendregt, and G. F. Froment (1993). Relative rates of coke formation from hydrocarbons in steam cracking of naphtha. 2. parraffins, naphthenes, mono-, di-, and cycloolefins, and acetylenes. *Ind. Eng. Chem. Res. 32*(1), 56–61.

Kumar, P. and D. Kunzru (1987). Coke formation during naphtha pyrolysis in a tubular reactor. *Can. J. Chem. Eng. 65*, 280–285.

Kunii, D. and O. Levenspiel (1991). *Fluidization Engineering* (2^{nd} ed.). Boston: Butterworth-Heinemann.

Lambourn, G. A. and M. Durrieu (1983). Fouling in crude oil preheat trains. In J. Taborek, G. F. Hewitt, and N. Afgan (Eds.), *Heat Exchangers Theory and Practice.* Hemisphere Publishing Co.

Lewis, I. C. (1980). Thermal polymerization of hydrocarbons. *Carbon 18*, 191–196.

Litovitz, T. A. (1952). Temperature dependence of the viscosity of associated liquids. *J. of Chemical Physics 20*(7), 1088–1089.

Lott, R. K., H. A. Rangwala, C. Hsi, M. Zhao, and Y. M. Xu (1996). Mechanisms of coke formation and fouling in thermal cracking. In *Proc. Sixth UNITAR Conference on Heavy Crude and Tar Sands*, pp. 379–383.

Lu, B. C. Y. (1989). Phase equilibria and pvt properties. In L. G. Hepler and C. Hsi (Eds.), *AOSTRA Technical Handbook on Oil Sands, Bitumens and Heavy Oils*, AOSTRA Technical Publication Series #6, pp. 132. AOSTRA.

Madison, J. J. and R. M. Roberts (1958). Pyrolysis of aromatics and related heterocyclics. *Ind. Eng. Chem. 50*, 237–250.

Makhorin, K. E. and N. V. Kharchenko (1964). The rate of heat transfer between a fluidized bed and an immersed body at high temperatures. *International. Chem. Eng. 4*(4), 650–654.

Martin, H. (1984). The effects of pressure and temperature on heat transfer to gas-fluidized beds of solids particles. In *Heat and Mass Transfer in Fixed and Fluidized Beds*, XVI ICHMT Symp., Dubrovnik, pp. 143–157. Hemisphere pub. corp.

Mathur, A., S. C. Saxena, and A. Chao (1986). Heat transfer from a immersed vertical tube in a gas-fluidized bed. *Ind. Eng. Chem. Process Des. Dev. 25*, 156.

Mehrotra, A. K. (1994). Comments on modeling the viscosity of middle-east crude oil mixtures. *Ind. Eng. Chem. Res. 33*, 1410.

Mehrotra, A. K., R. R. Eastick, and W. Y. Svrcek (1989). Viscosity of cold lake bitumen and its fractions. *Can. J. Chem. Eng. 67*, 1004–1009.

Mehrotra, A. K., W. D. Monnery, and W. Y. Svrcek (1996). A review of practical calculation methods for the viscosity of liquid hydrocarbons and their mixtures. *Fluid Phase Equilibria 117*, 344–355.

Mehrotra, A. K. and W. Y. Svrcek (1988). Properties of cold lake bitumen saturated with pure gases and gas mixtures. *Can. J. Chem. Eng. 66*(4), 656–665.

Miadonye, A. and V. R. Puttagunta (1996). Viscosity correlations for unrefined petroleum liquids. In N. P. Cheremisinoff and P. J. Agarwal (Eds.), *Advances in*

Engineering Fluid Mechanics, Mixed-Flow Hydrodynamics, pp. 51–82. Gulf Pub. Co.

Mickley, H. S. and D. F. Fairbanks (1955). Mechanism of heat transfer to fluidized beds. *AIChE J. 1*(3), 374.

Mickley, H. S., D. F. Fairbanks, and R. D. Hawthorn (1961). The relation between the transfer coefficient and thermal fluctuations in fluidized-bed heat transfer. *Chem. Eng. Prog. Symp. Ser. 57*(32), 51.

Molerus, . and K. E. Wirth (1997). *Heat transfer in fluidized beds.* New York: Chapman & Hall.

Molerus, O., A. Burschka, and S. Dietz (1995). Particle migration at solid surfaces and heat transfer in bubbling fluidized beds–ii.prediction of heat transfer in bubbling fluidized beds. *Chem. Eng. Sci. 50*(5), 879–885.

Molerus, O. and W. Mattmann (1992). Heat transfer mechanisms in gas fluidized beds part i: Maximum heat transfer coefficients. *Chem. Eng. Technol. 15*, 139–150.

Murphy, G. and J. Campbell (1992). Fouling in refinery heat exchangers: causes, effects, measurement and control. In *Fouling Mechanisms*, pp. 249–261. GREThSeminar.

Oblad, R. F., H. G. Davis, and R. T. Eddinger (1979). *Thermal hydrocarbon chemistry*, Volume 183. Washington: American Chemical Society.

Obot, N. T., L. Das, D. E. Vakili, and R. A. Green (1997). Effect of Prandtl number on smooth-tube heat transfer and pressure drop. *Int. Comm. Heat Mass Transfer 24*(6), 889–896.

Perry, R. H. and D. Green (1984). *Perry's Chemical Engineers' Handbook* (6^{th} ed.). New York: McGraw Hill Inc.

Polikar, M. (1980). Internal report of Alberta Research Council.

Puttagunta, V. R., A. Miadonye, and B. Singh (1993). A simple concept for prediction of viscosity of heavy oils and bitumens. *Oil and Gas Journal 91*(9), 71–73.

Reid, R., J. M. Prausnitz, and T. K. Sherwood (1977). *The properties of gases and liquids* (3^{rd} ed.). McGraw-Hill.

Roberts, R. A. and C. T. Mullis (1987). *Digital Signal Processing.* Massachusetts: Addison-Wesley Pub. Co.

Sakai, T. (1983). Thermal reaction of olefins and diolefins, and formation of aromatics. In L. F. Albright, B. L. Crynes, and W. H. Corcoran (Eds.), *Pyrolysis: Theory and industrial practice*, Chapter 5. New-York: Academic Press Inc.

Sanaie, N. (1998). Effect of minerals on coke formation. *M.A.Sc. Thesis*. University of British Columbia.

Saxena, S. C. (1989). Heat transfer between immersed surfaces and gas-fluidized beds. In J. P. Hartnett and T. F. Irvine (Eds.), *Advances in Heat Transfer*, Volume 19, pp. 97–190. New-York: Academic Press Inc.

Saxena, S. C. and V. L. Ganzha (1984). Heat transfer to immersed surfaces in gas-fluidized beds of large particles and powder characterization. *Powder Technol. 39*, 199–208.

Speight, J. G. (1991). *The Chemistry and Technology of Petroleum.* New York: Marcel Dekker.

Strausz, O., T. W. Mojelsky, and E. M. Lown (1992). The molecular structure of asphaltenes. *Fuel 71*, 1355–1363.

Tassios, D. and E. Goletz Jr. (1977). An Antoine type equation for liquid viscosity dependency to temperature. *Ind. Eng. Chem., Process Des. Dev. 16*(1), 75–79.

Taylor, W. F. (1969). Kinetics of deposit formation from hydrocarbons: fuel composition studies. *Ind. Eng. Chem. Prod. Res. Dev. 8*, 375–380.

TEMA (1978). *Standards of Tubular Exchanger Manufacturers Association* (6 ed.). New York: TEMA.

Trimm, D. L. (1983). Fundamental aspects of the formation and gasification of coke. In L. F. Albright, B. L. Crynes, and W. H. Corcoran (Eds.), *Pyrolysis: Theory and industrial practice*, Chapter 9. New-York: Academic Press Inc.

Van Nostrand Jr., W. J., S. H. Leach, and J. L. Holuska (1981). Economic penalties associated with the fouling of refinery heat transfer equipment. In E. F. C. Somer-

scales and J. G. Knudsen (Eds.), *Fouling of Heat Transfer Equipment*, pp. 619–643. Hemisphere Publishing Co.

Varygin, N. N. and I. G. Martyushin (1959). Calculation of heat-exchange in fluidized beds. *Khim. Mashinostroenie 5*, 6–9.

Verma, R. S. and S. C. Saxena (1983). Heat transfer from an immersed vertical tube to a gas fluidized bed. *Energy 8*(12), 909–925.

Vranos, A., P. J. Marteney, and B. A. Knight (1981). Determination of coking rate in jet fuel. In E. F. C. Somerscales and J. G. Knudsen (Eds.), *Fouling of Heat Transfer Equipment*, pp. 489–499. Hemisphere Publishing Co.

Vreedenburg, H. A. (1960). Heat transfer between a fluidized bed and a vertical tube. *Chem. Eng. Sci. 11*, 274–285.

Watkinson, A. P. (1988). Critical review of organic fluid fouling. Technical report, Argonne National Laboratory.

Watkinson, A. P. (1992). Chemical reaction fouling of organic fluids. *Chem. Eng. Technol. 15*, 82–90.

Watkinson, A. P. and N. Epstein (1969). Gas oil fouling in a sensible heat exchanger. *Chem. Eng. Prog. Symp. Ser. 65*(92), 84–90.

Watkinson, A. P. and C. B. Panchal (1993). Chemical reaction fouling model for single-phase heat transfer. *AIChE Symp. Ser. 89*(295), 323–334.

Watkinson, A. P. and D. I. Wilson (1997). Chemical reaction fouling: a review. *Experimental Thermal and Fluid Science. 14*, 361–374.

Watkinson, A. P., C. Yue, M. Simard, and E. Kwok (1998). Deposition of coke in heating of heavy hydrocarbons, progress report, phase II. Technical report, University of British Columbia.

Wender, L. and G. T. Cooper (1958). Heat transfer between fluidized-solids beds and boundary surfaces–correlation of data. *AIChE J. 4*, 15–23.

Wiehe, I. A. (1993). A phase-separation kinetic model for coke formation. *Ind. Eng. Chem. Res. 32*, 2447–2454.

Xavier, A. M. and J. F. Davidson (1985). Heat transfer in fluidized beds: Convective heat transfer in fluidized beds. In J. F. Davidson, R. Clift, and D. Harrison (Eds.), *Fluidization* (2^{nd} ed.)., pp. 437. Orlando: Academic Press Inc.

Yue, C. and A. P. Watkinson (1998). Deposition of coke in heating of heavy hydrocarbons, final report phase i. Technical report, University of British Columbia.

Zabrodsky, S. S., N. V. Antonishin, and A. L. Parnas (1976). On fluidized bed-to-surface heat transfer. *Can. J. Chem. Eng. 54*, 52–58.

Zuiderweg, F. J. (1967). Report. In A. A. H. Drinkenburg (Ed.), *Proceedings of The International Symposium of Fluidization*, pp. 739. Amsterdam: Netherlands University Press.

Appendix A

Calibrations

The calibration curves for the orifice plates are shown in Figures A.2 and A.3 for different operating temperatures. The numbers in parentheses in the upper figures refer to the run number while the numbers in the lower figures corresponds to the discharge coefficient values. The calibration curve for the fluidized bed air rotameter is given in Figure A.1.

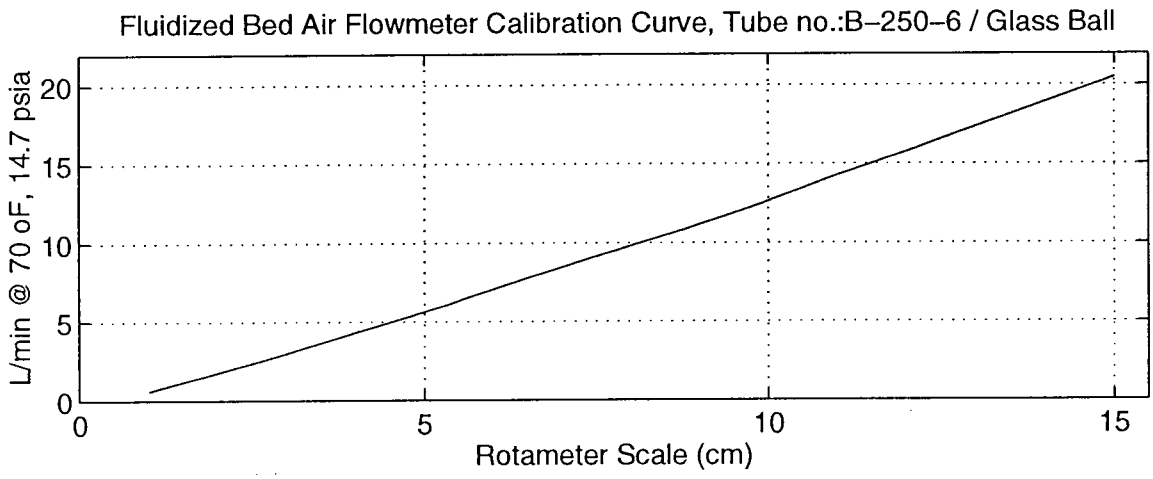

Figure A.1: Air rotameter calibration curve.

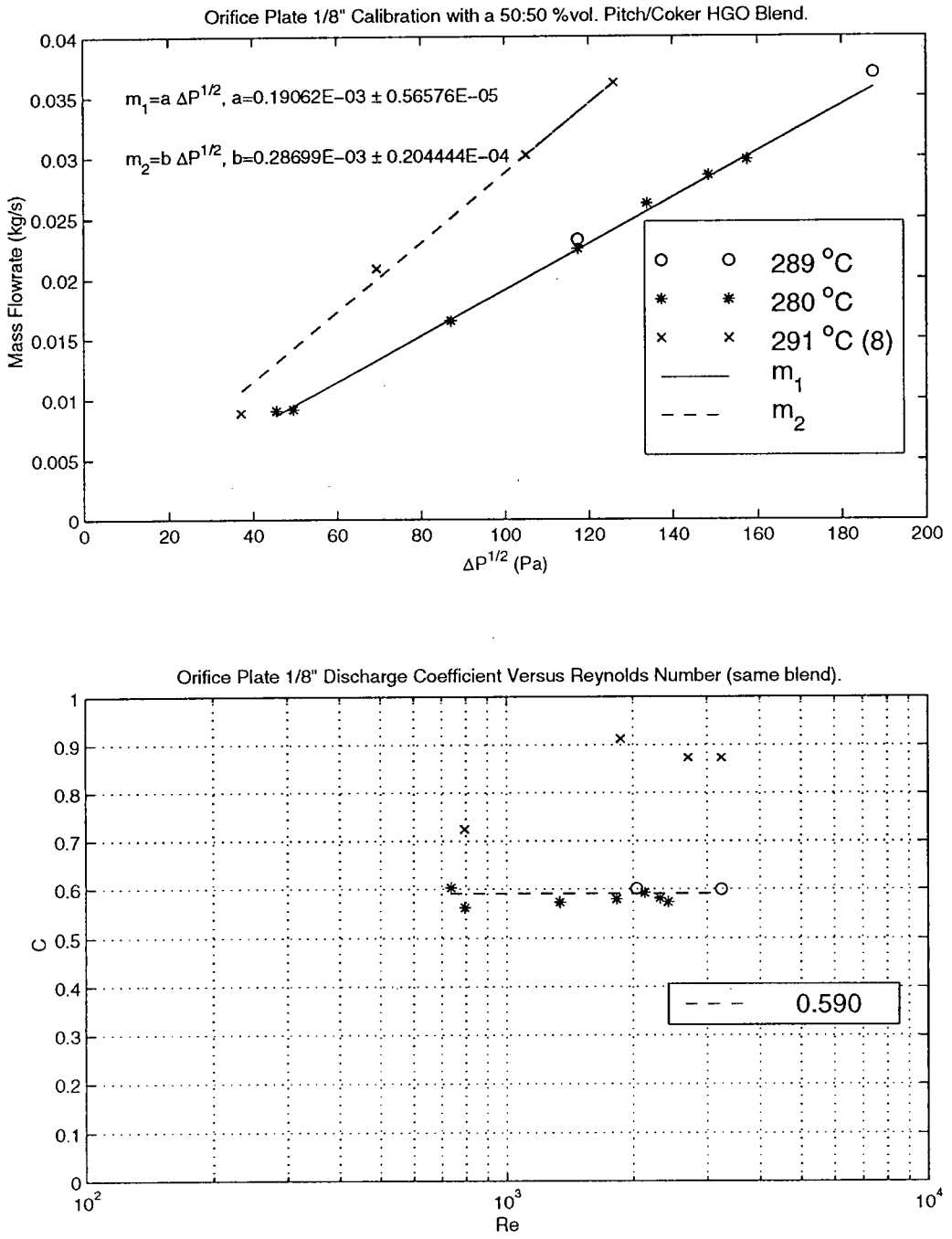

Figure A.2: Orifice 1/8" calibration and discharge coefficient; symbols in lower graph represent same data as in upper graph; bulk inlet temperature indicated in legend of upper graph and Run 8 indicated in parentheses.

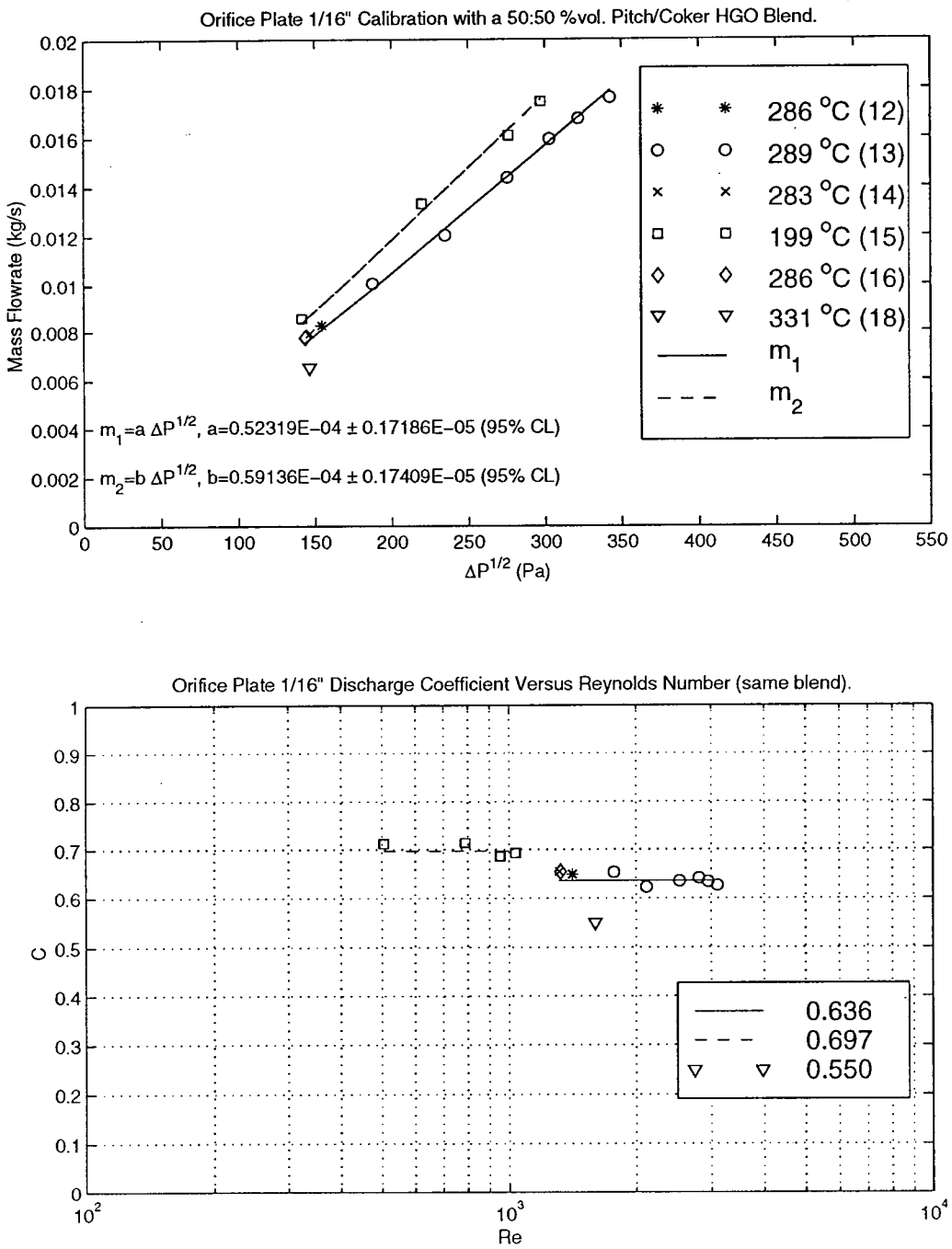

Figure A.3: Orifice 1/16" calibration and discharge coefficient; symbols in lower graph represent same data as in upper graph; bulk inlet temperature indicated in legend of upper graph and run number indicated in parentheses.

Appendix B

Properties of Fluids and Distillation TBP curves

Table B.1: Properties of pitch and CHGO

Parameter	Pitch	CHGO
Carbon, wt.%	81.6	84.0
Hydrogen, wt.%	9.1	10.5
Sulfur, wt.%	5.3	4.3
Nitrogen, ppm	6557	3810
Aromatic Carbon (C_{13} NMR), %	34.2	-
MCR, wt.%	27.1	2.8
Ash, wt.%	1.5	-
Density (25°C), g/mL	1.071	0.960
Ni, ppm	159	0.0
V, ppm	422	2.3

Table B.2: Some properties of Fuel Oil, Cold Lake Heavy Oil and De-Asphalted Oil

Parameter	Cold Lake Heavy Oil	Fuel Oil	De-Asphalted Oil
Saturates, wt.%	23.14	69.62	20.72
Aromatics, wt.%	49.84	27.71	68.45
Resins, wt.%	10.4	2.72	10.08
Asphaltenes, wt.%	16.63	Trace	0.76
Polars, wt.%	27.03	2.72	10.84
Carbon, wt.%	80.27	86.41	86.71
Hydrogen, wt.%	10.52	12.76	11.15
Nitrogen, wt.%	0.41	0.21	0.28
Sulphur, wt.%	4.51	0.56	3.54
H/C atomic ratio	1.57	1.77	1.58

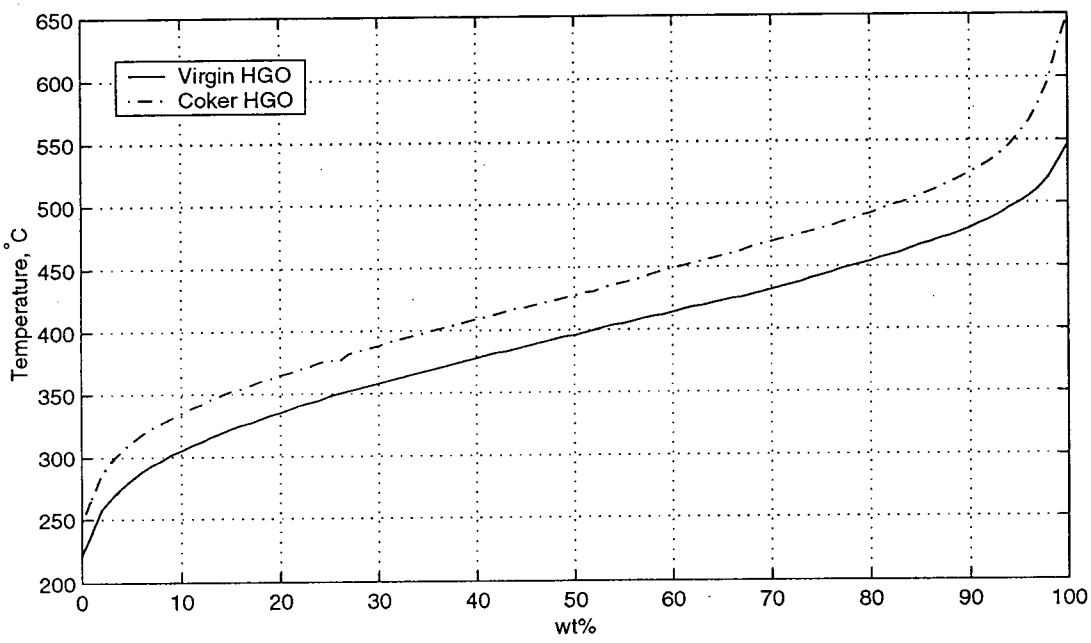

Figure B.1: SIMDIST for Virgin and Coker HGOs.

Appendix C

Size Distribution of Quartz Sand Used in Fluid Bed

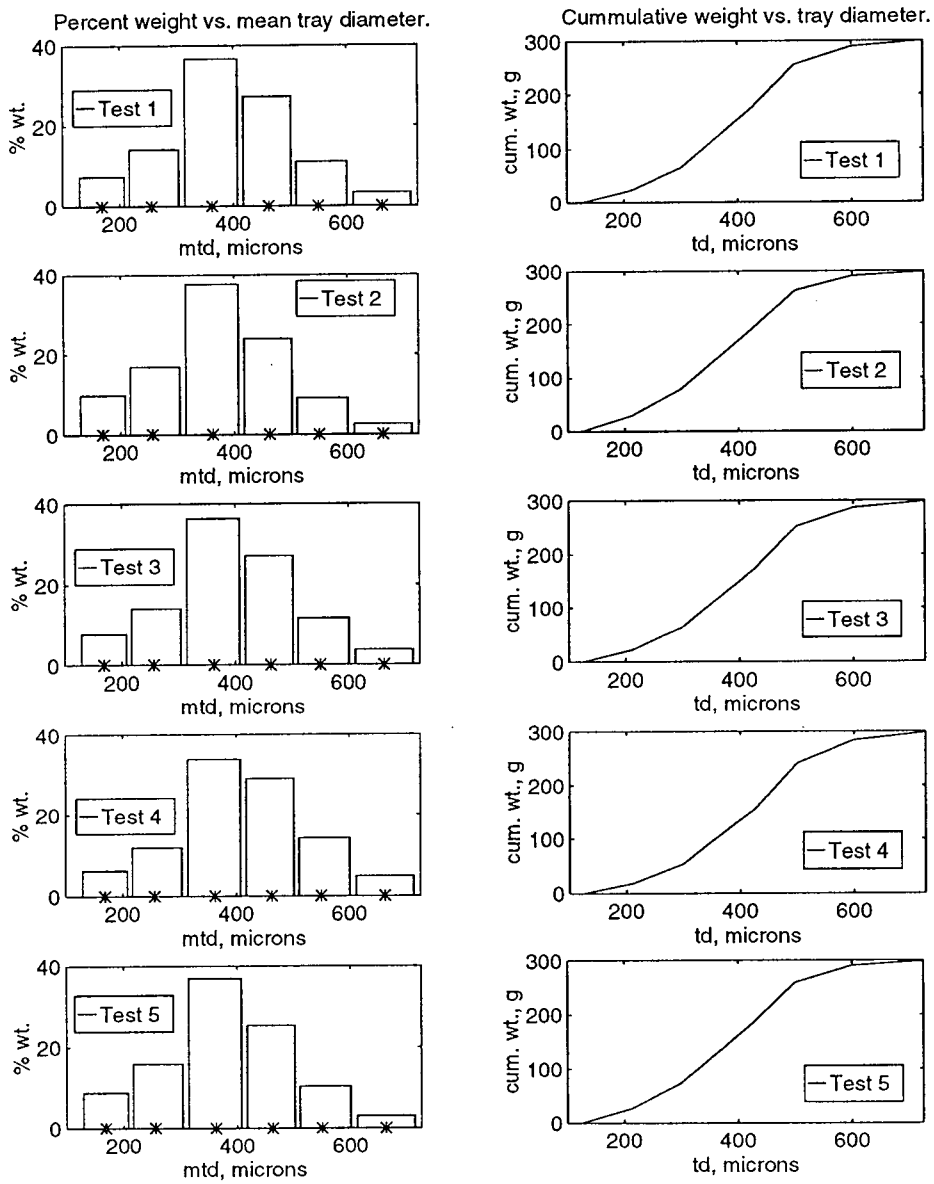

Figure C.1: Size distribution of quartz sand used in fluidized bed; mean particle diameter=0.34 mm.

Appendix D

Sample Calculations

D.1 Tube Side Velocity, and Reynolds Number.

For $\dot{m}_c = 9.2 \times 10^{-3}$ kg/s, $D_i = 5.33 \times 10^{-3}$ m, and ρ calculated at $\overline{T_b} = 287°C$ from Equation 3.2 (conditions of Run 10):

$$v_c = \frac{4 \cdot \dot{m}_c}{\rho \cdot \pi D_i^2} = 0.48 \text{ [m/s]} \tag{D.1}$$

For the same Run, with ν calculated at $\overline{T_b}$ from Equation 3.9 where A, B, and C are given in Table 3.4 (51.7%wt. pitch and Dutt), the Reynolds number is:

$$Re_c = \frac{v_c \cdot D_i}{\nu} = 487 \tag{D.2}$$

D.2 Heat Flow, Overall Heat Transfer Coefficient, and Thermal Fouling Resistance

$$Q_v(t) = \dot{m}(t) \int_{T_{in}(t)}^{T_{out}(t)} C_p(T) \cdot dT_b(t) \text{ [kW]} \tag{D.3}$$

where $C_p = (0.055 + 6.818 \times 10^{-3} \cdot T(t) - 4.464 \times 10^{-6} \cdot T^2)$ [kJ/kg·K] (see Lu (1989)) and $\dot{m}$ is given by Eq. 6.12. With $D_o = 6.35 \times 10^{-3}$ m and $L = 0.46$ m, the overall heat transfer coefficient at time t based on the actual mass flowrate is:

$$U_{o,v} = \frac{Q_v(t)}{\pi D_o L \cdot \Delta T_{lm}} \quad [\text{m}^2\cdot\text{K/kW}] \tag{D.4}$$

$$\text{where } \Delta T_{lm} = \frac{(T_{top} - T_{out}) - (T_{bot} - T_{in})}{ln[(T_{top} - T_{out})/(T_{bot} - T_{in})]} \tag{D.5}$$

The thermal fouling resistance is calculated as the difference between the reciprocals of overall heat transfer coefficients under clean conditions and at time t:

$$R_{f,v} = \frac{1}{U_{o,v}(t)} - \frac{1}{U_{o,v}(0)} \text{ [m}^2\cdot\text{K/kW]} \tag{D.6}$$

where $U_{o,v}(0)$ is an average of twenty-one points calculated from the S.S. value reported in Table 6.1.

D.3 Superficial Gas Velocity, U, and Minimum Fluidization Velocity, U_{mf}.

$$U = \frac{4 \cdot V_g}{\pi D_b^2} \tag{D.7}$$

where D_b=0.05 m and V_g, the volumetric flowrate of air, is obtained by correcting the value read from Figure A.1 for the appropriate conditions of pressure and temperature of the fluid bed. The minimum fluidization velocity is given by:

$$\frac{1.75}{\phi_s \cdot \epsilon_{mf}^3}\left(\frac{d_p \cdot \rho_g \cdot U_{mf}}{\mu_g}\right)^2 + \frac{150 \cdot (1-\epsilon_{mf}) \cdot d_p \cdot \rho_g \cdot U_{mf}}{\epsilon_{mf}^3 \cdot \phi_s^2 \cdot \mu_g} = \frac{d_p^3 \cdot \rho_g \cdot (\rho_s - \rho_g) \cdot g}{\mu_g^2} \tag{D.8}$$

D.4 Experimental Bed-to-Wall and Oil Side Heat Transfer Coefficients.

The bed-to-tube wall heat transfer coefficient measured in Runs 16, 20, and 23 was calculated from:

$$h_o = \left[\left(\frac{1}{U_{o,v}}\right) - \frac{\pi D_o \cdot L \cdot \Delta T'_{lm}}{Q_v}\right]^{-1} \tag{D.9}$$

$$\Delta T'_{lm} = \frac{(T_{top,w} - T_{out}) - (T_{bot,w} - T_{in})}{ln[(T_{top,w} - T_{out}) - (T_{bot,w} - T_{in})]} \tag{D.10}$$

where the subscript w refers to outer wall temperature. The tube side heat transfer coefficient measured was calculated according to:

$$\frac{A_i}{A_o} \cdot h_i = \left[\frac{\pi D_o \cdot L \cdot \Delta T'_{lm}}{Q_v} - \frac{A_o \cdot ln(D_o/D_i)}{2\pi \cdot L \cdot k}\right] \tag{D.11}$$

D.5 Effect of h_o on Sensitivity of Unit to detect Coke Formation.

Al-Atar (2000) obtained a fouling resistance of 0.3 m^2·K/kW—final value—after recirculating a 75% FO/10% HO/15% DAO blend for 380 min. at an average bulk temperature of 85.5 °C, average surface temperature of 222 °C, and liquid velocity of 0.75 m/s. What change in $1/U_o$ would result in our unit given this final value?

The change in $1/U_o$ is calculated from

$$\frac{\left(\frac{1}{U_{o,F}} - \frac{1}{U_{o,C}}\right)}{\left(\frac{1}{U_{o,C}}\right)} = \frac{\frac{A_o}{A_i} \cdot R_{f,i}}{\left(\frac{A_o}{A_i \cdot h_i} + R_w + \frac{1}{h_o}\right)} \tag{D.12}$$

and can be expected to be at least 10% if evident detection is to be made. The subscripts C and F refer to clean and fouled conditions respectively. Table D.1 gives the results for three values of h_o, the heat transfer coefficient in the fluid bed. The value of 489 and 451 W/m^2·K for h_o and h_i respectively are the predicted values for Run 16.

Table D.1: Effect of h_o on the change in $1/U_o$.

h_o (W/m^2·K)	h_i (W/m^2·K)	Change in $1/U_o$ (%)
489	451	8
1500	451	11
3000	451	12

From these results it may be inferred that the sensitivity of the unit is rather low. Also, it is shown that as h_o increases, the change in $1/U_o$ becomes more significant. Al-Atar (2000) reported a value of $(1/U_C)$=0.317 m^2·K/kW for this run, and hence the change in $(1/U)$ was 95% given a final R_f of 0.3 m^2·K/kW.

D.6 Calculation of parameters presented in Table 6.1

$$\overline{T}_{fb} = \frac{1}{N}\sum_{t=S.S.}^{t_r}\left(\frac{T_{top}(t)+T_{mid}(t)+T_{bot}(t)}{3}\right) \tag{D.13}$$

$$\overline{T}_{in} = \frac{1}{N}\sum_{t=S.S.}^{t_r} T_{in}(t) \tag{D.14}$$

$$\overline{T}_{b} = \frac{1}{N}\sum_{t=S.S.}^{t_r}\left(\frac{T_{in}(t)+T_{out}(t)}{2}\right) \tag{D.15}$$

$$\overline{Q} = \frac{1}{N}\sum_{t=S.S.}^{t_r} Q(t) \tag{D.16}$$

$$\overline{\Delta T_{lm}} = \frac{1}{N}\sum_{t=S.S.}^{t_r} \Delta T_{lm}(t) \tag{D.17}$$

(D.18)

where t_r is the total recirculation time, N is the number of data points from S.S. to t_r, and $\Delta T_{lm}(t)$ is given by Equation D.5.